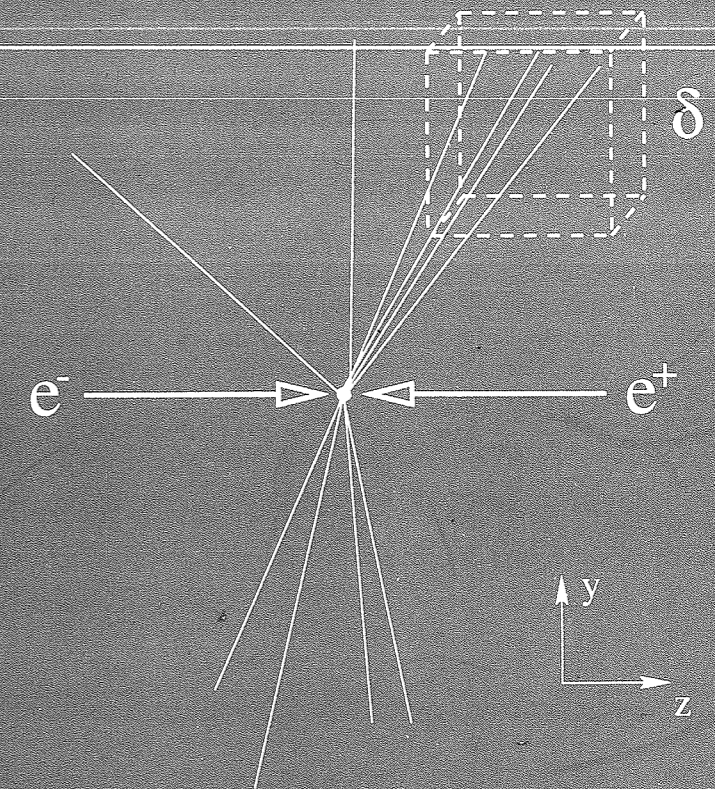


LOCAL MULTIPLICITY FLUCTUATIONS
AND INTERMITTENT STRUCTURE
INSIDE JETS



Thesis-1997-Chekanov

Sergei Chekanov

**LOCAL MULTIPLICITY FLUCTUATIONS
AND INTERMITTENT STRUCTURE
INSIDE JETS**

**LOCAL MULTIPLICITY FLUCTUATIONS
AND INTERMITTENT STRUCTURE
INSIDE JETS**

Doctoral Dissertation

to obtain the degree of doctor
from the University of Nijmegen
according to the decision of the Council of Deans
to be defended in public
on Thursday, June 12, 1997,
at 1.30 pm

by

Sergei Chekanov

born in Minsk (Belarus) on June 9, 1969

LOCAL MULTIPLICITY FLUCTUATIONS AND INTERMITTENT STRUCTURE INSIDE JETS

Een wetenschappelijke proeve op het gebied
van de Natuurwetenschappen.

Proefschrift

ter verkrijging van de graad van doctor
aan de Katholieke Universiteit Nijmegen,
volgens besluit van het College van Decanen
in het openbaar te verdedigen
op donderdag 12 juni 1997,
des namiddags om 1.30 uur precies,

door

Sergei Chekanov

geboren op 9 juni 1969 te Minsk (Belarus)

910222

Promotores: **Prof. Dr. E. W. Kittel**
Prof. Dr. V. I. Kuvshinov (Minsk, Belarus)

Manuscriptcommissie: **Prof. Dr. J. -L. Meunier** (Nice, France)
Dr. W. J. Metzger

This work is part of the research program of the “Stichting voor Fundamenteel Onderzoek der Materie (FOM)”, which is financially supported by the “Nederlandse Organisatie voor Wetenschappelijk Onderzoek (NWO)”. The research was partly supported by the International Soros Science Educational Program and the Fund for Fundamental Research of the Republic of Belarus.

Chekanov, Sergei Vladimirovich

Local Multiplicity Fluctuations
and Intermittent Structure
Inside Jets,

Thesis, Nijmegen, The Netherlands, 1997

ISBN 90-9010518-2

Acknowledgements

It is a pleasure to thank all those who have encouraged and supported me since the beginning of this work.

Special thanks go to my promoter Prof. Dr. E. W. Kittel, who taught me an innumerable amount of experimental high-energy physics and who offered me an opportunity to work on the L3 experiment. His guidance, advice and criticism on the contents and structure of this thesis are very much appreciated.

I am grateful to my promoter Prof. Dr. V. I. Kuushinov for introducing me the topic of multiparticle fluctuations/correlations and many discussions on the subject. He has continuously guided my steps in my discovery of the world of intermittent fluctuations.

I thank Prof. Dr. J. -L. Meunier and Dr. W. J. Metzger for discussions, careful reading of the manuscript and for their suggestions which greatly improved the readability of this thesis.

I thank all members of the Laboratory of Theoretical Physics of the Academy of Science of Belarus who provided me with a good atmosphere to work on this subject. My thanks go to my colleagues and friends D. Klenitsky, S. Sakovich, S. Shatohin, A. Saprykin, R. Shulyakovsky and V. Shaporov for their friendship and a pleasant time I shared with them. Being always special, special thanks go to A. Zagorskaya for friendship. I am indebted to Dr. L. F. Babichev with whom I could always discuss all software problems.

I thank all members of the high-energy physics group in Nijmegen. I greatly benefited from discussions with A. Buytenhuijs, H. De Boeck, S. Costantini, R. Hakobyan, H. Kuijten. I would like to thank M. van Hoek, A. van Mil, D. Mangeol, B. Petersen, M. Sanders, V. Sokovin and E. Visser for their friendship. I thank Dr. J. Schotanus who helped me on various matters. I thank the secretaries of the group E. Dikmans, J. Lodesteijn and M. van Wees for their help in administrative matters. I thank A. Oosterhof for being always available to help me. I am indebted to P. Klok and R. Bergman who taught me computing. I thank Prof. Dr. R. T. Van de Walle, who gave me the chance to broaden my horizon at CERN. I thank D. Bourilkov, D. Duchesneau and J. Field for useful discussions at CERN.

I would like to thank my colleagues E. Boudinov, J. Czyzewski, I. M. Dremin, E. Grinbaum-Sarkisyan, P. Lipa, V. Nechitailo, A. Tomaradze, W. Ochs and R. Peschanski for inspiring discussion on the subject of multiparticle fluctuations.

I would like to thank Els Hopman (and her family) for warm hospitality and constant support.

My stay in Nijmegen would not have been as nice as it was if it were not for all the friends that I made here. I would like to thank them for their warm friendship. I thank, last but not least, my parents and my sister for their heartfelt guidance, a lot of patience and support across the years.

LIST OF ABBREVIATIONS

AFD - anomalous fractal dimension
BE - Bose-Einstein (correlations)
BPs - bunching parameters
CERN - European Laboratory for Particle Physics
DCA - distance of closest approach
DGLAP - Dokshitzer-Gribov-Lipatov-Altarelli-Parisi (equation)
DLLA - Double Leading Log Approximation (of QCD)
ECAL - electromagnetic calorimeter (of the L3 detector)
GF - generating function
HWHM - half-width at half-maximum of Gaussian distribution
HCAL - hadron calorimeter (of the L3 detector)
LEP - Large Electron Positron Collider
LLA - Leading Logarithmic Approximation (of QCD)
ME - matrix element approach
MC - Monte Carlo
MLLA - Modified Leading Log Approximation (of QCD)
NBD - negative-binomial distribution
NFM - normalized factorial moment
QCD - quantum chromodynamics theory
PS - parton shower approach
SIL3 - simulation program (of the L3 detector)
SMD - silicon microvertex detector (of the L3 detector)
SRCs - smallest resolvable cluster
TEC - time expansion chamber (of the L3 detector)

Contents

1	Introduction	1
2	Local fluctuations and their characteristics	5
2.1	Local multiplicity distribution and its properties	5
2.2	Normalized factorial moments and statistical noise	7
2.3	Bunching parameters	10
2.4	Guide for further reading	11
3	Bunching Parameter and Intermittency in High-Energy Collisions	15
3.1	Introduction	16
3.2	The bunching parameter	16
3.3	The BPs for the negative-binomial distribution	18
3.4	The Lévy-law approximation	18
3.5	Simple approximation of the high-order BPs	20
3.6	Conclusion	21
4	Multifractal Multiplicity Distribution in Bunching-Parameter Analysis	23
4.1	Introduction	24
4.2	Bunching-parameter approach	25
4.3	Recurrence relations and generating functions	26
4.4	Non-linear Markov process and MNBD	30
4.5	Application to experimental data	31
4.6	Conclusion	33
5	Generalized Bunching Parameters and Local Fluctuations	35
5.1	Introduction	36
5.2	Poissonian noise suppression and other properties	38
5.2.1	The problem of Poissonian noise	38
5.2.2	Multifractal and monofractal behavior	40
5.2.3	Examples	40
5.2.3.1	Random-cascade model	40
5.2.3.2	Second-order phase transition	41
5.2.3.3	Perturbative QCD cascade	41
5.3	Experimental definitions of BPs	41
5.3.1	Bin-averaged BPs	41
5.3.2	Generalized distance measure	42
5.3.2.1	Definitions of spike size	42

5.3.2.2	Bunching parameters	4
5.3.2.3	Propagation of the statistical error for generalized BPs	4
5.4	Statistical fluctuations and BPs	4
5.4.1	The bin-averaged BPs	4
5.4.1.1	Flat phase-space distribution	4
5.4.1.2	Non-flat phase-space distribution	5
5.4.1.3	Theoretical aspect of the problem	5
5.4.2	GHP counting topology	5
5.5	Local fluctuations in the JETSET 7.4 model	5
5.6	Conclusions	5
6	Bin-Bin Correlation Measurement by the Bunching-Parameter Method	6
6.1	Introduction	6
6.2	Bunching correlators	6
6.3	The lowest-order bunching correlator and its behavior	6
6.4	Conclusions	6
7	Hadron production in e^+e^- collisions	7
7.1	Theoretical description of e^+e^- collisions	7
7.2	Lund Monte-Carlo generator (JETSET 7.4)	7
7.3	Description of final-state hadrons	7
7.3.1	Single-particle variables	7
7.3.2	Event-shape variables	7
8	L3 Detector and data acquisition	8
8.1	The L3 Detector	8
8.2	Data acquisition and reconstruction	8
8.2.1	Trigger system	8
8.2.2	Event reconstruction	8
8.2.3	Event simulation	8
9	Charged-hadron selection	9
9.1	Calorimeter-based selection of hadronic events	9
9.2	Charged-particle selection	9
9.2.1	Cuts on full events	9
9.2.2	Selection of charged tracks	9
9.3	Inclusive distributions	9
10	Resolution	10
10.1	Resolution of variables with respect to the beam axis	10
10.2	Resolution of variables with respect to the thrust axis	10
10.3	Resolution of the squared four-momentum difference	10
10.4	Determination of the smallest bin size	11

11 Transformation of variables	113
11.1 Motivation	113
11.2 One-dimensional cumulative variable	114
11.3 Multi-dimensional transformation	116
12 Experimental Analysis of Local Fluctuations	119
12.1 Motivation	119
12.2 Experimental definitions	120
12.3 In the detector frame	123
12.3.1 Factorial-moment method	123
12.4 In the event frame	126
12.4.1 All charge combinations	126
12.4.2 Like-charged and unlike-charged particle combination	128
12.5 In the four-momentum difference	130
12.5.1 Generalized integral BPs	130
12.5.2 Generalized differential BPs	133
12.6 Discussion	133
13 Test of Analytical QCD Predictions	139
13.1 Introduction	139
13.2 Analytical predictions	139
13.3 Experimental procedure	141
13.4 Analysis	142
13.5 Conclusion	144
14 Summary	149
15 Samenvatting	151
Curriculum Vitae	153
List of Publications	155

1

Introduction

The main problems addressed in this thesis concern the description and interpretation of local particle-multiplicity fluctuations observed in high-energy collision experiments. In fact, the quest for dynamical local fluctuations is the quest for chaotic behavior in any multiparticle system: At the simplest level, such a chaotic behavior means that particles have a tendency to form so-called “spikes” according to some dynamical process. In high-energy physics, spikes are seen as high-density peaks of dynamical origin in the phase-space distribution for individual events.

Dynamical occurrence of peaks is familiar in other fields of physics, particularly in hydrodynamics, where peaks are observed in velocity and temperature distributions and where the effect has been given the name “intermittency”. Another example of intermittency can be observed near the critical point in a system undergoing a first- or second-order phase transition.

In a high-energy experiment, an unusual bunch of particles in a single event is not yet a signal for intermittency because such a group of particles may be formed randomly, even without any dynamical reason. Indeed, from probability theory, we know that for a random distribution of particles in phase space, the probability $P_n(\delta)$ to find n particles in a phase-space cell of size δ is non-zero but proportional to δ^n . For a random distribution, this quantity is very small for large n and small δ . However, if there is a dynamical reason for the clustering, the probability of observing n particles in a small phase-space interval can become significantly larger. This leads to a multiplicity distribution that is broader, with large fluctuations near the average value of observed multiplicity than in the case of no correlations. In particular, an increase of the fluctuations according to a power law of phase-space size δ , corresponds to intermittency in particle spectra [1]. This effect is intimately linked to (multi)fractal properties of the underlying physical process. Reviews on the present status of experimental and theoretical studies of intermittency in high-energy physics are given in [2].

In order to reveal intermittency in high-energy experiments, it is necessary to consider a large number of experimental events, i.e., to have a large event sample. For a given event sample, we can qualitatively and quantitatively estimate the strength of an intermittent signal from the characteristics of the multiplicity distribution in small phase-space intervals.

Fluctuations in multiparticle systems can be described by correlations between particles. Positive correlations between particles produce clustering and lead to spikes. Negative correlations produce anti-clustering and lead to “dips” in phase-space distributions for single

experimental events. In fact, the concepts of fluctuations and correlations are equivalent, because both descriptions have the same physical content. One can, in principle, choose either method; this choice only depends on the specific system and the actual questions under study. In this thesis, we will mainly use the fluctuation approach in which one studies the characteristics of multiplicity distributions in ever smaller phase-space intervals.

A peculiarity of this thesis is that it combines some theoretical progress in the theory of local fluctuation measurements with new experimental investigations using the highest statistics obtained in the L3 experiment. This thesis, therefore, contains two main parts: a theoretical and an experimental.

While the introduction to the theoretical part will be given just after this general introduction, a few words about the experiment should be given already here. First of all, I would like to mention that I had the rare opportunity to test new theoretical ideas in this rapidly developing field using the data on hadrons produced in e^+e^- interactions - one of the fundamental point-like processes. Since the initial state of this interaction is completely known, the study of such a process opens up the possibility of a precision test of the Standard Model incorporating our present knowledge on elementary particles and their interactions. In particular, e^+e^- annihilation into a quark and an antiquark is one of the most important experimental probes of interactions of quark and gluons - according to present knowledge the basic building blocks of matter.

The interaction of quarks and gluons (partons) is described by the theory of quantum chromodynamics (QCD), which exhibits two remarkable properties: "asymptotic freedom" and "color confinement". The first property means that at short distances, below the proton size ($\sim 10^{-13}$ cm), the color interaction becomes weak and quarks are almost free particles. Asymptotic freedom corresponds to large transverse momentum, when the QCD coupling constant α_s becomes small. In this case, the QCD characteristics of partons can be calculated as a power expansion in α_s (perturbative calculations). Color confinement, on the other hand, means that, at distances comparable to or larger than the proton size, the color interaction becomes so strong that it confines quarks and gluons into composite particles as pions, protons and neutrons. In this case, perturbative calculations become impossible (non-perturbative regime of QCD).

Another property of QCD, which is strongly related to color confinement, is hadronization. In the hadronization process, quarks and gluons are converted into the hadrons that are actually seen in the detector. At present, the only detailed description of the hadronization process is provided by models, one of which, the string fragmentation model, will be discussed briefly in this thesis.

There is another difficulty in forming a complete description of particles produced in an e^+e^- experiment. For high energies, this process is a multiparticle one, i.e., at the perturbative stage a large number of partons is involved. Hence, many variables are necessary for the description of the process. For this reason, an exact treatment according to Feynman diagrams is a very difficult task even at the perturbative stage.

The experimental study of a multiparticle system produced in an e^+e^- reaction is, therefore, very important. Because of their large information content on the dynamics involved the investigation of multiplicity fluctuations and their interpretation is one of the most important directions in such a study. Apart from the fact that it is a new area of confrontation between (not complete) theory and experiment, the search, description and interpretation of local fluctuations give rise to many new methods in this field of physics. For example

the study of self-similar structure of the dynamics responsible for local fluctuations has been started quite recently, together with the study of intermittency in high-energy experiments. Within the framework of QCD, the self-similar structure is a natural consequence of parton branching: In this process, each hard parton branches into two new partons, which in turn branch into new ones, and so on, down to a final hadronization stage. This stage again gives rise to a self-similar pattern. Such a self-similar mechanism can produce a self-similar structure of local fluctuations which becomes very transparent in fully dimensional momentum phase space.

Recently, there have been many attempts to formulate and explain local multiplicity fluctuations: within the framework of QCD, cascade models, quantum statistics, phase transition of a quark-gluon plasma, fractal space-time and so on [2]. For an e^+e^- interaction, one can be confident that, at least on the parton level of this reaction, perturbative QCD calculations can give a hint for an understanding of the problem. Calculations based on the Double Leading Log Approximation (DLLA) of perturbative QCD show that the multiplicity distribution of partons in ever smaller opening angles is inherently intermittent [3] (for a review see [4]). However, the first comparison [5] of asymptotic theoretical predictions for multiparton angular correlations with experimental results from e^+e^- annihilations revealed poor agreement. There can be a number of reasons for the observed disagreement: the data are far away from an asymptotic energy and various approximations had to be made for the analytical QCD calculations. Another obstacle in the way of a comparison of an observed intermittent signal with QCD predictions is that the perturbative description is forbidden for a very small phase-space window because of the large value of the running coupling constant α_s . This leads to the breakdown of the intermittent behavior for small phase-space intervals due to the filling-up of phase space by soft gluons. The hadronization effect, therefore, appears to be important for our understanding of the dynamical reason for intermittency at small phase-space intervals.

Note, however, that the self-similar dynamics of perturbative QCD and hadronization are not the only phenomena that can lead to the observed fluctuations. For example, another candidate to explain intermittency is Bose-Einstein (BE) interference between identical bosons. In this context, the study of large local fluctuations opens up an intriguing question about the connection between (multi) fractal structures in four-momentum and ordinary space-time.

The main goal of this thesis is to try to reveal and understand the behavior of local fluctuations inside jets produced in e^+e^- reactions. For the first time we will use for this purpose a recently proposed approach which can precisely and comprehensively measure these fluctuations. This approach is applied to high statistics accumulated by the L3 experiment at LEP in 1994. These measurements, therefore, may form a new basis for further experimental tests of fluctuations in various reactions and the comparison with theoretical predictions.

Bibliography

- [1] A.Białas and R.Peschanski, Nucl. Phys. B273 (1986) 703; Nucl. Phys. B308 (1988) 857
- [2] A.Białas, Nucl. Phys. A525 (1991) 345;
R.Peschanski, J. of Mod. Phys. A21 (1991) 3681;
P.Bożek, M.Łosajczak and R.Botet, Phys. Rep. 252 (1995) 101;
E.A.De Wolf, I.M.Dremin and W.Kittel, Phys. Rep. 270 (1996) 1
- [3] W.Ochs and J.Wosiek, Phys. Lett B289 (1992) 152; Phys. Lett. B305 (1993) 144;
Yu.Dokshitzer and I.M.Dremin, Nucl. Phys. B402 (1993) 139;
Ph.Brax, J.-L.Meunier and R.Peschanski, Z. Phys. C62 (1994) 649
- [4] W.Ochs and J.Wosiek, Z. Phys. C68 (1995) 269
- [5] F.Mandl and B.Buschbeck (DELPHI Coll.), Multiparton angular correlations in e^+e^- interactions, Proc. 24 Int. Symp. on Multiparticle Dynamics, Salerno, Italy 1994, Eds: A.Giovannini et al. (World Scientific, Singapore, 1995) p.52;
B.Buschbeck, P.Lipa, F.Mandl (DELPHI Coll.), Angular correlations and QCD parameters, Proc. 7th Int. Workshop on Multiparticle Production "Correlations and Fluctuations", Nijmegen, The Netherlands 1996, Eds: R.C.Hwa et al. World Scientific, Singapore, 1997) p.175

2

Local fluctuations and their characteristics

The main goal of this chapter is to give a short introduction to the subject of local fluctuations necessary for reading the main theoretical part of this thesis. We summarize definitions and various relations used throughout this thesis.

2.1 Local multiplicity distribution and its properties

The first step to describe multiplicity fluctuations of charged particles produced in collisions of elementary particles is to study the multiplicity distribution P_N of observing N secondary particles in an inelastic event. This distribution can be defined as follows

$$P_N = \frac{\sigma_N}{\sigma_I}, \quad \sigma_I = \sum_{N=0}^{\infty} \sigma_N, \quad (2.1)$$

where σ_I is the total inelastic cross section and σ_N is the cross section for the production of N particles in an event. Such a distribution reflects only *event-to-event* fluctuations since it contains no information on the distribution of particles over phase space. The form of this distribution is strongly influenced by charge and energy-momentum conservation.

In practice, the multiplicity distribution P_N can be measured by counting the numbers N_N of events with N particles in the full phase space Δ :

$$P_N = \frac{N_N}{N_{\text{ev}}}, \quad N_{\text{ev}} = \sum_{N=0}^{\infty} N_N, \quad (2.2)$$

where N_{ev} is the total number of experimental events. For $N_{\text{ev}} \rightarrow \infty$, definition (2.2) would approach the true theoretical multiplicity distribution which is bounded by energy conservation, i.e. $P_N = 0$, for $N > N_{\text{en}}$ with N_{en} being the maximum number of particles possible at given energy. However, since in any experiment N_{ev} is finite, the distribution is also statistically truncated by a finite multiplicity N_{stat} (randomly) depending on N_{ev} , i.e., $P_N = 0$, for $N > N_{\text{stat}}$, $N_{\text{stat}} < N_{\text{en}}$.

While the study of the multiplicity distribution in full phase space deals with limited dynamical information influenced by charge and energy-momentum conservation, the investigation of the evolution of the multiplicity distribution with decreasing size of phase-space

windows (bins), however, can provide us with detailed information on multihadron production without these trivial constraints. A deviation of the local multiplicity distribution from that expected for purely independent particle production can be attributed to local dynamical multiplicity fluctuations.

In order to study the phase-space distribution of particles locally, i.e., in restricted phase space intervals, it is necessary to measure the multiplicity distribution $P_n(\delta_m)$ of observing n particles in the phase-space bin m of size δ_m inside the full phase-space interval Δ . In analogy with (2.2), this distribution can be defined as

$$P_n(\delta_m) = \frac{N_n(\delta_m)}{N_{\text{ev}}}, \quad (2.3)$$

where $N_n(\delta_m)$ is the number of events with n particles in bin m .

In contrast to P_N , $P_n(\delta_m)$ drops very rapidly with increasing n . As a consequence of finiteness N_{ev} , n_{max} defined by $P_n(\delta_m) = 0$ observed for $n > n_{\text{max}}$, becomes much smaller than N_{sta} and, for $\delta_m \rightarrow 0$, even tends to zero ($P_0(\delta_m) \rightarrow 1$, $\delta_m \rightarrow 0$). So, for such a (local) multiplicity distribution, the problem of finite statistics leading to the truncation of the observed $P_n(\delta_m)$ becomes of primary importance.

The average value of multiplicity n_m in bin m is given by

$$\langle n_m \rangle = \sum_{n=1}^{\infty} n P_n(\delta_m). \quad (2.4)$$

The next important step in studying the distribution $P_n(\delta_m)$ is to find out how particles fluctuate around $\langle n_m \rangle$. For this aim, one can define the moments $\langle n_m^q \rangle$ of the multiplicity distribution in bin m

$$\langle n_m^q \rangle = \sum_{n=1}^{\infty} n^q P_n(\delta_m). \quad (2.5)$$

These characteristics of $P_n(\delta_m)$ contain redundant information, since they depend on $\langle n_m \rangle$. To reduce this effect, one can define the scaled or normalized moments C_q as

$$C_q = \frac{\langle n_m^q \rangle}{\langle n_m \rangle^q}. \quad (2.6)$$

Such quantities are frequently used to compare multiplicity distributions in restricted phase space bins for various processes or for different energies with different average multiplicities. In particular, the multiplicity distribution P_N for full phase space Δ is said to admit asymptotic Koba-Nielsen-Olesen scaling [1], if $C_q = \langle N^q \rangle / \langle N \rangle^q$ is an energy independent constant for all q . However, C_q are rarely used for the investigation of the structure of multiplicity fluctuations in the small δ_m , because they are contaminated by Poissonian statistical noise (see below).

Note that the measurement of $P_n(\delta_m)$ in ever smaller phase-space intervals reflects only reduced information on phase-space fluctuations. From a theoretical point of view, the complete information on the phase-space distribution of n particles is contained in the exclusive continuous distribution in 3-momentum phase space $P_n(\vec{p}_1, \vec{p}_2, \dots, \vec{p}_n)$, where \vec{p}_i , $i = 1, \dots, n$ represent the 3-momentum vectors needed to specify the position of each particle in a given phase space. If all final particles are identical, the distribution is symmetric in all variables

\vec{p}_i . Then, the observed multiplicity distribution $P_n(\delta_m)$ in a small momentum volume δ_m can be found as

$$P_n(\delta_m) = (n!)^{-1} \int_{\delta_m} P_n(\vec{p}_1, \vec{p}_2, \dots, \vec{p}_n) \prod_{i=1}^n d\vec{p}_i. \quad (2.7)$$

From an experimental point of view, to study $P_n(\vec{p}_1, \vec{p}_2, \dots, \vec{p}_n)$ is an extremely difficult task. This is due to the fact that in a given event, one can only know the number of particles in some minimally small bins defined by the experimental resolution. This leads naturally to the investigation of $P_n(\delta_m)$ for different phase-space intervals (bins). Of course, the dimension of δ_m should be smaller than or equal to that of the vectors \vec{p}_i .

2.2 Normalized factorial moments and statistical noise

The standard tool used to reveal local fluctuations of particles near the average $\langle n_m \rangle$ is the method of normalized factorial moments (NFM) introduced in high-energy physics by Białas and Peschanski [2]. The normalized factorial moment $F_q(\delta_m)$ of q -th order for bin m is defined as

$$F_q(\delta_m) = \frac{\langle n_m^{[q]} \rangle}{\langle n_m \rangle^q}, \quad n_m^{[q]} = n_m(n_m - 1) \dots (n_m - q + 1), \quad (2.8)$$

$$\langle n_m^{[q]} \rangle = \sum_{n=q}^{\infty} n_m^{[q]} P_n(\delta_m). \quad (2.9)$$

These moments have the following properties:

1) Contributions to the numerator (2.8) for a q -th order NFM come only from the events containing $n_m \geq q$ particles, i.e., the NFM acts as a filter for particle spikes.

2) If particles are distributed independently according to a Poissonian distribution, then $F_q(\delta_m) = 1$. In the general case, for an independent distribution of particles in phase space, $F_q(\delta_m) = \text{const}$. The value of the constant depends on event-to-event fluctuations.

In contrast to C_q , the NFMs have an important feature for the study of local fluctuations: They are not contaminated by statistical noise. To illustrate this important property, let us first define a theoretical particle density ρ_m in bin m of size δ_m as

$$\rho_m = \frac{n_m}{\delta_m}, \quad (2.10)$$

where n_m is the number of particles in bin m in a single event. For a local-fluctuation analysis, we need to consider very small bin sizes, i.e., $\delta_m \rightarrow 0$. ρ_m , therefore, is an asymptotic density, since it can be defined in the limit of infinite multiplicity N (or n_m) for a given event.

After that, we can define $\omega(\rho_m)$ as a continuous probability density to observe a given value of ρ_m in the limit $N_{\text{ev}} \rightarrow \infty$. This density is normalized by

$$\int_0^{\infty} \omega(\rho_m) d\rho_m = 1. \quad (2.11)$$

Of course, the density ρ_m in bin m of size δ_m fluctuates around the average value

$$\langle \rho_m \rangle \equiv f_1 = \int_0^{\infty} \rho_m \omega(\rho_m) d\rho_m. \quad (2.12)$$

Since we are interested in the deviation of ρ_m from the average value f_1 , the next step is to define the higher-order moments of $\omega(\rho_m)$ as

$$\langle \rho_m^q \rangle \equiv f_q = \int_0^\infty \rho_m^q \omega(\rho_m) d\rho_m. \quad (2.13)$$

However, in experimental studies, the multiplicity N per event is finite. In this case, the number of particles n_m in bin m fluctuates around the theoretical value

$$n_m = \rho_m \delta_m \quad (2.14)$$

due to statistical noise. Accepting this assumption and the assumption that such statistical noise does not introduce new fluctuations, then the observed (discrete) multiplicity distribution $P_n(\delta_m)$ of observing n particles in δ_m can be described by the following Poisson transformation

$$P_n(\delta_m) = \int_0^\infty \omega(\rho_m) \frac{(\rho_m \delta_m)^n \exp(-\rho_m \delta_m)}{n!} d\rho_m. \quad (2.15)$$

Expression (2.15) represents a convolution of the statistical poissonian noise with mean $\rho_m \delta_m$ with a true, dynamical distribution $\omega(\rho_m)$.

The next problem is how to compare model fluctuations described by $\omega(\rho_m)$ with the experimental fluctuations defined by $P_n(\delta_m)$. Substituting (2.15) into definition (2.9), one has

$$\langle n_m^{[q]} \rangle = \int_0^\infty \omega(\rho_m) \exp(-\rho_m \delta_m) \left[\sum_{n=q}^\infty \frac{(\rho_m \delta_m)^n}{(n-q)!} \right] d\rho_m. \quad (2.16)$$

Defining $n' = n - q$, the expression in square brackets can be rewritten as

$$\sum_{n'=0}^\infty \frac{(\rho_m \delta_m)^{n'+q}}{n'!} = (\rho_m \delta_m)^q \exp(\rho_m \delta_m). \quad (2.17)$$

Hence, one has

$$\langle n_m^{[q]} \rangle = \delta_m^q f_q, \quad q = 1, 2, 3, \dots, \quad (2.18)$$

where f_q are the moments defined by (2.12) and (2.13). Hence,

$$F_q(\delta_m) = \frac{f_q}{f_1^q}. \quad (2.19)$$

The right-hand side of this expression represents the normalized moments given by a model distribution $\omega(\rho_m)$. Hence, to study this distribution in experiments with finite N is equivalent to measuring the NFMs $F_q(\delta_m)$.

Experimental definitions of NFMs

To study NFMs in an experiment, it is necessary to use available statistics as efficient as possible, in order to obtain a stable result for local quantities in small bins. For this purpose one divides the full phase-space volume Δ into M non-overlapping bins of size $\delta = \Delta/M$ and averages of these bins. Then one can define two kinds of NFMs:

1) *Vertical NFMs*:

$$F_q^{\text{ver}}(\delta) = \frac{1}{M} \sum_{m=1}^M \frac{\langle n_m^{[q]} \rangle}{\langle n_m \rangle^q}. \quad (2.20)$$

Since these moments are normalized locally, they are sensitive only to multiparticle fluctuations inside each bin, but do not depend on the form of the phase-space distribution.

2) *Horizontal NFMs*:

$$F_q^{\text{hor}}(\delta) = \frac{1}{M} \sum_{m=1}^M \frac{\langle n_m^{[q]} \rangle}{\langle \bar{n} \rangle^q}, \quad (2.21)$$

where $\langle n \rangle = \bar{N}/M$ and \bar{N} is the average multiplicity for full phase space. Due to the non local normalization, this kind of NFM is sensitive to the shape of the single-particle density. To reduce this trivial effect, a transformation of the original non-flat particle density into a new flat density is frequently used (see Chapter 11).

Intermittency

As stated earlier, if particles are distributed independently in phase space, then $F_q(\delta) = \text{const}$. The remarkable property of the NFMs is that, in reality, the $F_q(\delta)$ are functions rising with decreasing bin size δ due to dynamical correlations between particles. Experimental data on various processes have revealed such a tendency over a wide range of energy (see recent reviews [3]). In particular, if experimentally observed $F_q(\delta)$ follow inverse power-law functions of the bin size δ ,

$$F_q(\delta) \propto \delta^{-\phi_q}, \quad \phi_q > 0, \quad (2.22)$$

we call this effect *intermittency* and the ϕ_q *intermittency indices*.

For finite multiplicity per event, this phenomenon reflects the peculiarity of $P_n(\delta)$ to become broader with decreasing δ . This is widely regarded as evidence of short-range correlations exhibiting a self-similar underlying dynamics, since (2.22) satisfies the *scaling property*

$$F_q(\lambda\delta) = \lambda^{-\phi_q} F_q(\delta). \quad (2.23)$$

The subject of intermittency has motivated many theoretical investigations [3]. Since this type of scaling is an inherent property of (multi)fractal objects, intermittency can be related to (multi)fractal properties of phase-space distributions [4]. In this context, intermittency indices define the *anomalous fractal dimensions* (AFDs) d_q and the *Rényi dimensions* D_q as follows

$$d_q = \frac{\phi_q}{q-1}, \quad D_q = D - d_q, \quad (2.24)$$

where D is the topological dimension of the phase space under study. Note that a strict relation between the Rényi dimensions and ϕ_q is valid only for a single event. Therefore, different D_q should be attributed for each event after splitting the total phase space into an infinite number of bins, for an infinite total number of particles per event. If one averages the measurements over many events, D_q has to reflect an averaged property of the event sample. In such a treatment, D_q can be considered as a characteristic of a single phase-space bin for many events.

For monofractal distributions, d_q and D_q are q -independent constants. Any deviation of particle spectra from a monofractal distribution leads to a q -dependence of both AFDs and Rényi dimensions. In this case one says that the distribution exhibits a multifractal property.

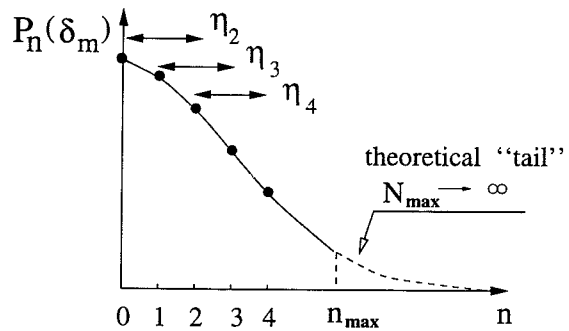


Figure 2.1: A schematic representation of the bunching-parameter measurement.

2.3 Bunching parameters

From the experimental point of view, the measurement of NFMs suffers from a few important disadvantages. NFMs were designed to select the high-multiplicity tail of a multiplicity distribution, since only events with $n \geq q$ particles can contribute to q -th order NFM. However, in practice, $P_n(\delta_m)$ is truncated at some n_{\max} which can be rather small for small δ_m . This means that the observed $F_q(\delta)$ are not only a function of δ and q , but also of n_{\max} ($\propto N_{ev}$). As a consequence of finite N_{ev} , in the limit of $\delta \rightarrow 0$, the NFMs obtained experimentally never coincide with the true ones [5]. Hence, the normalized factorial moments are an ideal tool to avoid the bias caused by finite particle statistics ($N \neq \infty$), but they suffer from another kind of statistical bias - finiteness of the number of experimental events ($N_{ev} \neq \infty$).

Secondly, the NFMs are able to extract dynamical information only on spikes, but the equally important information on dips is lost. This is an essential shortcoming for the investigation of reactions with a high density of secondary particles. For example, in nuclear collisions, where the multiplicity per event is very large, unusually large dips in the density distribution of individual events can be explained as dynamical effects as well.

The problem of “dips” can be solved with the help of G-moments [6] which take into account both “spike” events and events with large gaps. However, there is no clear link of this tool with the multiplicity distribution $P_n(\delta_m)$ itself.

Thirdly, for an accurate measurement of the NFM of order q , one needs to know the $n \geq q$ particle resolution. If only q -particle resolution is used, the calculation of the q th order NFM is affected by the systematic bias due to contributions from the tail of the multiplicity distribution measured with insufficient resolution.

To avoid these problems, one can measure the local fluctuations by means of so-called bunching parameters (BPs) [7–10] which are subject of the thesis. For a single phase-space bin, the BPs are defined as

$$\eta_q(\delta_m) = \frac{q}{q-1} \frac{P_q(\delta_m)P_{q-2}(\delta_m)}{P_{q-1}^2(\delta_m)}, \quad q > 1. \quad (2.25)$$

A complete list of properties of the BPs is given in the introduction of Chapter 5. Here, we only note that the measurement of local fluctuations by means of BPs merely involves knowl

edge on the behavior of $P_n(\delta_m)$ near multiplicity $q = n - 1$ without contributions from the tail of this distribution (see Fig. 2.1). This ultimately leads to a significant reduction of the statistical and systematical bias arising in the case of the normalized-factorial-moment measurements. Besides, the definition of the second-order BP $\eta_2(\delta)$ involves $P_0(\delta_m)$ containing information on bins with zero content not included in the definition of NFMs.

It was found [10] that, as in the case of NFMs, $\eta_q(\delta_m) = \text{const}$ for an independent distribution of particles in phase space. As an example, for a Poisson distribution of particles in bin m , one obtains $\eta_q(\delta_m) = 1$ for all q and δ_m .

The most important property of the BPs is that these quantities are very sensitive to the content of local fluctuations: It was shown that very different samples may lead to rather similar power-like behavior of the NFMs, while the BPs show the different trend [10, 11]. More properties of BPs will be given in the chapters following.

2.4 Guide for further reading

In the following four chapters, we shall give a reproduction of four selected papers dealing with the local fluctuation analysis and published during the years 1994-1997. A complete list of publications is given at the end of this thesis.

The papers are arranged in logical rather than in chronological order. The reproductions contain minor editorial alterations in order to keep close to the standard of abbreviations and definitions used throughout this thesis. It should be remarked that each chapter is to a great extent self-contained and can be read separately.

For convenience of reading of these papers, we here sketch the major theoretical results concerning the bunching-parameter approach:

• Chapter 3

This chapter contains the first article dealing with BPs in high-energy physics. We introduce these parameters following an analogy with quantum optics [13], where the BPs are used for the investigation of the radiation photon field in the theory of continuous quantum measurement. We derive a general form of the generating function (GF) for multiplicity distributions with δ -independent BPs and study the case of a negative-binomial distribution (NBD). Using Lévy-law approximation, we consider the possible behavior of BPs for various high-energy processes. In addition, we illustrate that

$$\eta_{q>2}(\delta) = \eta_2^r(\delta), \quad \eta_2(\delta) \propto \delta^{-d_2}, \quad (2.26)$$

for $r > 0$ is a good approximation for a multifractal behavior of AFDs in various reactions. Such an assumption leads to the following linear form of the AFDs

$$d_q = d_2(1 - r) + d_2 r \frac{q}{2}. \quad (2.27)$$

In this context, the parameter r can be considered as a degree of multifractality ($r = 0$ corresponds to a monofractal behavior).

- **Chapter 4**

An essential feature of BPs is that they have a direct link to the form of $P_n(\delta)$ itself. Inspired by this property, we derive a general form of $P_n(\delta)$ leading to both mono- and multifractal behavior. At the simplest phenomenological level, such a distribution can have only three free parameters: a , b and the degree of multifractality r . The first two parameters are δ -dependent functions. One can write

$$P_n(\delta) = P_n(a, b, r). \quad (2.28)$$

Such a general multiplicity distribution can lead to the following cases:

- 1) $a \neq 0, b = r = 0$, a Poisson distribution.
- 2) $b \neq 0, a = r = 0$, a logarithmic distribution
- 3) $a = b \neq 0, r = 0$, a geometric distribution.
- 4) $a \neq 0, b \neq 0, r = 0$, a negative binomial distribution.

The first three distributions do not lead to any fractal behavior. In the limit of $\delta \rightarrow 0$ the last case can lead to a monofractal behavior. However, if $r \neq 0$, the distribution (2.28) can lead to the multifractal behavior with the AFDs of the form (2.27).

We also propose a new definition of generating functions which are convenient for the study of BPs. Using this mathematical tool, we derive a general form of the generating function for the multifractal multiplicity distributions.

- **Chapter 5**

This chapter contains a paper most important for the experimental investigation of local multiplicity fluctuations by means of the bunching-parameter method. Here, we show that, in the limit of $\delta \rightarrow 0$, the BPs suppress the statistical noise as do the NFM (see (2.19)). We summarize the main properties of BPs and propose definitions of the BPs involving the bin-splitting method (in analogy with the definitions of NFMs (2.20) and (2.21)), as well as definitions making use of the interparticle distance-measurement technique. Special attention is paid to an exact expression for the statistical error for the latter definition of BPs.

Using theoretical and numerical investigations, we illustrate that for purely statistical phase-space fluctuations, the BPs are δ -independent functions at small δ . We have also show that the BPs provide tools for a better understanding of the differences between samples with approximately the same power-like behavior of the NFMs.

- **Chapter 6**

When one measures the local quantities inside restricted phase-space regions by means of the bin-splitting technique, one loses important information on fluctuations. More details on the local fluctuations can be obtained from the multivariate probability distribution. Due to the very complex structure of this quantity, however, one usually resorts to the study of a bivariate moment containing the information on bin-bin correlations. In this paper, the bunching-parameter method is, therefore, extended to measure the bin-bin correlations.

Bibliography

- [1] Z.Koba, H.B.Nielsen and P.Oleson, Nucl. Phys. B40 (1972) 317
- [2] A.Białas and R.Peschanski, Nucl. Phys. B273 (1986) 703; B308 (1988) 857
- [3] P.Bożek, M.Łosajczak and R.Botet, Phys. Rep. 252 (1995) 101;
E.A.De Wolf, I.M.Dremin and W.Kittel, Phys. Rep. 270 (1996) 1
- [4] P.Lipa and B.Buschbeck, Phys. Lett. B223 (1989) 465;
H.Satz, Santa Fe Workshop "Intermittency in High Energy Physics", Eds. F.Cooper et al., (World Scientific, Singapore, 1990) p.182
- [5] E.M.Friedlander, Mod. Phys. Lett. A4 (1989) 2457;
W.Kittel, Santa Fe Workshop "Intermittency in high-energy collisions", Ed. F.Cooper et al., (World Scientific, Singapore, 1991) p.83;
P.Lipa et al., Z. Phys. C54 (1992) 115
- [6] R.C.Hwa, Phys. Rev. D41 (1990) 1456;
C.B.Chiu and R.C.Hwa, Phys. Rev. D43 (1991) 100
- [7] S.V.Chekanov and V.I.Kuvshinov, Acta Phys. Pol. B25 (1994) 1189 (see Chapter 3)
- [8] S.V.Chekanov and V.I.Kuvshinov, J. Phys. G22 (1996) 601 (see Chapter 4)
- [9] S.V.Chekanov, W.Kittel and V.I.Kuvshinov, Acta Phys. Pol. B26 (1996) 1739 (Dedicated to A.Białas in honor of his 60th birthday), (see Chapter 6)
- [10] S.V.Chekanov, W.Kittel and V.I.Kuvshinov, Z. Phys. C74 (1997) 517 (see Chapter 5)
- [11] S.V.Chekanov, Talk presented at 5th Int. Sem. "Nonlinear Phenomena in Complex Systems", (Minsk, Belarus, 1996), J. Phys. G (1997) (in press)
- [12] F.Meijers, "Multiplicities in Phase-Space Intervals and Bose-Einstein Correlations in Hadronic Interactions at 250 GeV/c", Ph.D. Thesis Univ. of Nijmegen 1987, The Netherlands
- [13] S.Ya.Kilin and T.M.Maevskaya, preprint IPAS No.686 (1993), Belarus (in Russian)

Bunching Parameter and Intermittency in High-Energy Collisions

S.V.Chekanov and V.I.Kuvshinov

*Institute of Physics, Academy of Sciences of Belarus
F.Skaryna Av. 70, 220072 Minsk, Belarus*

Published in Acta Phys. Pol. B25 (1994) 1189 - 1197

Abstract

We introduce the parameter of bunching for an analysis of the intermittent structure of multihadron production in high-energy collisions following an analogy with photon counting in quantum optics. A power-law singularity is shown to exist for second-order bunching parameters in small phase-space intervals for the case of a monofractal structure of the multiplicity distribution and a similar form for the high-order parameters for the case of multifractality. The approximation of the high-order bunching parameters by the second-order provides a good description of the anomalous fractal dimensions for a number of experimental data with multifractal behavior.

3.1 Introduction

The idea of applying stochastic methods developed to study photon counting statistics in quantum optics to particle production processes has been used for a long time [1]. At present, a systematic and careful investigation of multihadron production by the application of methods borrowed from quantum optics is very useful because there is a large analogy between these fields of physics. For instance, the interpretation of multiplicity distributions in terms of hadronic field states by analogy to photon counting [2] and the study of squeezed gluon states [3] seem to be important directions for theoretical research. The problem of damping of the statistical noise and the concept of factorial-moment analysis to study multihadron production [4] have long been known in quantum optics [5]. Correlators in terms of moments [6] have an analogous form in quantum optics as well [7].

The purpose of the present paper is to extend some methods of continuous quantum measurement in quantum optics to high-energy physics. We introduce the bunching parameter for the analysis of fractal structure of multihadron production. For intermittent structure of the multiplicity distribution, a non-trivial behavior of the bunching parameters is obtained for small phase-space intervals.

3.2 The bunching parameter

In the theory of continuous quantum measurement, the bunching parameter $\tilde{\eta}_q(\delta t)$ of order q for an one-mode photon field can be expressed in terms of the probability $P_n(\delta t)$ to have n photons in the time interval δt as follows [8]

$$\tilde{\eta}_q(\delta t) = \frac{q}{q-1} \frac{P_q(\delta t)P_{q-2}(\delta t)}{P_{q-1}^2(\delta t)}, \quad q > 1. \quad (3.1)$$

This parameter determines how the probability to detect q photons in δt changes relatively to the probability to detect $q-1$ photons in the same time interval. If the source of light is completely coherent, then $\tilde{\eta}_q(\delta t) = 1$. The corresponding multiplicity distribution is a Poissonian one. A radiation field is said to be statistically anti-bunched in order q if $\tilde{\eta}_q(\delta t) < 1$. When $\tilde{\eta}_q(\delta t) > 1$, then it is said to be bunched in δt . For a wide class of states the bunching parameters are independent of the time interval [8].

By analogy with (3.1), let us consider the bunching parameters (BPs) $\eta_q(\delta)$ for the multiplicity distributions of secondary particles produced in high-energy interactions

$$\eta_q(\delta) = \frac{q}{q-1} \frac{P_q(\delta)P_{q-2}(\delta)}{P_{q-1}^2(\delta)}, \quad q > 1, \quad (3.2)$$

where $P_n(\delta)$ is the probability to have n particles in the phase-space interval δ defined in rapidity, azimuthal angle, transverse momentum or a (multi-dimensional) combination of these variables.

There is a large class of distributions which has δ -independent BPs. By applying formula (3.2), any multiplicity distribution can be expressed as

$$P_n(\delta) = P_0(\delta) \frac{\lambda^n(\delta)}{n!} \prod_{m=2}^n [\eta_m(\delta)]^{n+1-m}, \quad n > 1, \quad (3.3)$$

where $\lambda(\delta) = P_1(\delta)/P_0(\delta)$. If $\eta_q(\delta)$ is independent of δ , one gets the following general form of the generating function for such a distribution,

$$G(z, \delta) \equiv \sum_{n=0}^{\infty} z^n P_n(\delta) = G(z=0, \delta) Q(z\lambda(\delta)), \quad (3.4)$$

where $G(z=0, \delta) = P_0(\delta)$, the $Q(z\lambda(\delta))$ is some analytic function of the auxiliary variable z multiplied by a function $\lambda(\delta)$ under the condition $Q(\lambda(\delta)) = 1/G(z=0, \delta)$. It is easy to see that condition (3.4) is fulfilled for well-known distributions, such as the Poissonian, binomial and geometric ones. The case of a negative-binomial distribution will be discussed later.

Let us remind that the observed behavior of the normalized factorial moments (NFM) is

$$F_q(\delta) \equiv \frac{\langle n^{[q]} \rangle}{\langle n \rangle^q} \propto \delta^{-d_q(q-1)}, \quad \delta \rightarrow 0, \quad q \geq 2 \quad (3.5)$$

is a straightforward manifestation of non-statistical intermittent fluctuations in the distribution of secondary particles produced in high-energy interactions [4, 9, 10]. In (3.5), n denotes the number of particles in δ , $n^{[q]} \equiv n(n-1) \dots (n-q+1)$, $\langle \dots \rangle$ is the average over all events. The right side of (3.5) represents the definition of the intermittent behavior characterized by an anomalous fractal dimensions (AFDs) d_q depending on the rank q of the NFM for multifractal behavior and $d_q = \text{const}$ for monofractality.

Now we shall prove the following statement: an inverse-power δ -dependence of the second-order BP and δ -independence of high-order BPs are necessary and sufficient conditions for the monofractal behavior of AFDs. An inverse-power δ -dependence of all BPs is necessary and sufficient for multifractality.

Sketch of a proof. By applying (3.3), for the NFM in terms of BPs, we have

$$F_q(\delta) = \frac{P_0(\delta)}{\langle n \rangle^q} \sum_{n=q}^{\infty} \frac{n^{[q]} \lambda^n(\delta)}{n!} \prod_{m=2}^n [\eta_m(\delta)]^{n+1-m}, \quad (3.6)$$

$$\langle n \rangle = P_0(\delta) \lambda(\delta) + P_0(\delta) \sum_{n=2}^{\infty} \frac{\lambda^n(\delta)}{(n-1)!} \prod_{m=2}^n [\eta_m(\delta)]^{n+1-m}. \quad (3.7)$$

Assuming the approximate proportionality of $\langle n \rangle$ and δ at small δ and the condition $P_0(\delta) \rightarrow 1$, for $\delta \rightarrow 0$, we have the following approximate expression for the small interval δ

$$F_q(\delta) \simeq \prod_{m=2}^q [\eta_m(\delta)]^{q+1-m}. \quad (3.8)$$

In the case of a power-law dependence of NFM (3.5) with monofractal behavior of AFDs $d_q = d_2 = \text{const}$, we must require the following properties of BPs

$$\eta_2(\delta) \propto \delta^{-d_2}, \quad 0 < d_2 < 1, \quad (3.9)$$

$$\eta_s(\delta) \simeq \text{const}, \quad s > 2. \quad (3.10)$$

From expression (3.8), one can conclude that for multifractality a power-law singularity of the BPs of the order $q = s > 2$ is necessary. Using (3.8), it is easy to show the sufficient conditions of an inverse power-law behavior of BPs for both the monofractal and multifractal cases.

Now we have the possibility to write down the general form of the generating function $G^{\text{mon}}(z, \delta)$ for the multiplicity distribution with monofractal behavior of AFDs

$$G^{\text{mon}}(z, \delta) = G^{\text{mon}}(z=0, \delta) \left(1 + \eta_2^{-1}(\delta) Q^{\text{mon}}(\lambda(\delta)\eta_2(\delta)z)\right), \quad (3.11)$$

where $\eta_2(\delta)$ is defined by (3.9), Q^{mon} is some analytic function with variable $\lambda(\delta)\eta_2(\delta)z$ with the following conditions

$$Q^{\text{mon}}(\lambda(\delta)\eta_2(\delta)z=0) = 0, \quad (3.12)$$

$$Q^{\text{mon}}(\lambda(\delta)\eta_2(\delta)z = \lambda(\delta)\eta_2(\delta)) = \eta_2(\delta) \left(\frac{1}{G^{\text{mon}}(z=0)} - 1 \right). \quad (3.13)$$

The general formal form of the generating function for multifractal behavior can be obtained from (3.3).

3.3 The BPs for the negative-binomial distribution

Since a few years, many high-energy multiparticle data at various energies have been successfully fitted by the negative-binomial distribution (NBD) [11] with the generating function

$$G^{\text{NBD}}(\delta y, z) = \left(1 + \frac{\langle n(\delta y) \rangle}{k(\delta y)}(1-z)\right)^{-k(\delta y)}, \quad (3.14)$$

where $\langle n(\delta y) \rangle$ is the average multiplicity of final hadrons in the restricted rapidity (or pseudorapidity) interval δy and $k(\delta y)$ is a positive parameter. If $k(\delta y)$ does not depend on δy , we do not have any fractal type of behavior for the NFMs of this distribution. Indeed, in this case one can rewrite the generating function in the form (3.4).

In the general case, the BPs of a NBD are given by the expression

$$\eta_q^{\text{NBD}}(\delta y) = \frac{k(\delta y) + q - 1}{k(\delta y) + q - 2}, \quad q = 2, \dots, \infty. \quad (3.15)$$

Let us assume that $k(\delta y) \propto \delta y^{d_2}$. In this case, $\eta_2^{\text{NBD}}(\delta y) \propto \delta y^{-d_2}$ and $\eta_s^{\text{NBD}}(\delta y) \simeq \text{const.}$, for $s > 2$ at small δy . According to Sect. 3.2, one gets the monofractal type of behavior for AFDs, i.e., $d_q = d_2 = \text{const.}$. Such a monofractal behavior has already been discussed in [12]. This analysis only illustrates the simplicity of our approach to intermittency in terms of BPs.

3.4 The Lévy-law approximation

In this section, we shall show the possible behavior of the bunching parameters in rapidity bins for different high-energy collisions.

At the beginning, let us note that for an investigation of intermittency in rapidity bins δy one usually averages [4] the factorial moments over all bins of equal width δy normalizing to the overall average number per bin $\langle n \rangle \equiv \sum_{m=1}^M \langle n_m \rangle / M$, where $\langle n_m \rangle$ is the average multiplicity in the m th bin, $M = Y/\delta y$, Y being the full rapidity interval,

$$\bar{F}_q(\delta y) \equiv \frac{1}{M} \sum_{m=1}^M \frac{\langle n_m^{[q]} \rangle}{\langle n \rangle^q} \simeq c_q \delta y^{-d_q(q-1)}, \quad (3.16)$$

where c_q is some constant. Similarly, one can introduce the BPs by averaging the probability $P_n^m(\delta y)$ for the m th bin over all M bins,

$$\bar{\eta}_q(\delta y) = \frac{q}{q-1} \frac{\bar{P}_q(\delta y) \bar{P}_{q-2}(\delta y)}{\bar{P}_{q-1}^2(\delta y)}, \quad q > 1, \quad (3.17)$$

where $\bar{P}_n(\delta y) = \frac{1}{M} \sum_{m=1}^M P_n^m(\delta y)$.

Following the same procedure as in Sect. 3.2, we can see that the approximate expression for the NFMs (3.16) in terms of the BPs (3.17) has the same form for $\delta y \rightarrow 0$ as (3.8), if we substitute $\bar{F}_q(\delta y)$ for $F_q(\delta)$ and $\bar{\eta}_s(\delta y)$ for $\eta_s(\delta)$. Then, we have

$$\bar{\eta}_2(\delta y) \simeq \bar{F}_2(\delta y), \quad \bar{\eta}_s(\delta y) \simeq \frac{\bar{F}_s(\delta y) \bar{F}_{s-2}(\delta y)}{(\bar{F}_{s-1}(\delta y))^2}, \quad (3.18)$$

where $\bar{F}_1(\delta y) = 1$ and $s > 2$. Using (3.16) and (3.18), we obtain the following expression for the BPs

$$\bar{\eta}_2(\delta y) \simeq c_2 \delta y^{-\beta_2}, \quad \bar{\eta}_s(\delta y) \simeq \frac{c_s c_{s-2}}{c_{s-1}^2} \delta y^{-\beta_s}, \quad (3.19)$$

where $C_1 = 1$ and

$$\beta_2 = d_2 \quad (3.20)$$

$$\beta_s = d_s(s-1) + d_{s-2}(s-3) - 2d_{s-1}(s-2), \quad s > 2. \quad (3.21)$$

Note that we can obtain (3.21) using the approximation $\langle n_m^{[q]} \rangle \simeq q! P_q^m(\delta y)$ for $\langle n \rangle \ll 1$ (a similar analysis of factorial moments in terms of the probabilities for one bin can be found in [13]).

For an analysis of the parameters β_n , we shall use the Lévy-law approximation for the AFDs, which has been introduced to describe random cascading models,

$$d_q = \frac{d_2}{2^\mu - 2} \frac{q^\mu - q}{q-1}, \quad (3.22)$$

with the Lévy index μ . The Lévy index is known as a degree of multifractality and allows a natural interpolation between the monofractal case ($\mu = 0$) and multifractality ($\mu > 0$). The case $\mu = 2$ ($d_q = qd_2/2$) corresponds to the log-normal approximation. Substituting (3.22) into (3.21), one gets the following expression

$$\beta_q = d_2 E_q, \quad E_q \equiv \frac{q^\mu + (q-2)^\mu - 2(q-1)^\mu}{2^\mu - 2}. \quad (3.23)$$

In the limit of monofractal behavior of the AFDs ($\mu = 0$), we have $\beta_s = 0$ for $s > 2$, i.e., the high-order BPs are independent of δy . Then, the values of $\bar{\eta}_s(\delta y)$ are completely determined by the coefficients c_q . Note, that in the case of multifractality, the values of E_q are positive for all q and the BPs increase indefinitely for $\delta y \rightarrow 0$. As we see, in the case of multifractal behavior, one can speak of a strong high-order bunching of particles in δy . For the log-normal approximation ($\mu = 2$), we obtain $E_q = 1$, $\beta_q = d_2$, i.e. all bunching parameters have the same power-law behavior $\bar{\eta}_q \propto \delta y^{-d_2}$.

Thus, there are two important limiting cases which correspond to monofractality and log-normal approximation for multifractality :

$$\mu = 0, \quad \bar{\eta}_2(\delta y) \propto \delta y^{-d_2}, \quad \bar{\eta}_s = \text{const.}, \quad \text{for all } s \geq 3, \quad (3.24)$$

$$\mu = 2, \quad \bar{\eta}_q(\delta y) \propto \delta y^{-d_2}, \quad \text{for all } q \geq 2. \quad (3.25)$$

In actual physical situations, the Lévy index μ is different for different reactions [10, 14–16] and, strictly speaking, it is not equal to an integer value:

(i) Nucleus-nucleus reaction S-AgBr: The Lévy index is $0 \leq \mu < 0.55$ (in fact, it is almost a monofractal system) [14]. The value of E_q is almost zero and the BPs approximately are δy independent. This behavior is typical for the intermittency at second-order phase transition and thus has been advocated [17] in favor of the formation of a quark-gluon plasma.

(ii) e^+e^- , pA, AA, hh reactions with $\mu \simeq 1.3 - 1.6$ [16] corresponding to the parameter $0 < E_q < 0.7$. In the case of μ p deep inelastic scattering, the Lévy index is largest, $\mu \simeq 2.6 - 3.7$ [14, 15] and $1 < E_q < 5$. In these cases, we have a power-law singularity in the behavior of the BPs.

3.5 Simple approximation of the high-order BPs

Using only one free parameter μ , the Lévy-law approximation allows a simple description of multifractal properties of random-cascade models. However, using the interpretation of intermittency via the BPs, we can make some approximation of high-order BPs in order to obtain a more simple linear expression for the AFDs, maintaining the number of free parameters.

Let us make the assumption that the high-order BPs can be expressed in terms of the second-order BP and a constant $r > 0$ as

$$\bar{\eta}_s(\delta y) = \bar{\eta}_2^r(\delta y), \quad s > 2 \quad (3.26)$$

with

$$\bar{\eta}_2(\delta y) \propto \delta y^{-d_2}. \quad (3.27)$$

For the given case, the multiplicity distribution with multifractal behavior has the following form ($n > 1$)

$$\bar{P}_n(\delta y) = \bar{P}_0(\delta y) \frac{\bar{\lambda}^n(\delta y)}{n!} [\bar{\eta}_2(\delta y)]^{n-1+\frac{1}{2}(n-n^2+\delta)(1-\delta_{2n})}, \quad (3.28)$$

where $\bar{\lambda}(\delta y) = \bar{P}_1(\delta y)/\bar{P}_0(\delta y)$ and $\delta_{22} = 1$, $\delta_{2n} = 0$ for $n \neq 2$. Using (3.18), (3.26-3.27), the AFDs of such a distribution are given by the linear expression

$$d_q = d_2(1 - r) + d_2 r \frac{q}{2}. \quad (3.29)$$

This linear approximation, in our opinion, is very interesting, because it allows interpolation between the monofractal case ($r = 0$) and the log-normal approximation ($r = 1$) as does the Lévy-law approximation (3.22). The results of fits of some experimental data [18–20] by the expression (3.29) are presented in Fig. 3.1. This analysis gives good agreement with the experimental data. Thus, the approximation (3.26) of high-order BPs by the second-order BP is valid for such reactions.

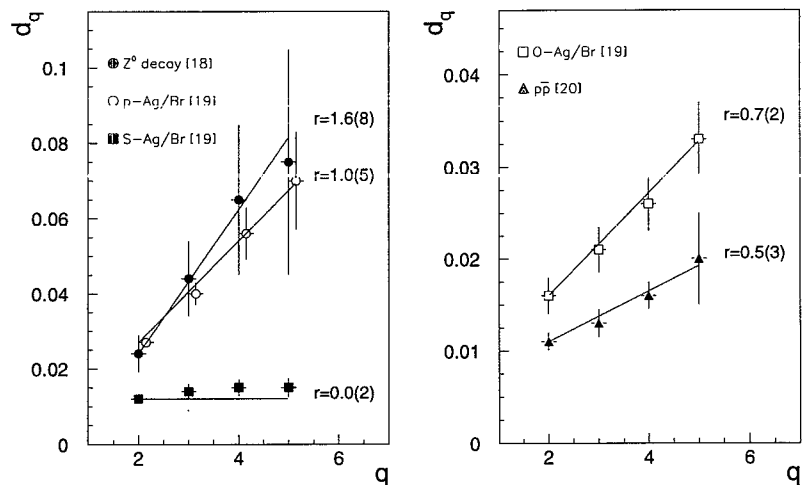


Figure 3.1: *Experimental data for the behavior of AFDs [18–20]. Continuous lines show fits using (3.29).*

3.6 Conclusion

We have introduced the bunching parameters for the analysis of multiparticle production in high-energy physics by analogy with the theory of continuous quantum measurement for one-mode photon fields. It is shown that an inverse power-law singularity of the second-order BP leads to monofractal behavior of the AFDs at small rapidity intervals if all high-order BPs are independent of phase-space intervals. Using such a dependence of the second-order BP on the phase-space interval size, we have found a general form of the generating function with monofractality. For multifractality, an inverse power-law singularity for all order BPs is necessary and sufficient.

Using the experimental data, we can conclude that, for $\delta y \rightarrow 0$, some reactions indeed show a strong bunching of particles in all orders. We have shown that the investigated experimental behavior of the AFDs can be understood as a simple approximation of the high-order BPs in terms of the second order. We believe this to be an important conclusion as it leads to a description of the multifractal multiplicity distribution with a minimum number of free parameters.

The use of BPs is interesting because it gives a general answer to the problem of finding a multiplicity distribution leading to intermittency. This method is also interesting since it may provide a link between theory of continuous quantum measurement and the investigations of multifractal structure of multiplicity distributions in particle collisions at high energies. Furthermore, it grants the possibility to analyze the intermittency phenomenon in quantum optics.

Bibliography

- [1] W.Knox, Phys. Rev. D10 (1974) 65;
A.Giovannini, Nuovo Cimento 15A (1973) 543
- [2] Bindu A.Bambah and M.Venkata Satyanarayana, Phys. Rev. D38 (1988) 2202;
A.Vourdas and R.M.Weiner, Phys. Rev. D38 (1988) 2209
- [3] V.I.Kuvshinov et al., 2nd Int. Workshop on Squeezed States and Uncertainty Relations
NASA, Conf. Publ. No.3219, 1993, p.301
- [4] A.Białas and R.Peschanski, Nucl. Phys. B273 (1986) 703; B308 (1988) 857
- [5] G.Bedard, Proc. Phys. Soc. 90 (1967) 131
- [6] R.Peschanski and J.Seixas, preprint CERN-TH-5903/90, DF/IST-3.90
- [7] C.D.Cantrell and J.R.Fields, Phys. Rep. A7 (1973) 2063
- [8] S.Ya.Kilin and T.M.Maevskaya, preprint of IP Academy of Sciences, No. 686 (1993)
Belarus, (in Russian)
- [9] A.Białas, Nucl. Phys. A525 (1991) 345
- [10] R.Peschanski, J. of Mod. Phys. A21 (1991) 3681
- [11] UA5 Coll., G.J.Alner et.al., Phys. Lett. B160 (1985) 193;
NA22 Coll., M.Adamus et al., Z. Phys. C32 (1986) 475;
UA5 Coll., R.E.Ansorge et al., Z. Phys. C43 (1989) 357;
M.Derrick et al., Phys. Lett. B168 (1986) 299
- [12] B.Buschbeck, P.Lipa, R.Peschanski, Phys. Lett. B215 (1988) 788;
L.Van Hove, Phys. Lett. B232 (1989) 509
- [13] L.Van Hove, Mod. Phys. Lett. A19 (1989) 1869
- [14] Ph.Brax and R.Peschanski, Phys. Lett. B253 (1991) 225
- [15] EHS/NA22 Coll, N.Agababyan et al., Z. Phys. C59 (1993) 405
- [16] W.Ochs, Z. Phys. C50 (1991) 339
- [17] A.Białas and R.C.Hwa, Phys. Lett. B253 (1991) 436
- [18] DELPHI Coll., P.Abreu et al., Phys. Lett. B247 (1990) 137
- [19] KLM Coll., R.Holynski et al., Phys. Rev. C40 (1989) 2449
- [20] UA1 Coll., C.Albajar et al., Nucl. Phys. B345 (1990) 1

Multifractal Multiplicity Distribution in Bunching-Parameter Analysis

S.V.Chekanov¹,

*High Energy Physics Institute Nijmegen (HEFIN), University of Nijmegen/NIKHEF,
NL-6525 ED Nijmegen, The Netherlands*

V.I.Kuvshinov

Institute of Physics, AS of Belarus, Skaryna Av.70, Minsk 220072, Belarus

Published in J. Phys. G22 (1996) 601 - 610

Abstract

A new multiplicity distribution with multifractal properties is proposed which can be used in high-energy physics and quantum optics. It may be considered as a generalization of the negative-binomial distribution. We derive the structure of the generating function for this distribution and discuss its properties.

¹On leave from Institute of Physics, AS of Belarus, Skaryna Av.70, Minsk 220072, Belarus

4.1 Introduction

Multifractal analysis in high-energy physics and quantum optics has received great interest in recent years due to the possibility to obtain quantitative and qualitative results concerning multiparticle production in different processes. In addition, the analysis is becoming an important theoretical tool to discriminate between multiparticle production models.

The fact that the normalized factorial moments (NFM's)

$$F_q = \frac{\langle n(n-1)\dots(n-q+1) \rangle}{\langle n \rangle^q} \quad (4.1)$$

(n is the number of particles in a restricted phase-space interval δ , $\langle \dots \rangle$ is the average over all events) depend on the size of the phase-space interval (bin) as $F_q \sim \delta^{-\phi_q}$ (intermittency phenomenon) is a manifestation of non-statistical fluctuations in the multiplicity distribution of secondary particles produced in high-energy physics [1]. The multifractal behavior, where the anomalous fractal dimension $d_q = \phi_q/(q-1)$ depends on q , is particularly important because such a behavior is typical for the vast majority of experiments. It is more pronounced in two- and three-dimensional phase-space domains. This behavior has also been found in photon counting experiments on laser fluctuations near threshold, where δ is the counting time interval T [2]. Thus, the problem of multifractality is a common one, applying both to high-energy physics and quantum optics.

In this paper, we shall discuss the theoretical aspect of the problem in the context of high-energy physics by means of bunching parameters (BPs) [3]. We have introduced this quantity in order to get a simple and efficient method for the analysis of complicated multiplicity distributions in restricted phase-space regions. Our consideration can be used in any field of research, where local dynamical fluctuations are a subject of investigation.

As is well known, the negative-binomial distribution has become the focus of interest in view of its applicability to the study of multiparticle production in high-energy physics. However, it has been noted that this distribution has no multifractal properties for small phase-space intervals [3, 4].

The UA5 collaboration has observed that the negative-binomial distribution fails to give a good fit to the data at a center of mass energy of 900 GeV [5] in full phase space due to a shoulder structure. This structure is explained by the superposition of 2-jet events of low multiplicities and 3-jet and 4-jet events yielding much larger multiplicities. Moreover, the study of charged-particle multiplicity distributions in restricted rapidity intervals confirms that the negative-binomial distribution is not sufficient to describe the data in Z^0 hadronic decays due to the shoulder structure of the experimental distributions [6, 7]. For example, in [7] it was shown that the negative-binomial distribution does not describe the experimental data, either in restricted rapidity intervals or in full phase space.

The conclusion must be that the negative-binomial distribution is not sufficient to describe the experimental distributions, both for restricted rapidity windows and for full phase space in definite experimental situations and, hence, true multiplicity distribution must be more complicated.

In this paper we propose a new multiplicity distribution which has multifractal properties for small phase-space intervals and is very similar to the conventional negative-binomial form for large phase-space intervals. We shall analyze this distribution in terms of BPs and

bunching moments. As we shall see, such an investigation is simpler than the analysis of multiplicity distributions with the help of NFMs. Moreover, recurrence relations for probabilities can lead to a non-traditional form of generating functions, both for well-known distributions (Poisson, geometric, logarithmic, positive-binomial, negative-binomial distributions) and the multiplicity distribution with multifractal properties for small phase-space intervals.

In Sect. 4.2, we give a short introduction to the bunching parameter method. In Sect. 4.3, we consider the general form of a multifractal negative-binomial-like distribution and derive its generating function. In Sect. 4.4, the properties of Markov branching leading to this multiplicity distribution are considered. In Sect. 4.5, we discuss a particular form of such a generalization of the negative-binomial distribution and illustrate its multifractal properties. In Sect. 4.6, we present the conclusions.

4.2 Bunching-parameter approach

Normalized factorial moments have become an important and popular topic of experimental and theoretical investigations in high-energy physics and quantum optics. Measuring the NFMs is equivalent to measuring the multiplicity distribution. On the other hand, recently another simple mathematical tool to investigate the behavior of the multiplicity distribution in different phase-space intervals has been proposed. In order to reveal “spike” structure of events, one can study the behavior of probabilities themselves by means of BPs. The definition of the BPs is given by the formula [3]

$$\eta_q = \frac{q}{q-1} \frac{P_q P_{q-2}}{P_{q-1}^2}, \quad q \geq 2, \quad (4.2)$$

P_q being the probability of finding q particles inside the limited phase-space interval δ ¹. For example, $\eta_q = 1$ for a Poisson distribution. If the size of the phase-space interval is small and the average number of particles in this interval is approximately proportional to δ , then the following approximate relation between the NFMs and the BPs holds [3]

$$F_q \simeq \prod_{i=2}^q \eta_i^{q+1-i}. \quad (4.3)$$

For intermittent fluctuations, one expects $\eta_2 \propto \delta^{-d_2}$ (d_2 is the second-order anomalous fractal dimension), while the high-order BPs may have a different dependence on δ . In [3] it has been shown that for high-energy collisions with multifractal behavior of the NFMs, $d_q = d_2(1-r) + d_2 r q/2$, power-like behavior of the BPs, $\eta_2 \propto \delta^{-d_2}$, $\eta_s = \eta_2^r$, $s > 2$ is valid. The positive parameter r can be interpreted as a degree of multifractality (for $r = 0$ we have exact monofractal behavior). Thus, the problem of a multifractal multiplicity distribution with inverse-power δ -dependence of *all* BPs is the central issue.

As discussed in [3], the use of BPs can give a general answer to the problem of finding a multiplicity distribution leading to the observed intermittency. Indeed, any multiplicity distribution can be expressed as

$$P_n = \frac{P_0}{n!} \left(\frac{P_1}{P_0} \right)^n \prod_{i=2}^n \eta_i^{n+1-i}. \quad (4.4)$$

¹In [3] we introduced the BPs by averaging the probabilities over all bins of equal width. Here we consider only one fixed bin. We do this only for the sake of simplicity and it is not a physical restriction.

On the contrary, a multiplicity distribution can not be expressed in terms of its factorial moments if this distribution is not truncated.

4.3 Recurrence relations and generating functions

A necessary and sufficient condition for a multiplicity distribution P_n to be of negative binomial type (P_n^N) is the recurrence relation [8]

$$\frac{P_n^N}{P_{n-1}^N} = C_{n-1} = \frac{a + b(n-1)}{n}, \quad n \geq 1, \quad (4.5)$$

where a, b are positive constants for fixed δ ($b < 1$). Note, that throughout this paper we shall treat the probabilities and the parameters C_{n-1}, a, b as continuous functions of the phase-space interval δ . If $a \neq 0, b \neq 0$, iterations of (4.5) with the normalization condition $\sum_{n=0}^{\infty} P_n^N = 1$ give the negative-binomial distribution. In the limit $b \rightarrow 0$, the recurrence relation gives a Poisson distribution. The case $a \rightarrow 0$ at constant b shows that the negative binomial distribution reduces to a logarithmic distribution. For $a = b$ we get a geometric multiplicity distribution. For $a > 0, b < 0$ and a/b integer we have a positive-binomial distribution. Using the definition of the BPs, expression (4.5) and the theorem of [3], it is easy to see that none of these distributions leads to multifractality, for any assumption chosen for the behavior of a, b in small phase-space bins.

Thus, it is important to find a multifractal generalization of the commonly used multiplicity distributions. From a physical point of view, to find such a multiplicity distribution means to understand the reasons of intermittency with multifractal behavior of the anomalous fractal dimension. However, the level of theoretical understanding of this phenomenon is still insufficient (hadronization problem) and is quite different for various types of collision processes [1]. Nevertheless, from a mathematical point of view, we can propose a distribution that has *a priori* multifractal behavior.

There is a natural way to include BPs with power-law behavior into a new recurrence relation, in order to obtain a modification of (4.5) which can generate the multifractal multiplicity distribution in the limit of small δ . To see this, let us rewrite the definition (4.2) of BPs as follows

$$\frac{P_q}{P_{q-1}} = \eta_q \frac{q-1}{q} \frac{P_{q-1}}{P_{q-2}}. \quad (4.6)$$

As mentioned in Sect. 4.2, for a multifractal behavior with $r = 1$, all BPs have the same power-law behavior, i.e, in the simplest case, we can write

$$\eta_q = g \propto \delta^{-\beta}. \quad (4.7)$$

The β is a positive constant and is taken as a measure of the strength of the multifractal effect. After that, by combining (4.5) and (4.6), we assume the following recurrence relation

$$\frac{P_n}{P_{n-1}} = \frac{a + b(n-1)}{n} + g \frac{n-1}{n} \frac{P_{n-1}}{P_{n-2}}, \quad (4.8)$$

where $n \geq 1$. Here, in fact, g can be either a new parameter or some combination of the parameters a and b (the latter case will be discussed below). Equation (4.8) is a sufficient

condition to construct a distribution which for a large phase-space interval ($g \ll 1$) is very similar to the multiplicity distribution (4.5) and has multifractal behavior for a small phase-space interval (g is not small).

The expression (4.8) can be rewritten as

$$\frac{P_n}{P_{n-1}} = \tilde{C}_{n-1} = \sum_{l=0}^{n-1} \frac{g^l}{n} (a + b(n-l-1)) \quad (4.9)$$

with the sum equal to

$$\begin{cases} b(n-ng)^{-1}[k(1-g^n) + n + (g^n-1)(1-g)^{-1}], & \text{for } g \neq 1, \\ b(k+0.5(n-1)), & \text{for } g = 1, \end{cases} \quad (4.10)$$

where $k^{-1} = b/a$ was called aggregation coefficient by Giovannini and Van Hove [8] for the usual negative-binomial distribution. For a compact description of the recurrence relation, we shall use an expression for \tilde{C}_{n-1} in the form of sum (4.9). Using (4.8) and (4.9), we get for the BPs

$$\eta_q = \frac{1 + k^{-1}(q-1)}{\sum_{l=0}^{q-2} g^l (1 + k^{-1}(q-l-2))} + g. \quad (4.11)$$

We have multifractal behavior because the second term in (4.11) has power-law behavior and, for small enough δ , will be the leading one. The multiplicity distribution corresponding to (4.8), (4.9) is

$$P_n = \frac{P_0}{n!} \prod_{s=0}^{n-1} \sum_{l=0}^s g^l (a + b(s-l)). \quad (4.12)$$

Throughout this paper, we consider the probability $P_0 = 1 - \sum_{n=1}^{\infty} P_n$ to have no particles in δ as a normalization constant. Since in the limit $g \rightarrow 0$ expression (4.12) reduces to a negative-binomial distribution, we shall call this distribution a multifractal negative-binomial distribution (MNBD) and denote it as P_n^M .

Let us note that we can analyze a multiplicity distribution written in terms of the recurrence relations by means of the generating function for P_n/P_{n-1} .

Let us define

$$G(z) = \sum_{n=1}^{\infty} \frac{z^n}{(n-1)!} \frac{P_n}{P_{n-1}}. \quad (4.13)$$

Then, the BPs are given by

$$\eta_q = \frac{G^{(q)}(z) |_{z=0}}{G^{(q-1)}(z) |_{z=0}}. \quad (4.14)$$

For example, the generating function of the negative-binomial distribution has the following form

$$G^N(z) = (a-b)(e^z - 1) + b z e^z. \quad (4.15)$$

For the Poisson distribution

$$G^P(z) = a(e^z - 1). \quad (4.16)$$

In terms of the generating function, the recurrence relation (4.8) can be rewritten in the form of the following differential equation

$$\frac{dG^M(z)}{dz} = \frac{dG^N(z)}{dz} + g G^M(z) \quad (4.17)$$

with the initial condition (see (4.13))

$$G^M(z=0) = G^N(z=0) = 0. \quad (4.18)$$

Using (4.17), we can get the generating function in integral form as follows

$$G^M(z) = G^N(z) + \sum_{i=1}^{\infty} g^i \int G^N(z) d^i z. \quad (4.19)$$

Using (4.15) and condition (4.18), one obtains the analytical solution of the equation (4.17)

$$G^M(z) = \frac{e^z}{1-g} \left(a + bz - \frac{b}{1-g} \right) - e^{gz} \frac{a(1-g) - b}{(1-g)^2} \quad (4.20)$$

for $g \neq 1$ and, using (4.9) and (4.13), $G^M(z) = e^z(az + bz^2/2)$ for $g = 1$. Further on we shall not consider the trivial case, when $g = 1$.

Now we mention two limiting cases:

a) In the simplest Poisson case, when $b = 0$, we have the following multifractal Poisson distribution with the generating function in the form

$$G^{MP}(z) = \frac{a}{1-g} (e^z - e^{zg}). \quad (4.21)$$

Then, from (4.11) and (4.12), one has

$$P_n^{MP} = P_0 \frac{a^n}{n!} \prod_{s=0}^{n-1} \sum_{l=0}^s g^l, \quad (4.22)$$

$$\eta_q^{MP} = \frac{1}{\sum_{l=0}^{q-2} g^l} + g. \quad (4.23)$$

Here a is not an average multiplicity as would be in the case of a usual Poisson distribution

b) The limit $a \rightarrow 0$ is also interesting since it leads to the multifractal logarithmic distribution

$$G^{ML}(z) = \frac{be^z}{1-g} \left(z - \frac{1}{1-g} \right) + e^{gz} \frac{b}{(1-g)^2}. \quad (4.24)$$

From (4.11) and (4.12) one gets

$$P_n^{ML} = P_1 \frac{b^{n-1}}{n!} \prod_{s=0}^{n-2} \sum_{l=0}^s g^l (s-l+1), \quad (4.25)$$

$$\eta_q^{ML} = \frac{q-1}{\sum_{l=0}^{q-2} g^l (q-l-2)} + g, \quad (4.26)$$

where $q > 2$ and P_1 is a normalization constant (for the logarithmic multiplicity distribution $P_0 = 0$). We see that these multiplicity distributions have the same power-law behavior of the high-order BPs for small δ . In this sense, the distributions are equivalent for small phase-space intervals.

It is important to emphasize here that an infinite sequence of probabilities P_n can be normalized if it converges, i.e if $P_n \rightarrow 0$ for $n \rightarrow \infty$. This is possible if, for every i greater than some number ζ , we have the following condition

$$\frac{P_i}{P_{i-1}} < 1 \quad (4.27)$$

(ratio test). For the MNBD (4.9) this is possible if

$$0 < g < 1, \quad 0 < \frac{b}{1-g} < 1. \quad (4.28)$$

For any other domain of g , we have to truncate the MNBD, putting $P_i^M = 0$ for $i > \zeta$.

One can understand, from the definition (4.2), that BPs are sensitive to the local multiplicity fluctuations (or to the behavior of the multiplicity distribution in small phase-space intervals) near the multiplicity $q = n - 1$. In order to study the total contribution from multiplicity fluctuations for large values of n , it is appropriate to introduce ‘‘bunching moments’’ b_q as follows

$$b_q \equiv G^{(q)}(z) \Big|_{z=1} = \sum_{s=q}^{\infty} \frac{s}{(s-q)!} \frac{P_s}{P_{s-1}}, \quad (4.29)$$

following an analogy with factorial moments. So, the knowledge of the generating function gives us a possibility to calculate both the BPs and the bunching moments. The higher the rank of the b_q , the more sensitive they are to the ‘‘tail’’ of the multiplicity distribution for large n . As normalized bunching moments B_q we define

$$B_q \equiv \frac{b_q}{b_1} = \frac{G^{(q)} \Big|_{z=1}}{G^{(1)} \Big|_{z=1}}. \quad (4.30)$$

Then, for the Poisson distribution (4.16), we have

$$B_q^P = 1, \quad q = 1 \dots \infty. \quad (4.31)$$

For the negative-binomial distribution (4.15), one obtains a very simple expression,

$$B_q^N = \frac{k+q}{k+1}, \quad q = 1 \dots \infty. \quad (4.32)$$

This means that the negative-binomial distribution is broader than the Poisson distribution ($B_q^N > B_q^P$). For the geometric multiplicity distribution ($k = 1$), the normalized bunching moments are larger than those of the negative-binomial distribution with $k > 1$. In this case, we can say that the geometric distribution is broader than the negative-binomial one. For the positive-binomial multiplicity distribution, where $k < 0$ and integer, the normalized bunching moments are smaller than unity, because this distribution is narrower than Poisson.

For MNBD (4.20) one obtains

$$B_q^M = \frac{k(g-1)(g^q e^{g-1} - 1) + g^q e^{g-1} - g(q+1) + q}{k(g-1)(g e^{g-1} - 1) + g e^{g-1} - 2g + 1}, \quad (4.33)$$

$q = 1 \dots \infty$. For a small g (or for a large phase-space interval), the MNBD slightly differs from the negative-binomial distribution. For $g \rightarrow 0$ ($B_q^M \rightarrow B_q^N$), the MNBD tends to the

negative-binomial distribution. The situation drastically changes when a large g (or the small δ) is considered. The B_q^M becomes larger than B_q^N , since the MNBD becomes *broader* than the negative-binomial distribution for all k . Bear in mind of this property; It is not surprising that for this region of phase space the MNBD reflects the increase of the local intermittent fluctuations and can lead to a multifractal behavior of the anomalous fractal dimension.

The generating function $Q = \sum_{n=0}^{\infty} z^n P_n$ commonly considered in probability theory and its applications can also be used in the multifractal generalization [9]. To analyze this generating function, it is appropriate to use usual NFMs or normalized cumulant moments. In fact, these two "languages", using the BPs and the NFMs for the study of multiplicity distributions in terms of the generating functions G and Q , are equivalent. Nevertheless, the analysis of multiplicity distributions at small δ with the help of BPs and the bunching moments is simpler, because an analytical form of the NFMs is too complicated for a number of multiplicity distributions. For example, to find a simple form of the generating function for multifractal distributions (4.12), (4.22), (4.25) is rather difficult. The technical advantage of the use of these quantities comes mainly from the fact that, as a rule, the structure of the ratio P_n/P_{n-1} is simpler than the form of the probabilities P_n themselves.

It is appropriate to make some remarks here on the relationship between the form of the recurrence relation (4.8) and the definition of the generating function (4.13). The particular form of recurrence relation (4.8) is chosen because of its simplicity. For example, the factor $(n-1)/n$ in the last term of (4.8) is used only because it is possible to rewrite this relation in the form of generating function (4.13). It is easy to check that other similar forms involving P_{n-1} and P_{n-2} in the recurrence relation can lead to qualitatively similar results, providing a singular form of BPs for all orders. However, in these cases, one needs to introduce other forms of generating function in order to obtain a differential equation for the MNBD with simple solutions.

4.4 Non-linear Markov process and MNBD

Now we shall show that the form of MNBD can be obtained from a stochastic Markov process with non-linear birth rate. Let $P_n(t)$ be the probability to have n particles at time t . Of course, such a choice of an evolution parameter is not unique. In principle, the evolution variable t can be connected, for example, with the squared mass of the branching parton in the parton shower. For simplicity, we shall assume that the process starts at time $t = 0$, with the initial condition $P_0(t = 0) = 1$, $P_n(t = 0) = 0$, $n > 0$. We shall consider a very general birth-death process with an infinitesimal birth rate w_n^+ and an infinitesimal death rate w_n^- of particles, treating these parameters as continuous functions of t . The corresponding Markov equation is [10]

$$P_n'(t) = w_{n-1}^+ P_{n-1}(t) + w_{n+1}^- P_{n+1}(t) - (w_n^+ + w_n^-) P_n(t). \quad (4.34)$$

For a stationary process, when time goes to infinity, the $P_n(t)$ are t -independent constants. Then, from (4.34) one has $\pi_n - \pi_{n+1} = 0$, $n = 1, 2, \dots$, $\pi_n = w_n^- P_n - w_{n-1}^+ P_{n-1}$. Since $\pi_0 = 0$ we have $\pi_n = 0$, $n \geq 1$ and, hence, a solution of (4.34) in the form of the recurrence relation

$$\frac{P_n}{P_{n-1}} = \frac{w_{n-1}^+}{w_n^-}. \quad (4.35)$$

The negative-binomial distribution can be considered as a stationary solution of (4.34) if we assume linear forms for w_n^+ and w_n^- as

$$w_n^+ = \gamma + \beta n, \quad w_n^- = \rho n, \quad (4.36)$$

where $a = \gamma/\rho$ and $b = \beta/\rho$ (γ, β, ρ are t -independent). If we admit that the parameter w_n^+ is a non-linear function of n , i.e.

$$w_n^+ = \sum_{l=0}^n g^l [\gamma + \beta(n-l)], \quad w_n^- = \rho n, \quad (4.37)$$

then the MNBD can be found as a stationary solution of the evolution equation (4.34). Here, the parameter g represents the strength of the influence of the non-linearity in the equation. For $\delta \rightarrow 0$ the non-linearity of the birth rate increases.

The multifractal structure of MNBD, therefore, can be caused by the non-linearity of a stationary Markov process. From the point of view of high-energy physics, the multiparticle production in QCD and the subsequent transition to hadrons have a strongly non-linear nature. In this sense, the form of (4.37) can reflect the non-linearity of the underlying multiparticle dynamics leading to multifractality.

4.5 Application to experimental data

Up to now, we have considered g as a free parameter with the power-law behavior $g \propto \delta^{-\beta}$. The next question is, how does one choose g if one wants to obtain a multiplicity distribution with a degree of multifractality r (see Sect. 4.2). The simplest way is to assume the following form

$$g = \omega(r) \left(\frac{b}{a} \right)^r = \omega(r) k^{-r}, \quad (4.38)$$

where $\omega(r)$ is some function which tends to zero for $r \rightarrow 0$ (in a simplest case, $\omega(r) = r$). The parameter r allows interpolation between the negative-binomial distribution with monofractal behavior ($r = 0$) and the MNBD with multifractal behavior ($r > 0$). Let us remind that the aggregation coefficient k^{-1} is related to the mean multiplicity $\langle n \rangle = a/(1-b)$ and the dispersion D of the negative-binomial distribution as $D^2 = \langle n \rangle + \langle n \rangle^2 k^{-1}$.

From the point of view of high-energy physics, our choice is justified by the following reasons:

i) If we have the negative-binomial distribution, then for a large (pseudo)rapidity interval k^{-1} has a small value ($k^{-1} \sim 0.1 - 0.01$). Applying a fit by (4.12), we can expect that g in the MNBD would be small also and this distribution would be similar to the negative-binomial distribution.

ii) It is essential that the negative-binomial distribution is approximately valid, not only for large phase-space intervals, but also for small ones. For the negative-binomial distribution, the behavior $k^{-1} \propto \delta^{-\beta}$ lies in the framework of the assumption that intermittency is governed only by the aggregation coefficient. In [4], Van Hove has shown that, if $k^{-1} \propto \delta^{-\beta}$ for small δ , then the negative-binomial distribution has monofractal behavior $F_q \propto \delta^{-d_q(n-1)}$, $d_q = \beta$. Then $\eta_2 \propto \delta^{-\beta}$, $\eta_s = \text{const.}$, $s > 2$ [3]. In our case, the assumption $w(r) \neq 0$ can yield intermittency with multifractal behavior of the anomalous fractal dimension. From

the experimental point of view, a good approximation for the aggregation coefficient of the negative-binomial distribution is [11]

$$k^{-1} = c M^{d_2}, \quad M = \frac{\Delta}{\delta}, \quad (4.39)$$

where Δ and δ are three-dimensional full and limited phase-space intervals, respectively, d_1 is the anomalous fractal dimension of second order. For different reactions, the parameters c and d_2 are of the same order of magnitude. For example, d_2 has an almost universal value of ~ 0.4 [11]. Expression (4.39) has been obtained from the relation $F_2^N = 1 + k^{-1}$ between the second-order NFM and the aggregation coefficient which is correct for the negative-binomial distribution.

iii) Since the fits for different reactions show a logarithmic increase of k^{-1} with increasing energy \sqrt{s} , one may expect that we shall obtain a similar effect for the MNBD as well. Then the distribution (4.12) in full phase space may differ significantly from the standard negative binomial distribution for large energies. This is very important because, as mentioned already in the introduction, the usual negative-binomial distribution fails to describe multiplicity distributions at 900GeV in $p\bar{p}$ collisions and in Z^0 hadronic decay for full phase space.

Let us obtain the anomalous fractal dimension for the MNBD in the particular case, when $g = \omega(r)k^{-r}$. The calculation of the NFMs can be simplified when the average multiplicity in δ is small. Then, the NFMs are given by expression (4.3). Let us discuss two domains of the parameter r :

(i) $0 \leq r \leq 1$. From (4.11) we have

$$\eta_2 = 1 + k^{-1} + w(r)k^{-r}, \quad (4.40)$$

$$\eta_s = \frac{1 + k^{-1}(s-1)}{\sum_{l=0}^{s-2} \omega^l(r)k^{-rl}(1 + k^{-1}(s-l-2))} + w(r)k^{-r}, \quad s > 2. \quad (4.41)$$

We see that, if $k \propto \delta^{d_2}$, the leading terms of the BPs have the following behavior: $\eta_2 \propto \delta^{-d_2}$, $\eta_s \propto \delta^{-rd_2}$, $s > 2$. Then

$$F_q \propto \delta^{-d_q(q-1)}, \quad d_q = d_2(1-r) + d_2r\frac{q}{2}. \quad (4.42)$$

For $r = 0$, we have the monofractal behavior $d_q = d_2$ and the MNBD reduces to the negative binomial distribution.

(ii) $r > 1$. The leading terms of the BPs are given by the expression $\eta_q \propto \delta^{-rd_2}$, $q \geq 2$. The corresponding anomalous fractal dimension is

$$d_q = d_2r\frac{q}{2}. \quad (4.43)$$

The values of r for different reactions have been discussed in [3].

4.6 Conclusion

We proposed a new multiplicity distribution with multifractal properties for small phase-space intervals basing on the simplicity of the analysis of multifractality in terms of BPs and bunching moments. Guided by the fact that, for the multifractality of normalized factorial moments the same power-law behavior for all orders of the BPs is necessary and sufficient, we have focused our attention on the analysis of the MNBD with multifractal behavior. The MNBD may be considered as a generalization of the negative-binomial distribution with a new free parameter g (or r for the particular case, when $g = \omega(r)k^{-r}$), which has a power-like behavior for small phase-space interval.

Theoretically, the question arises what is the physical reason of such a multifractal distribution. The problem of multifractality is very complicated and requires further examination both in high-energy physics and quantum optics. Note, as an example, that some versions of cascade models can lead to this distribution because they have the same anomalous fractal dimension (see the α -model [12], where the anomalous fractal dimension has the form (4.43) with $r = 1$).

On the experimental side of the question, we hope that the MNBD is interesting since it yields a new possibility to describe experimental data.

Bibliography

- [1] A. Białas and R.Peschanski, Nucl. Phys. B273 (1986) 703;
A. Białas, Nucl. Phys. A525 (1991) 345;
R.Peschanski, J. of Mod. Phys. A21 (1991) 3681;
E.A.De Wolf, I.M. Dremin and W.Kittel, Phys. Rep. 270 (1996) 1
- [2] M.R.Young, Y.Qu.Surendra Singh and R.Hwa, Opt. Comm. 105 (1994) 325
- [3] S.V. Chekanov and V.I.Kuvshinov, Acta Phys. Pol. B25 (1994) 1189 (see Chapter 3)
- [4] L.Van Hove, Phys. Lett. B232 (1989) 509
- [5] UA5 Coll., R.E.Ansorge et al., Z. Phys. C43 (1989) 357
- [6] DELPHI Coll., P.Abreu et al., Z. Phys. C52 (1991) 271
- [7] ALEPH Coll., D.Buskulic et al., Z. Phys. C69 (1995) 15
- [8] A.Giovannini and L.Van Hove, Acta Phys. Pol. B19 (1988) 495
- [9] S.V.Chekanov, Acta Phys. Pol. B25 (1994) 1583
- [10] A.T.Bharucha-Reid, "Elements of the Theory of Markov Processes and Their Applications", 1960, McGraw-Hill Book Company Inc. p.87
- [11] K.Fiałkowski, Z. Phys. C61 (1994) 313
- [12] A.Białas and R.Peschanski, Nucl. Phys. B308 (1988) 857

Generalized Bunching Parameters and Local Fluctuations

S.V.Chekanov¹, W.Kittel

*High Energy Physics Institute Nijmegen (HEFIN), University of Nijmegen/NIKHEF,
NL-6525 ED Nijmegen, The Netherlands*

V.I.Kuvshinov

Institute of Physics, AS of Belarus, Skaryna Av.70, Minsk 220072, Belarus

Published in Z. Phys. C74 (1997) 517-529

Abstract

Experimental aspects of the use of bunching parameters are discussed. Special attention is paid to the behavior expected for the case of purely statistical fluctuations. We studied bin-averaged bunching parameters and propose a generalization of bunching parameters, making use of the interparticle distance-measure technique. The proposed method opens up the possibility of carrying out a comprehensive and sensitive investigation of multiplicity fluctuations inside jets.

¹On leave from Institute of Physics, AS of Belarus, Skaryna Av.70, Minsk 220072, Belarus

5.1 Introduction

In recent years, multiparticle density fluctuations have been studied in ever smaller phase space intervals δ in terms of normalized factorial moments (NFMs) $F_q(\delta)$ [1]. The NFM can be defined as

$$F_q(\delta) = \frac{\sum_{n=q}^{\infty} n^{[q]} P_n(\delta)}{(\sum_{n=1}^{\infty} n P_n(\delta))^q}, \quad n^{[q]} = n(n-1)\dots(n-q+1), \quad (5.1)$$

where n is the (charged) particle multiplicity and $P_n(\delta)$ is the multiplicity distribution in δ . The interval δ can be any interval in phase space, such as in rapidity, azimuthal angle, transverse momentum, or a (multi-dimensional) combination of these variables. This method has recently been improved by the use of density and correlation integrals [2] to avoid the problems of bin splitting and the insufficient use of experimental statistics inherent to definition (5.1).

From an experimental point of view, the most important properties of the NFMs are:

- 1) they filter out Poissonian statistical noise;
- 2) events can contribute to (5.1) only if $n \geq q$, so they resolve the high-multiplicity tail of $P_n(\delta)$;
- 3) if local self-similar dynamical multiplicity fluctuations exist, then $F_q(\delta) \propto \delta^{-\phi_q}$, $\phi_q > 0$. Such a power-law behavior is called intermittency and the ϕ_q are called intermittency indices. They are related to the anomalous dimensions of the corresponding fractal system by the simple relation $d_q = \phi_q/(q-1)$.

Additional advantages of density integrals are that they avoid the problem of bin splitting inherent to the definition of NFMs above, and that they allow the use of general distance measures. Correlation integrals, furthermore, are based on genuine q -particle correlations which avoid trivial contributions from lower-order densities. For reviews see [3] and references therein.

Recently, another simple mathematical tool has been proposed to investigate multiparticle fluctuations. In order to reveal intermittent structure of multiparticle production, it is, in fact, sufficient to study the behavior of the probability distribution near multiplicity $n = q - 1$ by means of the so-called bunching parameters (BPs) [4, 5]

$$\eta_q(\delta) = \frac{q}{q-1} \frac{P_q(\delta)P_{q-2}(\delta)}{P_{q-1}^2(\delta)}. \quad (5.2)$$

These quantities are formally identical to those used in quantum optics [6]. The bunching parameter method has also been extended to measure bin-bin correlations [7].

In the mathematical limit $\delta \rightarrow 0$, the relation between NFMs and the BPs is

$$F_q(\delta) \simeq \prod_{i=2}^q \eta_i^{q-i+1}(\delta). \quad (5.3)$$

In this limit, therefore, the BPs share with the NFMs the important property of suppression of Poissonian statistical noise.

In fact, for an event sample following a Poissonian multiplicity distribution, one finds $\eta_q(\delta) = 1$ for all q and δ . If all BPs are larger than 1, the corresponding multiplicity

distribution is broader than the Poisson distribution. On the other hand, a multiplicity distribution is narrower than Poisson if all its BPs are smaller than 1.

For a sample of events with a fixed finite number of particles N in full phase space, independent emission of these particles leads to a (positive) binomial distribution in the interval δ . Consequently, the BPs have the values $\eta_q^{\text{PBD}} = (q-1-N)/(q-2-N)$, i.e., are again independent of δ .

As shown in [4], there exists, in fact, a large class of multiplicity distributions for which the BPs are independent of δ for the full range of δ values. This result is the first important point investigated in detail in this paper.

The relevance of the bunching parameters for multiparticle production in high-energy collisions, however, lies in the following properties:

1) From (5.3) we can see that the second-order BP follows $\eta_2(\delta) \sim \delta^{-\phi_2}$ for intermittent fluctuations in the limit $\delta \rightarrow 0$ (bunching effect of the second order), while the higher-order BPs may have any type of dependence on δ [4].

2) In the case of monofractal behavior, the anomalous dimension d_q is independent of q . Variation of d_q with increasing q corresponds to a multifractal behavior. In contrast to the NFMs, only $\eta_2(\delta)$ increases with decreasing δ for monofractal behavior, while the $\eta_q(\delta)$ are constants for all $q > 2$ [4]. Any δ dependence of higher-order BPs, therefore, reveals a deviation from monofractal behavior of the multiplicity fluctuation.

3) The lower-order BPs are more sensitive than the NFMs to spikes with a small number of particles. Only spikes with $n \leq q$ particles can contribute to the bunching parameter of order q . Hence, the BPs act as a filter, but, in comparison to the NFMs, with a complementary property (see property 2 of NFMs above).

This feature of BPs is important for the study of high-multiplicity events, where unusually large dips in the density distribution of individual events can be treated as a dynamical effect as well as that of the appearance of spikes. In this case, the lowest-order BPs will be sensitive to such dips. On the other hand, for lower-multiplicity reactions, such as e^+e^- -annihilation, the use of BPs can provide high-precision measurements of local fluctuations, since they suffer less from the bias arising due to a finite number of experimental events than do the NFMs (see property 6 below).

4) The BPs have a more direct link than the NFMs to the multiplicity distribution itself [4]. Any multiplicity distribution can be expressed in terms of the BPs as

$$P_n(\delta) = P_0(\delta) \frac{\lambda^n(\delta)}{n!} \prod_{i=2}^n \eta_i^{n-i+1}(\delta), \quad \lambda(\delta) = \frac{P_1(\delta)}{P_0(\delta)}. \quad (5.4)$$

5) From the theoretical point of view, the BPs are useful when direct calculation of the NFMs from a model or theory becomes too tedious. Factorial moments are easily calculated from the generating function of the multiplicity distribution. A large class of distributions exists, however, without any simple analytical form of the generating function.

6) Moreover, from the experimental point of view, we expect that the BPs are less severely affected by the bias from finite statistics than are the NFMs: In practice, the multiplicity distribution $P_n(\delta)$ is always truncated at large n due to finite statistics in a given experiment. As a consequence, the values of high-order NFMs at small bin size are determined by the first

few terms in expression (5.1) only, which leads in most cases to a significant underestimation of the measured NFMs with respect to their true values [8–10]. Furthermore, the calculation of a given-order BP is simpler, since one is analyzing events for three given multiplicities only, without the requirement of normalization by an average multiplicity.

7) Another experimental advantage of the bunching-parameter measurements is that, for the calculation of the BP of order q , one needs to know only the q -particle resolution of the detector. In contrast, the precise calculation of the NFMs of order q always involves the knowledge of the resolution of $n \geq q$ particles. So, for a given q -track resolution, the behavior of the q th-order NFM may contain a systematic bias due to contributions from the tail of the multiplicity distribution measured with insufficient resolution.

The study of multiparticle production processes with the help of BPs, therefore, is expected to provide important information on multiplicity fluctuations in ever smaller phase-space intervals, in addition to and complementary to that extracted with NFMs.

In Sect. 5.2, we discuss the problem of Poissonian noise and the behavior of BPs for a number of theoretical models. In Sect. 5.3, we give experimental definitions of the BP and suggest an extension of the bunching-parameter method to avoid the problem of bin splitting and to allow a more general choice of distance measure, in analogy to the extension of NFMs to the density integrals mentioned above. The crucial question of the behavior of BPs and their extensions in the case of purely statistical phase-space fluctuations is shown in Sect. 5.4. In Sect. 5.5, we give, as an example, a comparison of the factorial-moment and bunching-parameter analysis of two different intermittent samples generated by the JETSET 7.4 model.

5.2 Poissonian noise suppression and other properties

5.2.1 The problem of Poissonian noise

As we noted in the introduction, the NFMs have an important feature for the theoretical study of local fluctuations: they are not contaminated by Poissonian statistical noise. First, let us show that the BPs reduce the statistical noise in the limit $\delta \rightarrow 0$, as well, meaning that BPs are not only a convenient experimental tool that can reduce the bias from finite statistics ($N_{\text{ev}} \neq \infty$), but also can suppress statistical noise arising due to the finite number of particles per event ($N \neq \infty$). The last point is of vital importance for the study of theoretical models with an infinite number of particles in an event.

Let us first define a particle density ρ in bin m for an individual event as

$$\rho = \frac{n}{\delta}, \quad (5.5)$$

where n is the number of particles in bin m of size δ . For a local-fluctuation analysis, we need to consider very small bin sizes, i.e., $\delta \rightarrow 0$. ρ , therefore, is an asymptotic density, since it can be defined in the limit of infinite multiplicity N (or n) for a given event.

Using another (theoretical) limit, $N_{\text{ev}} \rightarrow \infty$, we can define $\omega(\rho)$ as a continuous probability density to observe a given value of ρ . This density fulfills the normalization condition

$$\int_0^\infty \omega(\rho) d\rho = 1. \quad (5.6)$$

Of course, the density ρ for bin size δ fluctuates around the average value

$$\langle \rho \rangle \equiv f_1 = \int_0^\infty \rho \omega(\rho) d\rho. \quad (5.7)$$

Because we are interested in the deviation of ρ from the average value f_1 , the next step is to define the higher-order moments of $w(\rho)$ as follows

$$\langle \rho^q \rangle \equiv f_q = \int_0^\infty \rho^q \omega(\rho) d\rho. \quad (5.8)$$

In experimental studies, the multiplicity N is finite. In this case, the number of particles n in bin m fluctuates around the average value due to “statistical noise”. If we accept this assumption, and the additional assumption that such a statistical noise does not introduce new fluctuations, the observed (discrete) multiplicity distribution $P_n(\delta)$ to observe n particles in δ can be described by the following Poisson transformation [1]

$$P_n(\delta) = \int_0^\infty \omega(\rho) \frac{(\rho\delta)^n \exp(-\rho\delta)}{n!} d\rho. \quad (5.9)$$

Expression (5.9) represents a convolution of the statistical Poissonian noise of mean $\rho\delta$ with a true, dynamical distribution $\omega(\rho)$.

The next problem, therefore, is how to compare model fluctuations described by $\omega(\rho)$ with the experimental fluctuations defined by $P_n(\delta)$. Substituting (5.9) in the definition of factorial moments gives

$$\langle n^{[q]} \rangle \equiv \sum_{n=q}^\infty n^{[q]} P_n(\delta) = \delta^q f_q, \quad q = 1, 2, 3, \dots, \quad (5.10)$$

where f_q are ordinary moments defined by (5.7) and (5.8). Hence, for NFMs (5.1) one obtains

$$F_q(\delta) = \frac{f_q}{f_1^q}. \quad (5.11)$$

The right side of this expression represents the normalized moments given by a model distribution $\omega(\rho)$. Studying this distribution in experiments with finite N , therefore, is equivalent to measuring the NFMs $F_q(\delta)$.

Let us note that in the limit of small phase-space size, we can only keep the leading term in expression (5.9), i.e., $P_n(\delta)$ can be rewritten as

$$P_n(\delta) \simeq \frac{\delta^n}{n!} \int_0^\infty \omega(\rho) \rho^n d\rho, \quad (5.12)$$

if fluctuations in a model are investigated in the limit $\delta \rightarrow 0$. Substituting this expression in (5.2) gives

$$\eta_q(\delta) \simeq \frac{f_q f_{q-2}}{f_{q-1}^2}, \quad (5.13)$$

where $f_0 = 1$ according to (5.6) and (2.13). Therefore, $\eta_q(\delta)$ calculated from experiment gives information on the fluctuations described by the theoretical probability density $w(\rho)$, since Poissonian contributions cancel at small δ . From (5.13) and (5.11) one can obtain relation (5.3) given in the introduction.

The idea to express intermittency directly in terms of the probabilities has also been proposed by Van Hove [11]. Indeed, in the limit $\delta \rightarrow 0$, one can use the ratio $P_q(\delta)/P_1^q(\delta)$ instead of $F_q(\delta)$, since

$$\frac{P_q(\delta)}{P_1^q(\delta)} \propto \frac{f_q}{f_1^q} = F_q(\delta), \quad (5.14)$$

according to (5.12).

5.2.2 Multifractal and monofractal behavior

For a model with intermittent behavior, we can expect

$$\frac{f_q}{f_1^q} \propto \delta^{-\phi_q}. \quad (5.15)$$

Using this relation and (5.13), one obtains

$$\eta_q(\delta) \propto \delta^{2\phi_{q-1} - \phi_q - \phi_{q-2}}, \quad \delta \rightarrow 0, \quad (5.16)$$

where $\phi_0 = \phi_1 = 0$.

As a reminder, one should expect $\phi_q = d_2(q-1)$ for monofractality. For these types of fluctuations, the BPs have the following behavior

$$\eta_2(\delta) \propto \delta^{-d_2}, \quad \eta_{q>2}(\delta) \simeq \text{const.} \quad (5.17)$$

For monofractal behavior, therefore, what one obtains is that all high-order BPs $\eta_{q>2}(\delta)$ are δ -independent constants. This result is one of the important advantages of the bunching parameter method over factorial moments: to reveal multifractal behavior in an experimental sample, it is not necessary to interpolate an experimental slope by the power-law $F_q(\delta) \propto \delta^{-d_q(q-1)}$ in order to derive a q -dependence of d_q .

5.2.3 Examples

For illustrative purposes, we now consider examples of the behavior of BPs for various dynamical models:

5.2.3.1 Random-cascade model

This is the first model [1] used in high-energy fluctuation phenomenology. For this model the intermittency indices have the following form

$$\phi_q = \frac{1}{2}q(q-1)d_2. \quad (5.18)$$

From (5.16), one can see that all BPs follow the same power law

$$\eta_q(\delta) \propto \delta^{-d_2}, \quad \text{for all } q \geq 2. \quad (5.19)$$

This feature in the behavior of the cascade model can be revealed by calculating the BPs and by comparing their power-law behavior, without the necessity of any fit of NFMs by power-law.

5.2.3.2 Second-order phase transition

One expects [12] that for a system undergoing a second-order phase transition the corresponding intermittency indices would depend linearly on the rank of the moment,

$$\phi_q = d_2(q-1). \quad (5.20)$$

Such a behavior has been derived from a toy Ising model [13]. In this case, according to (5.17), all higher-order BPs are δ -independent constants.

5.2.3.3 Perturbative QCD cascade

In a QCD cascade with fixed coupling constant α_s , the intermittency indices have the following multifractal behavior [14]

$$\phi_q = D(q-1) - \gamma_0 r_q, \quad r_q = (q-1)(q+1)q^{-1}, \quad (5.21)$$

where D is the topological dimension of the phase space under consideration and $\gamma_0 = (6\alpha_s/\pi)^{1/2}$ is the QCD anomalous dimension. From (5.16), one can conclude that the behavior of all high-order BPs is D -independent for a fixed-coupling regime of QCD and is governed only by γ_0

$$\eta_q(\delta) \propto \delta^{\gamma_0 h_q}, \quad h_q = r_q + r_{q-2} - 2r_{q-1}, \quad q \geq 3, \quad (5.22)$$

where $r_1 = 0$. As a first rough test of the QCD prediction, therefore, a measurement of the third-order BP for different dimensions D can provide a qualitative answer to the applicability of this type of QCD calculations to real data. Note that this can be done very precisely, since statistical (and systematical) errors are small for a third-order BP.

5.3 Experimental definitions of BPs

5.3.1 Bin-averaged BPs

In order to increase the statistics and to reduce the statistical error of observed BPs when analyzing experimental data, we can use bin-averaged BPs as defined in analogy to the bin-averaged factorial moments:

1) *Flat phase-space distribution*: The following definition of horizontally normalized bin-averaged BPs can be used [4]:

$$\eta_q^{\text{hor}}(\delta) = \frac{q}{q-1} \frac{\bar{N}_q(\delta)\bar{N}_{q-2}(\delta)}{\bar{N}_{q-1}^2(\delta)}, \quad (5.23)$$

where

$$\bar{N}_q(\delta) = \frac{1}{M} \sum_{m=1}^M N_q(m, \delta). \quad (5.24)$$

Here, $N_q(m, \delta)$ is the number of events having q particles in bin m , $M = \Delta/\delta$ is the total number of bins, and Δ represents the full phase-space volume.

2) *Non-flat phase-space distribution*: In this case we need to use vertically normalized BPs defined as

$$\eta_q^{\text{ver}}(\delta) = M^{-1} \frac{q}{q-1} \sum_{m=1}^M \frac{N_q(m, \delta) N_{q-2}(m, \delta)}{N_{q-1}^2(m, \delta)}. \quad (5.23)$$

It should be pointed out that, in this case, the sum runs over non-zero bins only. This type of BPs, therefore, demands more statistics and may be unstable for small phase-space bins. In contrast, events with no particles in a bin can contribute to the horizontally normalized BP. For this reason, it may be more convenient to use the BPs (5.23) for non-flat distributions as well. To be able to do this, one must carry out a transformation from the original phase-space variable to one in which the underlying distribution is approximately uniform [15].

5.3.2 Generalized distance measure

5.3.2.1 Definitions of spike size

The main deficiency of definitions (5.23) and (5.25) (and the bin-averaged NFM) lies in the artificial splitting of particle spikes. Spikes do not contribute to the $N_q(m, \delta)$ if the boundaries of bins happen to split such spikes. This deficiency can be avoided by the choice of a proper distance $X_{i,j}$ between two particles, which as demonstrated in [16], would have the additional advantage of largely increasing the statistics effectively used in a given experiment, at a given resolution.

For a given event, let us define a g -particle spike of size ϵ as a group of g particles having mutual phase-space distance $X_{i,j}$ smaller than ϵ . According to this definition, the condition for particles to belong to a spike is

$$\prod_{i=1}^g \prod_{j=1}^g \theta(\epsilon - X_{i,j}) = 1, \quad i \neq j, \quad (5.24)$$

where θ is the Heaviside unit step function. To determine the spike size ϵ for a given event we have used here the so-called Grassberger-Hentschel-Procaccia (GHP) counting topology [17] for which a g -particle hyper-tube is assigned a size ϵ that corresponds to the maximum of all pairwise distances.

Alternative topologies are the so-called “snake” topology [2]

$$\prod_{i=2}^g \theta(\epsilon - X_{i-1,i}) = 1, \quad (5.25)$$

which corresponds to the longest distance between two particles connected by one joining line, and the “star” topology [16] defined as

$$\prod_{i=2}^g \theta(\epsilon - X_{1,i}) = 1. \quad (5.26)$$

The star topology involves all particles that are paired with a preselected center particle (index 1). It shares all the advantages of the GHP and snake forms, and is computationally more efficient.

5.3.2.2 Bunching parameters

After establishing the definitions of spike size ϵ , we can investigate the behavior of multiplicity fluctuations in ever smaller ϵ by means of the bunching-parameter method.

Differential BPs:

In any multiparticle process, the number of g -particle spikes fluctuates around an average value according to a certain probability distribution. Let $P_n(\epsilon, g)$ be the probability distribution of observing in an event a number n of g -particle spikes of size ϵ , irrespective of the presence of other spikes. This distribution can be characterized by the generating function $G(\epsilon, g)$ defined as

$$G(z, \epsilon, g) = \sum_{n=0}^{\infty} P_n(\epsilon, g) z^n. \quad (5.29)$$

For a purely independent production of spikes, the multiplicity distribution $P_n(\epsilon, g)$ follows a Poissonian law,

$$P_n^P(\epsilon, g) = (n!)^{-1} \bar{K}^n(\epsilon, g) e^{-\bar{K}(\epsilon, g)}, \quad (5.30)$$

with a generating function of the form

$$G^P(z, \epsilon, g) = e^{\bar{K}(\epsilon, g)(z-1)}, \quad (5.31)$$

where $\bar{K}(\epsilon, g)$ represents the average number of g -particle spikes of size ϵ in an event in the sample under study.

To measure the distribution $P_n(\epsilon, g)$ without the contribution from events with a large number of such spikes (or “tail” of the real distribution), one can calculate the following “differential” type of BPs

$$\chi_q(\epsilon, g) = \frac{q}{q-1} \frac{\Pi_q(\epsilon, g) \Pi_{q-2}(\epsilon, g)}{\Pi_{q-1}^2(\epsilon, g)}, \quad q = 2, 3, \dots, \quad (5.32)$$

where $\Pi_q(\epsilon, g)$ represents the number of events with a number q of g -particle spikes of size ϵ . For purely independent emission of spikes, $P_n(\epsilon, g)$ follows the Poissonian distribution (5.30) and all BPs (5.32) are equal to unity for all q and ϵ .

Integral BPs:

Of course, when analyzing experimental data, it is difficult to obtain all values of $\chi_q(\epsilon, g)$ as a function of ϵ . This is due to the large number ($= qg$) of possible configurations involved and the finite number of events available. We can, however, use a less informative and less differential definition suitable for an experiment with rather small statistics.

To understand these kinds of measurements, let us first define the probability distribution $P_n(\epsilon)$ to observe in an event a number n of multiparticle spikes, irrespective of how many particles are inside each spike. From a theoretical point of view, if all g -particle spikes are produced independently of each other, the generating function $G(z, \epsilon)$ for $P_n(\epsilon)$ has the form of a convolution of spike distributions with different particle content, i.e.,

$$G(z, \epsilon) = \prod_{g=2}^{\infty} G(z, \epsilon, g). \quad (5.33)$$

For purely independent spike production, one has from (5.31) and (5.33), again a Poissonian distribution, with the generating function

$$G(z, \epsilon) = G^P(z, \epsilon) = e^{\bar{K}(\epsilon)(z-1)} \quad (5.3)$$

and with the average number of multiparticle spikes

$$\bar{K}(\epsilon) = \sum_{g=2}^{\infty} \bar{K}(\epsilon, g). \quad (5.3)$$

As mentioned before, to measure a deviation from the Poissonian distribution, one can calculate the “integral” type of BPs

$$\chi_q(\epsilon) = \frac{q}{q-1} \frac{\Pi_q(\epsilon)\Pi_{q-2}(\epsilon)}{\Pi_{q-1}^2(\epsilon)}, \quad q = 2, 3, \dots, \quad (5.3)$$

where $\Pi_q(\epsilon)$ represents the number of events with q spikes of size ϵ , irrespective of how many particles are inside each spike. If $\chi_q(\epsilon) \neq 1$, then the conclusion of non-Poissonian spike production follows and a more sophisticated analysis can be performed with the help of the differential kind of BPs.

According to the definition above, all spikes with $g \geq 2$ particles contribute to $\chi_q(\epsilon)$. However, one can propose a more selective study of the spike fluctuations. Indeed, in the case of purely random (Poisson) fluctuations, the probability distributions to observe n spikes with $g \geq s$ or with $g \leq s$ particles (s is some integer number) also follow the Poissonian law due to the “reproductive” property of the Poisson distribution. In terms of generating functions, these two distributions can be expressed as

$$G(z, \epsilon, g \geq s) = \prod_{g=s}^{\infty} G(z, \epsilon, g) = \exp \left[\sum_{g=s}^{\infty} \bar{K}(\epsilon, g)(z-1) \right] \quad (5.3)$$

and

$$G(z, \epsilon, g \leq s) = \prod_{g=2}^s G(z, \epsilon, g) = \exp \left[\sum_{g=2}^s \bar{K}(\epsilon, g)(z-1) \right]. \quad (5.3)$$

To measure a deviation from these distributions, instead of $\Pi_i(\epsilon)$, one must use in (5.3) the number of events $\Pi_i(\epsilon, g \geq s)$ and $\Pi_i(\epsilon, g \leq s)$ having i spikes with $g \geq s$ and $g \leq s$ particles, respectively. The definition with $\Pi_i(\epsilon, g \leq s)$ is more preferable for high-precision measurements, because this quantity does not contain the contributions from spikes with high-multiplicity content.

Discussion:

The main reason for introducing the integral BPs (5.36) is that the $\chi_q(\epsilon)$ are more useful when the statistics of an experiment are small. In this case, the lower-order BPs (5.3) have large statistical errors¹, whereas higher-order BPs even vanish. In contrast, the BPs (5.36) have smaller statistical errors and high-order BPs can be still calculable. Moreover, the simplicity of this definition makes the latter very economical to calculate.

¹According to the Gauss law, the statistical error on the number of events Π is $\sqrt{\Pi}$ for large Π .

The actual choice of the definition of the BPs and of the value of ϵ strongly depends on the aims of the specific investigation. For example, at *large* ϵ the BPs are sensitive to the large scale of an event structure, where any jet behaves as a cluster (a spike of dynamical origin). The calculation of the BPs according to (5.36), therefore, corresponds to a study of a fluctuation in the number of jets, where each jet is considered, regardless of its inner structure. For an intermittent fluctuation, we expect that all second-order BPs are a power-like function of ϵ for $\epsilon \rightarrow 0$, whereas high-order ones can have any dependence on ϵ .

All these kinds of definitions have an important advantage over the conventional definition (5.23) or (5.25): we now can study the structure of spike fluctuations. In addition, we can investigate a given sample in a variety of new variables. For example, the squared four-momentum difference between any two particles $Q_{12}^2 = -(p_1 - p_2)^2$ is theoretically preferred for investigations of Bose-Einstein or effective mass correlations.

The question remains why we use the definitions of the generalized BPs in terms of the spike multiplicity distributions $P_n(\epsilon, g)$ and $P_n(\epsilon)$. Indeed, at first sight, it may seem more straightforward to use a conventional probability $\tilde{P}_n(\epsilon)$ of having n particles inside a hyper-tube of size ϵ . This probability can be found as

$$\tilde{P}_n(\epsilon) = \frac{K_n(\epsilon)}{\sum_{n=1}^{\infty} K_n(\epsilon)}, \quad (5.39)$$

where $K_n(\epsilon)$ is the number of n -particle spikes (hyper-tubes) of size ϵ found in $N_{\text{ev}} \rightarrow \infty$ experimental events. Clearly, $\tilde{P}_0(\epsilon)$ does not exist. Hence, the BPs

$$\eta_q(\epsilon) = \frac{q}{q-1} \frac{K_q(\epsilon)K_{q-2}(\epsilon)}{K_{q-1}^2(\epsilon)} \quad (5.40)$$

exist only for $q = 3, 4, \dots$, but not for $q = 2$. It is important to note, however, that $\tilde{P}_n(\epsilon)$ is not Poissonian even if particles are distributed independently (see Fig. 5.4 and the comments in Sect. 5.4.2)². In addition, we will show that $\eta_q(\epsilon)$ suffers from insufficient statistics. Of course, if we keep both these problems in mind, the $\eta_q(\epsilon)$ can be used for experimental study as well.

Note that for the generalized BPs (5.32) and (5.36) we use the letter χ_q in order to emphasize that these definitions are intended for measuring the bunching of spikes, rather than that of particles. From this point of view, no simple connection exists between $\eta_q(\delta)$ (or $\eta_q(\epsilon)$) and $\chi_q(\epsilon)$. The same is true for the conventional and the generalized NFMs [16]. Furthermore, the relation between the NFMs and the BPs $\chi_q(\epsilon)$ ceases to have a simple form. As a result, it is no longer possible to draw a conclusion on the ϵ -dependence of the $\chi_q(\epsilon)$ from the study of the generalized NFMs. The question of the relation between the generalized BPs and the generalized NFMs will be the subject of a future paper. Below, we will, however, demonstrate that, as is the case for the NFMs, a rise of the value of $\chi_q(\epsilon)$ with decreasing ϵ is inherent in realistic systems exhibiting intermittency.

Unfortunately, the problem of purely random (or statistical) fluctuations cannot always be reduced to the study of Poissonian distributions. Below, we will consider a general case of statistical phase-space fluctuations for which the property $\chi_q(\epsilon, g) = 1$, $\chi_q(\epsilon) = 1$ is only a particular case, corresponding to a full-phase-space Poissonian multiplicity distribution.

²Such a non-Poissonian form of $\tilde{P}_n(\epsilon)$ has also been realized in [16], where a complex event-mixing technique has been introduced to normalize generalized factorial moments.

5.3.2.3 Propagation of the statistical error for generalized BPs

As is the case for the extension of the usual NFMs to the density integrals, the estimation of the statistical error is simplified for generalized, as compared to, bin-averaged BPs. The calculation of the statistical error (i.e. the standard deviation) for the BPs (5.23) and (5.25) includes bin-bin correlation coefficients (all M bins are dynamically correlated) not present in the other definitions.

In the following, we derive an exact expression for the standard deviation of the generalized BPs using a distance measure ϵ . For simplicity, we shall use the symbolic expression

$$\chi_q = \frac{q}{q-1} \frac{\Pi_q \Pi_{q-2}}{\Pi_{q-1}^2}, \quad (5.41)$$

where Π_q stands for any definition of the number of events having a given *spike configuration* q as used in (5.32) and (5.36).

Let $W_q(t)$ be an indicator for the presence of a given spike configuration (index q) in an experimental event (integer argument t), i.e., for a given measurement t we set

$$W_q(t) = \begin{cases} 1, & \text{if spike configuration } q \text{ is occurring,} \\ 0, & \text{otherwise.} \end{cases} \quad (5.42)$$

After N_{ev} measurements, we get the sample mean of $W_q(t)$

$$\overline{W}_q = \frac{\sum_{t=1}^{N_{\text{ev}}} W_q(t)}{N_{\text{ev}}} = \frac{\Pi_q}{N_{\text{ev}}}. \quad (5.43)$$

It can be seen that the definition of generalized BPs (5.41) already represents an average value³ of BPs after N_{ev} measurements with the sample mean \overline{W}_q , since N_{ev}^2 cancels in definition (5.41). Let us note that all our BPs exist only as an average quantity, since we do not use any definition for BPs with $W_q(t)$ for a single experimental event.

The elements of the covariance matrix for an unbiased estimator are given by the standard expression

$$V_{q,q'} = \frac{1}{N_{\text{ev}}(N_{\text{ev}} - 1)} \left[\sum_{t=1}^{N_{\text{ev}}} W_q(t)W_{q'}(t) - N_{\text{ev}}\overline{W}_q\overline{W}_{q'} \right]. \quad (5.44)$$

For $q = q'$, the covariance matrix reduces to the unbiased sample variance s_q^2

$$V_{q,q} = s_q^2. \quad (5.45)$$

Given the covariance matrix, we can obtain the sample variance S_q^2 for the generalized BPs using a general rule for combining correlated errors [18],

$$S_q^2 = \left(\frac{q}{q-1} \right)^2 \left[\frac{\overline{W}_{q-2}^2}{\overline{W}_{q-1}^4} s_q^2 + \frac{4\overline{W}_q^2 \overline{W}_{q-2}^2}{\overline{W}_{q-1}^6} s_{q-1}^2 + \frac{\overline{W}_q^2}{\overline{W}_{q-1}^4} s_{q-2}^2 + \varrho_q \right], \quad (5.46)$$

³Here we applied the fundamental statistical assumption that, to a first approximation, $\overline{V} = V(\overline{x})$, where $V(x)$ is a function of the directly measured quantity x .

where ϱ_q is a function of non-diagonal elements of the covariance matrix describing the correlations between the W_q ,

$$\varrho_q = 2 V_{q,q-2} \frac{\overline{W}_q \overline{W}_{q-2}}{\overline{W}_{q-1}^4} - 4 V_{q,q-1} \frac{\overline{W}_q \overline{W}_{q-2}^2}{\overline{W}_{q-1}^5} - 4 V_{q-1,q-2} \frac{\overline{W}_q^2 \overline{W}_{q-2}}{\overline{W}_{q-1}^5}. \quad (5.47)$$

The standard deviation is the square root of the variance (5.46). Let us note that for the calculation of the standard deviation we did not use any assumption on a Gaussian distribution of W_q . In fact, a Gaussian distribution is, in general, not applicable for the calculation of statistical errors for small ϵ . The errors plotted in the forthcoming figures are the errors calculated according to (5.46).

5.4 Statistical fluctuations and BPs

As was shown in Sect. 5.2, BPs are not affected by Poissonian noise in the limit $\delta \rightarrow 0$. However, in order to use the BPs to extract information on dynamical fluctuations, one has to know their behavior in the case of purely random phase-space fluctuations for realistic values of δ .

The random fluctuations cannot always be described in terms of a Poissonian distribution, since in multiparticle experiments, the full-phase-space multiplicity distribution is often far from Poissonian. In addition, there is always a constraint on the maximum value of multiplicity because of energy conservation. This constraint can lead to non-Poissonian fluctuations in small phase-space intervals, even if the particles are produced in phase space randomly, without any dynamical correlations.

To study statistical fluctuations, therefore, we consider a *general* case of independent particle emission, when spikes appearing in phase space are caused by random properties of an experimental sample.

5.4.1 The bin-averaged BPs

5.4.1.1 Flat phase-space distribution

In order to understand the behavior of BPs (5.23) and (5.25) in the case of purely statistical fluctuations, we start with a phase-space distribution which is flat and equally wide for all multiplicities N . In this case, the number $N_q(m, \delta)$ of events having q particles in bin m does not depend on the position of the bin, i.e., $N_q(m, \delta) = N_q(\delta)$. Expressions (5.23) and (5.25), therefore, are reduced to (5.2).

An event sample with *purely statistical fluctuations in restricted phase space* can be described by the following expression [19–21] :

$$P_n^{\text{stat}}(\delta) = \sum_{N=n}^{\infty} P_N C_N^n p^n (1-p)^{N-n}, \quad p = \frac{\delta}{\Delta}, \quad (5.48)$$

where P_N is the multiplicity distribution for full phase space, the C_N^n are the binomial coefficients and p is the probability that a particle falls within a given interval δ . Expression (5.48) states that for each data subsample of events with fixed finite multiplicity N , particles fall into δ independently, i.e., according to a (positive) binomial distribution [22].

When we speak of purely statistical phase-space fluctuations in the case of a finite number of particles in a single event, we imply independent emission of the particles into a small phase-space interval, i.e., without any interaction between particles yielding dynamical spikes or clusters. Of course, for a single event, even independent emission can produce spikes, but only of statistical nature. In such a case, a multiplicity distribution obtained after $N_{ev} \rightarrow \infty$ experimental measurements can be expressed in the form of (5.48).

Let us note that the statistical fluctuations described by (5.48) have nothing to do with statistical noise described by Poisson transformation (5.9). The notion of statistical noise is necessary to take into account the finiteness of the number of particles in the counting bin (and, hence, in full phase space). We can get an ‘‘observed’’ discrete multiplicity distribution from a ‘‘true’’ continuous dynamical probability density using the so-called linear transformation (5.9) of the density with a Poisson kernel.

Let

$$G(z, \delta) = \sum_{n=0}^{\infty} P_n(\delta) z^n \quad (5.49)$$

be the generating function for the multiplicity distribution $P_n(\delta)$ of having n particles in a small phase-space interval $\delta \leq \Delta$. Then, if we multiply (5.48) by z^n and sum the result over n , we can find the generating function for $P_n(\delta)$ as follows:

$$G^{\text{stat}}(z, \delta) = \sum_{N=0}^{\infty} P_N(pz - p + 1)^N. \quad (5.50)$$

Using the relation between factorial moments and generating function

$$\langle n^{[q]} \rangle = G^{(q)}(z) |_{z=1}, \quad (5.51)$$

one finds that the NFMs for distribution (5.50) are δ -independent constants [23] of the form [20]

$$F_q^{\text{stat}}(\delta) = \frac{\langle N^{[q]} \rangle_N}{\langle N \rangle_N^q}, \quad (5.52)$$

where $\langle \dots \rangle$ denotes the average over all events following the probability distribution P_N :

$$\langle N^{[q]} \rangle_N = \sum_{N=0}^{\infty} P_N N^{[q]}, \quad q = 1, 2, \dots \quad (5.53)$$

Using definition (5.2) of the BPs, together with (5.48), we obtain the BPs for the case of purely statistical fluctuations

$$\eta_q^{\text{stat}}(\delta) = \frac{B_q}{B_{q-1}}, \quad B_q = \frac{\sum_{N=0}^{\infty} P_N N^{[q]} (1-p)^N}{\sum_{N=0}^{\infty} P_N N^{[q-1]} (1-p)^N}. \quad (5.54)$$

If the phase-space interval is small enough, then $(1-p) \rightarrow 1$ and (5.54) is reduced to

$$\eta_q^{\text{stat}}(\delta) \rightarrow \frac{\langle N^{[q]} \rangle_N \langle N^{[q-2]} \rangle_N}{\langle N^{[q-1]} \rangle_N^2}, \quad \delta \rightarrow 0, \quad (5.55)$$

i.e., the BPs become independent of δ .

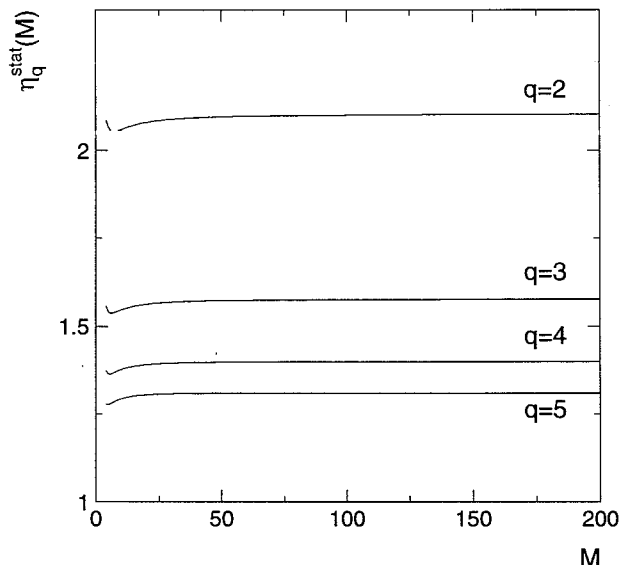


Figure 5.1: *The BPs as a function of M in the case of statistical phase-space fluctuations. Here we use an analytical description of the phase-space distribution in the form of a positive-binomial distribution and simulate the multiplicity distribution for full phase space by JETSET 7.4.*

If the multiplicity N for full phase space follows a Poissonian distribution with the average multiplicity \bar{N} , then the corresponding generating function has the form

$$G^P(z) = e^{\bar{N}(z-1)}, \quad (5.56)$$

and (5.50) again leads to the generating function for a Poissonian distribution in a small bin δ

$$G^{\text{stat}}(z) = e^{p\bar{N}(z-1)}, \quad p = \frac{\delta}{\Delta}. \quad (5.57)$$

In this case, the values of all-order BPs are unity for all δ . However, in many experiments P_N is far from the Poissonian distribution, and an additional study of the behavior of BPs for purely statistical phase-space fluctuations is necessary.

As an example, we present in Fig. 5.1 the behavior of the BPs as a function of $M = \Delta/\delta$ for the case of statistical fluctuations according to (5.48) with a truncated full-phase-space multiplicity distribution P_N obtained from the Monte-Carlo event generator JETSET 7.4 PS [24] simulating the decay of a Z^0 . The generator was tuned according to the parameter set of the L3 Collaboration [25]. The number of events generated is 750k. In this sample, $P_N = 0$ for $N < 4$ and $N > 70$ due to limited statistics. Let us stress that we are using the analytical expression (5.54), together with the P_N simulated for full phase space from

JETSET 7.4 PS, where P_N is not equal, but similar, to a negative-binomial distribution with the average charged-particle multiplicity $\bar{N} \simeq 21$.

As can be seen from Fig. 5.1, the values of the BPs are larger than unity, but the approximation $\eta_q^{\text{stat}}(\delta) \simeq \text{const}$ for $M > 10 - 20$ will be a good estimate of the statistical fluctuations in an experimental situation where P_N for full phase space is close to a truncated negative-binomial distribution. For intermittent fluctuations, as a rule, we need to study the behavior of the NFMs for much larger M . For such a situation, any observed dependence of the BPs (5.23) on the interval size must be caused by dynamical fluctuations.

5.4.1.2 Non-flat phase-space distribution

In the case of a non-flat phase-space distribution, the parameter p becomes a function of N , δ , and the position of the bin m in phase space. Mathematically, this can be written as [19]

$$p_m(N, \delta) = \frac{\int_{\delta_{m-1}}^{\delta_m} \frac{dN}{d\delta} d\delta}{\int_{\Delta} \frac{dN}{d\delta} d\delta}, \quad (5.58)$$

where the phase-space density $dN/d\delta$ is defined for a large set of events with a fixed total multiplicity N . For small δ and non-singular phase-space density, each term in the sum (5.25) is δ -independent according to (5.55) and, again, one has $\eta_q^{\text{ver}}(\delta) \simeq \text{const}$.

5.4.1.3 Theoretical aspect of the problem

From the theoretical point of view, there is a class of distributions, P_N , for which the BPs are δ -independent constants, also for large δ . Let $G^{\text{full}}(z)$ be the generating function for P_N in full phase space. After the composition with the positive-binomial distribution according to (5.50), the $G^{\text{full}}(z)$ becomes $G^{\text{stat}}(z, \delta) = G^{\text{full}}(pz - p + 1, \delta)$. Then, the BPs will be δ -independent if the generating function $G^{\text{full}}(pz - p + 1, \delta)$ can be expressed as

$$G^{\text{full}}(pz - p + 1, \delta) = G^{\text{full}}(1 - p, \delta)Q(z\lambda(\delta)), \quad (5.59)$$

where $Q(z\lambda(\delta))$ is some function containing only the combinations $z\lambda(\delta)$ (see (5.4), where $\lambda(\delta)$ is a function of δ). Here, $G^{\text{full}}(1 - p, \delta)$ is equal to $G^{\text{full}}(pz - p + 1, \delta)$ for $z = 0$. Expression (5.59) can be obtained from (5.4) by setting $\eta_q(\delta) = \text{const}$ [4].

If the multiplicity distribution for full phase space is Poisson, binomial, geometric, logarithmic, or negative binomial, then the BPs do not depend on δ , even if δ is not small [4].

As an example, we shall consider a negative-binomial distribution. The generating function for this distribution in full phase space is

$$G^{\text{NBD}}(z) = \left(1 + \frac{\bar{N}}{k}(1 - z)\right)^{-k}, \quad (5.60)$$

where \bar{N} represents the average number of particles in full phase space and k is a free parameter. Since they describe full phase space, both constants of course are δ -independent. After the composition (5.50), we obtain the generating function for the negative-binomial distribution in interval δ for the case of statistical phase-space fluctuations

$$G^{\text{NBD}}(z) = \left(1 + \frac{p\bar{N}}{k}(1 - z)\right)^{-k}. \quad (5.61)$$

Here, k is the same δ -dependent constant as in (5.60). For this distribution, the BPs (5.2) have the following form

$$\eta_q^{\text{stat}} = \eta_q^{\text{NBD}} = \frac{k + q - 1}{k + q - 2}, \quad (5.62)$$

i.e., are δ -independent.

Furthermore, even more complicated distributions exist which lead to δ -independent BPs for purely statistical fluctuations. For example, for a convolution of a number of different negative-binomial multiplicity distributions

$$G^{\text{conv}}(z) = \prod_{s=1}^{\mu} G_s^{\text{NBD}}(z), \quad (5.63)$$

the BPs can be shown not to depend on the interval size δ .

Let us note that dynamical fluctuations may be introduced into a model phenomenologically in the form of a projection (in analogy to (5.48)), if we require that for a subsample of fixed multiplicity N , the phase-space distribution differs from a positive binomial (so-called bunching projection method [20]). Another way to introduce dynamical fluctuations is by a two-projection method in which a two-step cluster mechanism with a generating function for full phase space is postulated in the form of a composition of two different generating functions. We, therefore, can apply a projection with two positive-binomial distributions, one for each stage (for the NBD (5.60) see [26], a general case is described in [27]). However, for this method only a monofractal behavior of intermittent fluctuations is characteristic. Therefore, as shown in [20], for multifractality it is necessary to use the bunching projection for both stages, cluster production and decay.

5.4.2 GHP counting topology

Now let us illustrate the behavior of the BPs (5.32) and (5.36) in the case of purely independent phase-space distribution, using the GHP counting topology. As we have noted in Sect. 5.3, if the full-phase-space multiplicity distribution is not Poissonian, then the values of the generalized BPs are not equal to unity.

An event sample is obtained with a random event generator ⁴ in the following way: For a given event of multiplicity N in full phase space, we generate N independent pseudo-random points in the “phase space” $0 < x < 1$. After that, we simulate the distribution for multiplicity N .

In Figs. 5.2 and 5.3 we present the $M = 1/\epsilon$ -behavior of differential BPs for two-particle spikes $\chi_q^{\text{stat}}(1/M, 2)$ and integral BPs $\chi_q^{\text{stat}}(1/M)$ for purely independent production of particles in the phase space x . The total number of events is 10^6 . Since the behavior of statistical fluctuations depends on the full-phase-space multiplicity distribution, we have considered the generalized BPs for the following cases:

1) N is fixed for all events ($N = 21$). This case is shown by open squares in the figures. Here, $\chi_q^{\text{stat}}(1/M, 2) < 1$ and $\chi_q^{\text{stat}}(1/M) < 1$. Such an anti-bunching effect is a consequence of trivial negative correlations that are present, when the probability of finding a spike is less if another spike has already been found.

⁴To generate N independent points for each event, we use the generator NRAN for uniformly distributed pseudo-random numbers (CERN Program Library).

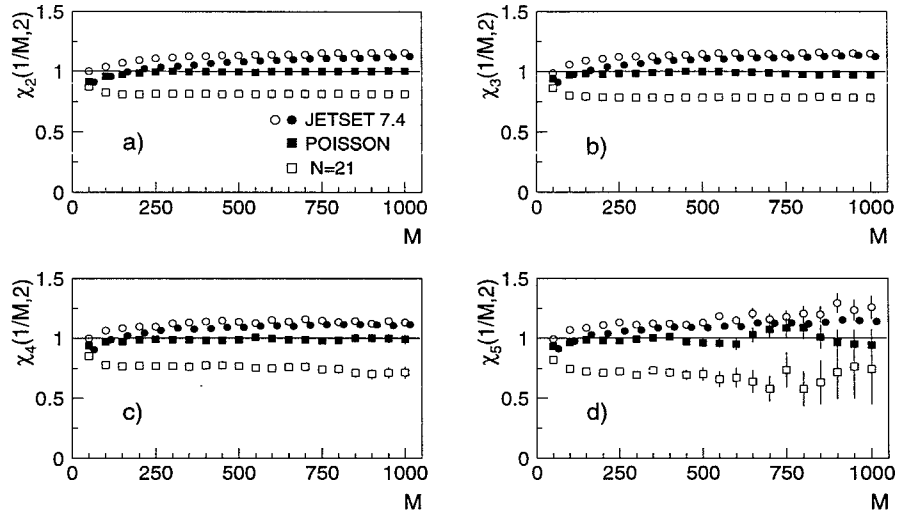


Figure 5.2: The values of differential BPs $\chi_q^{\text{stat}}(1/M, 2)$ as a function of $M = 1/\epsilon$ in the case of statistical fluctuations. The open circles represent the uniform single-particle density $\rho(x) = \text{const}$ and the full circles correspond to non-uniform density $\rho(x) = \text{const}(1+x)^{-6}$.

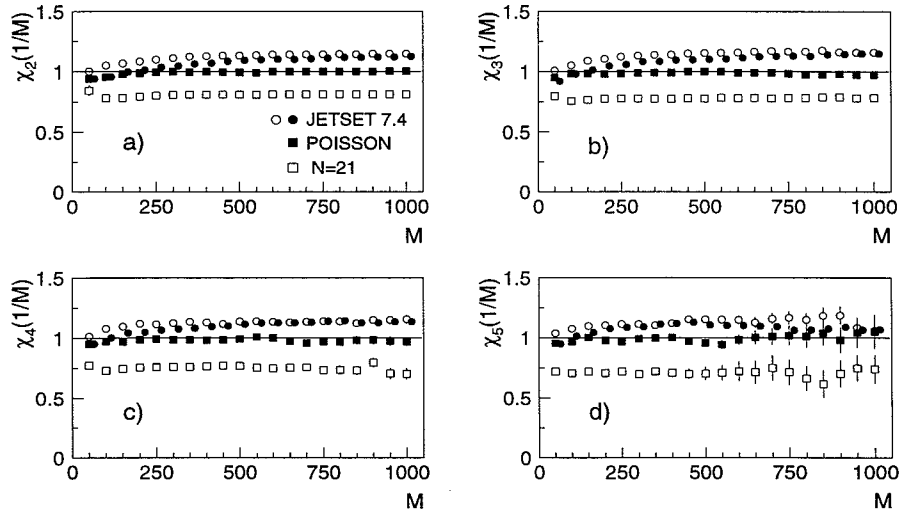


Figure 5.3: The values of integral BPs $\chi_q^{\text{stat}}(1/M)$ as a function of $M = 1/\epsilon$ in the case of statistical fluctuations.

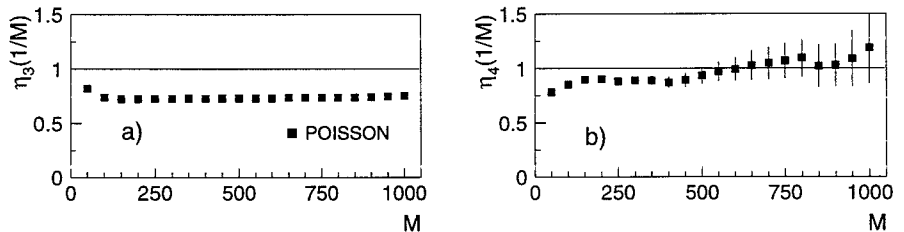


Figure 5.4: The values of BPs $\eta_q^{\text{stat}}(1/M)$ (5.40) as a function of $M = 1/\epsilon$ in the case of statistical fluctuations.

2) N is distributed according to a Poissonian distribution with average $\bar{N} = 21$ (full squares). As expected, the values of the bunching parameters are equal to unity.

3) In order to study a more realistic case, we generated the distribution for charged-hadron multiplicity N in full phase space according to JETSET 7.4 PS. To investigate the sensitivity of the BPs to various forms of single-particle distribution, we consider two different cases. In the first case, the phase-space density is uniform, i.e. $\rho(x) = dn/dx = \text{const}$ (open circles in the figures). For the second case, the phase-space density has the strongly non-uniform shape $\rho(x) = \text{const} (1+x)^{-6}$ (full circles)⁵. As we see from Figs. 5.2 and 5.3, the generalized distance-measure BPs have values larger than unity. Hence, the corresponding spike-multiplicity distributions are broader than a Poissonian distribution.

The most important feature of the generalized distance-measure BPs considered here is that, in the case of independent production of particles, they are approximately independent of the spike size ϵ . Only for the full-phase-space multiplicity distribution generated by JETSET 7.4 PS is a small rise of the generalized BPs visible for not very large M . In contrast to the bin-splitting definitions of BPs, the generalized BPs probably rise with decreasing ϵ even for very small values of ϵ due to the deviation in full-phase-space multiplicity distribution from a Poissonian distribution. However, to derive an exact conclusion on the full-phase-space dependence of generalized BPs, more investigation is needed, since statistical errors in the figures are comparable with the size of the symbols.

Figs. 5.2 and 5.3 show that the result obtained for JETSET 7.4 seems to be independent of the form of the single-particle density. It is important to note that a non-uniform phase-space density (full circles) leads to a more stable result for the M -dependence and significantly reduces the statistical error.

Fig. 5.4 shows the behavior of $\eta_q(1/M)$ (5.40) for $q = 3, 4$ as a function of $\epsilon = 1/M$ for the case of a Poissonian full-phase-space multiplicity distribution with average $\bar{N} = 21$. The total number of events is the same as that for Figs. 5.2 and 5.3. The independent particle distribution over phase space is simulated as for Figs. 5.2 and 5.3. Fig. 5.4 demonstrates that the corresponding multiplicity distribution $\tilde{P}_n(\epsilon)$ is narrower than Poisson ($\eta_q(1/M) < 1$), even if the particles are produced independently of each other. However, the main deficiency of definition (5.40) lies in the insufficient use of statistics available. This leads to large

⁵Such a single-particle inclusive density can easily be obtained as the product of two generators for uniformly distributed pseudo-random numbers.

statistical errors for large M . The calculation of $q = 5$ and $q = 6$ for $M > 100 - 200$ therefore, was found impossible due to limited statistics (not shown).

The subject of the behavior of generalized BPs is complex and, probably, must be solved separately for each particular type of BPs with a given definition of spike size, for a given multiplicity distribution of particles in full phase space. However, any ϵ -dependence of the BPs for purely statistical fluctuation due to full-phase-space fluctuations can be completely suppressed by using $1/\chi_q^{\text{stat}}$ or $1/\eta_q^{\text{stat}}$ as a correction factor. After the correction procedure any deviation in the behavior of the corrected generalized BPs from unity can be interpreted as being due to the presence of genuine local multiplicity fluctuations.

5.5 Local fluctuations in the JETSET 7.4 model

A widely used means to study general features of hadronic final-state fluctuations is to simulate hadronic events according to Monte-Carlo models. Below we will consider the behavior of BPs for hadrons produced in e^+e^- -annihilation at 91.2 GeV using the JETSET 7.4 PS model.

To study local fluctuations in this model, we use the bin-averaged BPs (5.23) with horizontal normalization. The azimuthal angle φ , calculated with respect to the beam axis, is used as a phase-space variable. Since there is no preferred direction for hadrons, the even- q averaged distribution in φ is uniform.

Fig. 5.5a shows for four different ranks q the value of η_q as a function of M , where $M = 2\pi/\delta\varphi$ is the number of partitions of the full azimuthal angle 2π . The number of events generated is 750k. From this figure it follows that there is a power-like behavior of the second-order BP, but all higher-order BPs tend to decrease with increasing M . Such an anti-bunching trend for higher-order BPs is the result of jet formation combined with energy-momentum conservation: particles belonging to different jets are separated by phase space.

In Fig. 5.5b we present the M -dependence of the BPs in azimuthal angle, but now calculated with respect to the thrust axis. Since the distribution for this kind of measurement is far from flat, the transformation [15] of the azimuthal-angle variable to a new cumulative variable with flat single-particle density was performed before the calculation of BP. Fig. 5.5b shows a power-law trend in the behavior of all BPs studied, without any visible saturation for large M , as is usually seen for NFMs in one-dimensional variables. We can conclude that the multifractal structure of intermittency is an inherent feature of fluctuations in the azimuthal angle defined with respect to the thrust axis. This means that multifractality is mainly a feature of fluctuations inside jets, rather than a property of fluctuations in the φ variable defined with respect to the beam.

Note that for small M , the behavior of the BPs is not meaningful: as we have seen in the previous section, in the domain $M \leq 10-20$ the value of the BPs can be affected by statistical fluctuations. In this case, an M -dependence of BPs can occur even without any dynamic reason. In addition, for small M , as is the case for NFMs, BPs are affected by the large-scale structure of fluctuations for which energy-momentum constraints are characteristic.

To compare the result obtained with NFMs, we present in Fig. 5.6a,b the behavior of NFMs as a function M , where we use the azimuthal angle φ calculated with respect to the beam axis (Fig. 5.6a) and the thrust axis (Fig. 5.6b). Both calculations show qualitative

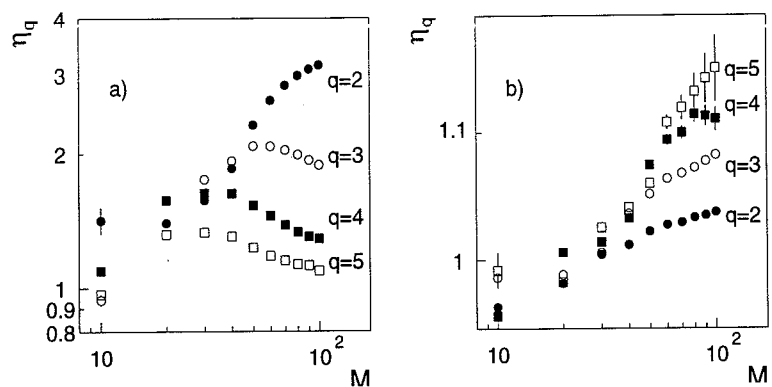


Figure 5.5: *BPs as a function of the number of bins in the azimuthal angle φ defined with respect to the a) beam axis and b) thrust axis. (JETSET 7.4 PS).*

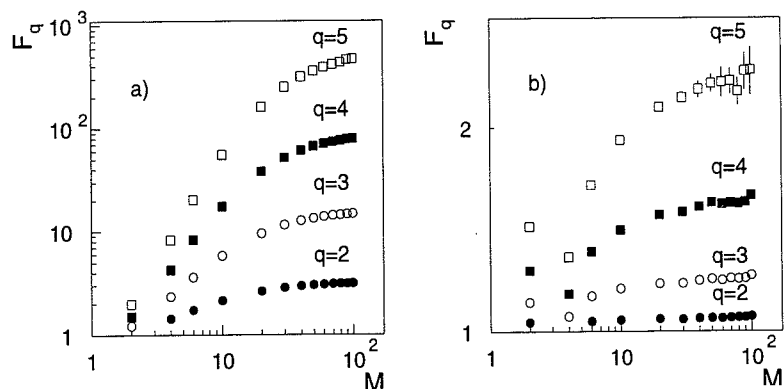


Figure 5.6: *NFMs as a function of the number of bins in the azimuthal angle φ defined with respect to the a) beam axis and b) thrust axis (JETSET 7.4 PS model).*

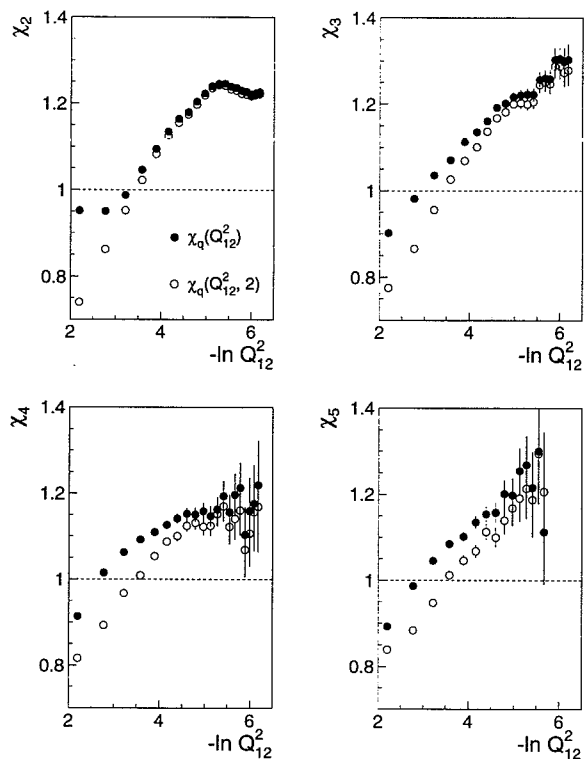


Figure 5.7: Integral (full symbols) and differential (open symbols) BPs as a function of the squared four-momentum difference Q_{12}^2 between two charged particles, calculated in the JETSET 7.4 PS model.

the same trend and it is very difficult to derive a conclusion on a different behavior of these two intermittent samples.

The same conclusion has been derived in [28], where a theoretical local-fluctuation model was studied with the help of both NFMs and BPs. It has been shown that two very different model samples can lead to rather similar power-law behavior of NFMs, while the BPs show a different trend. This means, in fact, that the NFMs are not sensitive to the details in the structure of intermittent fluctuations. The good agreement between experimental behavior of NFMs and Monte-Carlo predictions, as claimed recently [29], therefore, cannot provide a final proof of the similarity between experimental intermittent samples and samples generated by Monte-Carlo models in ever smaller phase-space intervals.

To demonstrate the behavior of generalized BPs, we use the squared four-momentum difference between two charged particles $Q_{12}^2 = -(p_1 - p_2)^2$ as a distance measure. Fig. 5.7 shows the behavior of integral $\chi_q(Q_{12}^2)$ (full circles) and differential $\chi_q(Q_{12}^2, 2)$ (open circles)

bunching parameters. The dashed line represents the behavior of these BPs in the case of a Poissonian distribution. Both kinds of BPs rise with decreasing Q_{12}^2 . This corresponds to a strong bunching effect. The saturation and downward bending of the second-order BPs at small Q_{12}^2 is caused by the influence of Dalitz pairs. We have verified that the power-like increase is stronger for like-charged particle combinations (not shown). The latter observation is very important, since the rise of BPs for identical pions with decreasing Q_{12}^2 can be attributed to Bose-Einstein correlations.

It is quite remarkable that the value of $\chi_q(Q_{12}^2)$ is always larger than $\chi_q(Q_{12}^2, 2)$, especially for not very small Q_{12}^2 . For small Q_{12}^2 , both definitions of BPs show the same trend and have similar values. The reason for such a similarity becomes clear when one realizes that the integral BPs include the contribution from two-particle spikes. For small interparticle distances, the integral BPs are then dominated by two-particle spikes.

For large Q_{12}^2 , the contribution of many-particle spikes to $\chi_q(Q_{12}^2)$ is more sizable. In such a case, the integral BPs are more sensitive, than are the differential ones, to jet events. This is due to the fact that jets can contribute to $\chi_q(Q_{12}^2, 2)$ only if they contain exactly two charged particles in each jet. In contrast, the integral BPs are affected by jets with a different number of particles. For example, for large Q_{12}^2 , the second-order integral BP is strongly influenced by two-jet events, the third-order BP is sensitive to both two- and three-jet events and so on.

5.6 Conclusions

Intermittency, as originally considered for particle physics by Białas and Peschanski [1], is a term borrowed from turbulence theory, as are most of the mathematical techniques used in this field. This is why intermittency was formulated in terms of continuous particle densities. In that approach, a convolution was assumed of an underlying dynamical density distribution with multi-Poissonian statistical noise. For such a situation, the method of removing statistical noise by the normalized factorial moments follows immediately.

However, the problem of intermittent dynamical fluctuations may, in principle, also be described in terms of bunching parameters. As is the case for bin-averaged normalized factorial moments, the bin-averaged BPs remove the influence of Poissonian statistical noise for small δ and become δ -independent constants if fluctuations have only statistical origin. Furthermore, definitions of the BPs are given which can be used for the study of fluctuations in various phase-space variables, without any artificial binning of phase space. This property is very important for the investigation of Bose-Einstein correlations and resonance decays.

As mentioned in the introduction, one of the most important properties of the BPs is that these quantities are not affected by the experimental statistical bias which arises in NFMs when the bin size becomes very small. Of course, the limitation in number of experimental events leads to an increase of the statistical errors with decreasing δ (or ϵ) for lower-order BPs and to the failure to calculate higher-order BPs. In contrast, the NFMs tend to be depressed at very small δ as compared to their values expected for an infinite sample [8].

Moreover, in studying intermittent fluctuations, there is a trivial tendency in the behavior of the NFMs: the higher the order of the NFM, the larger is its value for a given δ (or ϵ). On the contrary, the high-order BPs, in principle, can have any dependence on δ (or ϵ), i.e., the possible behavior of the BPs has a larger number of “degrees of freedom”. This

observation provides tools for a better understanding of the differences between samples with approximately the same power-law behavior of the NFMs and a selective study of fluctuations in terms of different types of spikes.

The last point has a primary importance for the investigation of local multiparticle fluctuations inside jets. The behavior of NFMs is qualitatively the same [29] for variables defined with respect to the beam axis and with respect to the sphericity axis. The informational content of these measurements, however, is rather different. The spikes dominating the distributions in variables defined with respect to the beam axis are due to the jets produced in a given event. Such spikes are separated in phase space because of energy-momentum conservation. This trivial effect always dramatically affects the observed behavior of local quantities measured in variables with respect to the beam axis. On the other hand, any local measurements of phase-space distributions in variables defined with respect to the sphericity or thrust axes mainly reflect the physical content of fluctuations that arise due to underlying stages (perturbative and fragmentation stages, resonance decays, Bose-Einstein interference) of multihadron production inside jets. Since the behavior of NFMs is not sensitive to the definition of a preferred axis, it is quite difficult to determine the physical nature of the intermittent signal observed for the two cases mentioned.

As we have seen, the different definitions of generalized BPs merely reflect the freedom of choice of event configurations. From the experimental point of view, this is very handy since we can choose a form of BPs optimized according to a given statistics of an experiment and according to the aims of the investigation.

We hope that the use of BPs will be useful for the investigation of details in the multifractal behavior of particle spectra, where it is important to find and to study the contribution from different multiparticle clusters and to compare theoretical or model multiplicity distributions with the experimental data.

Bibliography

- [1] A.Białas and R.Peschanski, Nucl. Phys. B273 (1986) 703; Nucl. Phys. B308 (1988) 857
- [2] P.Carruthers, Astrophys. J. 380 (1991) 24
- [3] A.Białas, Nucl. Phys. A525 (1991) 345;
R.Peschanski, J. of Mod. Phys. A21 (1991) 3681;
P.Bożek, M.Łosajczak and R.Botet, Phys. Rep. 252 (1995) 101;
E.A.De Wolf, I.M.Dremin and W.Kittel, Phys. Rep. 270 (1996) 1
- [4] S.V.Chekanov and V.I.Kuvshinov, Acta Phys. Pol. B25 (1994) 1189 (see Chapter 3)
- [5] S.V.Chekanov and V.I.Kuvshinov, J. Phys. G22 (1996) 601 (see Chapter 4)
- [6] S.Ya.Kilin and T.M.Maevskaya, preprint IPAS No.686 (1993), Belarus (in Russian)
- [7] S.V.Chekanov, W.Kittel and V.I.Kuvshinov, Acta Phys. Pol. B27 (1996) 1739 (see Chapter 6)
- [8] E.M.Friedlander, Mod. Phys. Lett. A4 (1989) 2457
- [9] W.Kittel: Proc. Santa Fe Workshop "Intermittency in High-Energy Collisions", Eds: F.Cooper et al. (World Scientific, Singapore, 1991) p.83
- [10] P.Lipa et al., Z. Phys. C54 (1992) 115
- [11] L.Van Hove, Mod. Phys. Lett. A4 (1989) 1867
- [12] A.Białas and R.C.Hwa, Phys. Lett. B253 (1991) 436
- [13] J.Wosiek, Acta Phys. Pol. B19 (1988) 863;
H.Satz, Nucl. Phys. B326 (1989) 613;
B.Bambah, J.Fingberg and H.Satz, Nucl. Phys. B332 (1990) 629
- [14] W.Ochs and J.Wośiek, Phys. Lett. B286 (1992) 159;
Yu.Dokshitzer and I.M.Dremin, Nucl.Phys. B402 (1993) 139
- [15] A.Białas and M.Gazdzicki, Phys. Lett. B252 (1990) 483;
W.Ochs, Z. Phys. C50 (1991) 339
- [16] E.C.Eggers, P.Lipa, P.Carruthers, B.Buschbeck, Phys. Rev. D. 48 (1993) 2041
- [17] P.Grassberger, Phys. Lett. A97 (1983) 227;
H.Hentschel and I.Procaccia, Physica D8 (1983) 43
- [18] Y.Beers: Introduction to the Theory of Errors, Addison-Wesley Publ. Com. Inc. (USA), 1958, p.28
- [19] G.J.H.Burgers, C.Fuglesang, R.Hagedorn, V.I.Kuvshinov, Z. Phys. C46 (1990) 465
- [20] S.V.Chekanov, Acta Phys. Pol., B25 (1994) 1583

- [21] A.I.Golokvastov, Z. Phys. C64 (1994) 301
- [22] C.V. Heer, Statistical Mechanics, Kinetic Theory, and Stochastic Process, Academic Press, INC (London), LTD, 1972, p.84
- [23] R.Hagedorn, private communication (1992)
- [24] T.Sjöstrand, Computer Phys. Commun. 82 (1994) 74
- [25] I.G.Knowles, T.Sjöstrand (conveners), "Physics at LEP2", eds. G.Altarelli, T.Sjöstrand and F.Zwirner, CERN 96-01 (1996) 103
- [26] L.Van Hove, Phys. Lett. B232 (1989) 509
- [27] D.V.Klenitski, V.I.Kuvshinov, Yad. Fiz. 59 (1996) 136
- [28] S.V.Chekanov, V.I.Kuvshinov, Proc. 5th. Int. Seminar "Non-Linear Phenomena in Complex Systems", Minsk, Belarus 1996, J. Phys. G (in press)
- [29] CELLO Coll., H.-J Behrend et al., Phys. Lett. B256 (1991) 97;
OPAL Coll., M.Z.Akrawy et al., Phys. Lett. B262 (1991) 351;
DELPHI Coll., P.Abreu et al., Nucl. Phys. B386 (1992) 47

Bin-Bin Correlation Measurement by the Bunching-Parameter Method

S.V.Chekanov¹, W.Kittel

*High Energy Physics Institute Nijmegen (HEFIN), University of Nijmegen/NIKHEF,
NL-6525 ED Nijmegen, The Netherlands*

V.I.Kuvshinov

Institute of Physics, AS of Belarus, Skaryna Av.70, Minsk 220072, Belarus

Published in Acta Phys. Pol. B27 (1996) 1739 - 1748

(Dedicated to A.Bialas in honor of his 60th birthday)

Abstract

A new method for the experimental study of bin-bin correlations is proposed. It is shown that this method is able to reveal important additional information on bin-bin correlations, beyond that of factorial-correlator measurements.

¹On leave from Institute of Physics, AS of Belarus, Skaryna Av.70, Minsk 220072, Belarus

6.1 Introduction

In order to obtain a comprehensive knowledge of the dynamics of particle production in high-energy reactions, two aspects of multiplicity fluctuations need to be studied:

1) the dependence of the multiplicity distribution (or its characteristics) on the size of the phase-space interval;

2) the dynamical correlations between two or more bins where this dependence is investigated.

The first point corresponds to the measurement of the local fluctuations, the second one to a simultaneous measurement of the local characteristics in two (or more) different bins in order to reveal correlations between these local fluctuations. If no correlations exist between fluctuations in different bins, then the complete information on an experimental sample can be obtained from local fluctuation measurements.

Dynamical information on fluctuations in a system with an infinite number of particles per event can be obtained from the multivariate density probability distribution $P(\rho_1, \rho_2, \dots, \rho_M)$ where ρ_m is the particle density in bin m ($m = 1, \dots, M$). This distribution can be studied by constructing the multivariate moments $\langle \rho_1^{q_1} \rho_2^{q_2} \dots \rho_M^{q_M} \rangle$. Due to the very complex structure of this quantity, however, one usually resorts to the study of only two moments: $\langle \rho_m^q \rangle$ and $\langle \rho_m^q \rho_{m'}^{q'} \rangle$, which contain a small fraction of the information on dynamical fluctuations in a system. The bivariate moment $\langle \rho_m^q \rho_{m'}^{q'} \rangle$ contains the information on bin-bin correlations.

In practice, bin-bin correlations always exist, i.e., $\langle \rho_m^q \rho_{m'}^{q'} \rangle \neq \langle \rho_m^q \rangle \langle \rho_{m'}^{q'} \rangle$, since final-state particles are not produced independently of each other. The production of a particle at high energy usually enhances the probability of producing other particles. The number of particles observed in a given phase-space bin, therefore, is always affected by the number of particles found in other bins. Moreover, there are more trivial (statistical) reasons for the observation of correlations in a system of finite fixed final-state multiplicity: for such a system, finding a particle in a single bin is less probable if another particle has already been counted in another bin. The latter case has no dynamical reason, but can influence the correlations observed in such a system.

In [1], Białas and Peschanski have adapted the method of normalized factorial moments to the measurement of dynamical bin-bin correlations by means of factorial correlators. The use of these quantities, as well as of the normalized factorial moments, has mainly been motivated by the Poissonian-noise suppression [2], thereby opening the possibility of modeling intermittency phenomena and bin-bin correlations by means of continuous densities.

In this paper we propose another experimental tool to measure bin-bin correlations by means of the bunching-parameter approach [3–6]. In the following, we shall discuss the experimental advantages of using such a method (Sect. 6.2). As an illustration, the bin-bin correlation measurement by the lowest-order bunching correlator is given in Sect. 6.3.

6.2 Bunching correlators

One of the characteristic features of any local multiplicity fluctuations in high-energy physics is the existence of bin-bin correlations. If we have two non-overlapping bins, m and m' of size δ , then the discrete two-dimensional multiplicity distribution $P_{n,n'}^{m,m'}(\delta)$ having n and n'

particles in bins m and m' , respectively, cannot be factorized, having

$$P_{n,n'}^{m,m'}(\delta) \neq P_n^m(\delta)P_{n'}^{m'}(\delta), \quad (6.1)$$

due to the existence of a bin-bin correlation between the bins m and m' ¹.

A procedure for investigating such bin-bin correlations is to measure so-called factorial correlators [1, 7], (for a review see [8]). In terms of $P_{n,n'}^{m,m'}(\delta)$, P_n^m , and $P_{n'}^{m'}$, the factorial correlators for two bins of equal size δ can be written as

$$F_{q,q'}^{m,m'}(\delta) = \frac{\sum_{n,n'} P_{n,n'}^{m,m'}(\delta) n^{[q]} n'^{[q']}}{\left(\sum_{n=1}^{\infty} P_n^m(\delta) n^{[q]}\right) \left(\sum_{n'=1}^{\infty} P_{n'}^{m'}(\delta) n'^{[q']}\right)}, \quad q', q > 1, \quad (6.2)$$

where $n^{[q]} = n(n-1)\dots(n-q+1)$. The quantity in the numerator is called the bivariate factorial moment. In contrast to the usual (univariate) factorial moment $\langle n^{[q]} \rangle = \sum_{n=1}^{\infty} P_n^m(\delta) n^{[q]}$, which characterizes only the local fluctuations in a single phase-space bin m , the bivariate factorial moment contains information on correlation between the local fluctuations in the two bins, m and m' .

If no correlation exists between bins m and m' , we get $F_{q,q'}^{m,m'}(\delta) = 1$ due to factorization of the multiplicity distribution in the numerator of (6.2).

To increase the statistics, one can assume translational invariance and average (6.2) over all bin combinations with the same bin-bin distance, D . After symmetrization, one has

$$F_{q,q'}(D) = \frac{1}{2(M-k)} \sum_{m=1}^{M-k} \left(F_{q,q'}^{m,m+k}(\delta) + F_{q',q}^{m,m+k}(\delta) \right), \quad (6.3)$$

where $M = \Delta/\delta$, Δ is a full phase-space interval, and $k = D/\delta$.

Correlators similar to (6.2) have also been proposed in [9]. In this approach, the bin of size δ is divided into two parts. If n_L and n_R are the number of particles in the left part and the right part of the bin, respectively, then one can define [9]

$$F_2(M) = \frac{1}{M} \sum_{m=1}^M \frac{\langle n_L n_R \rangle}{\langle n_L \rangle \langle n_R \rangle}. \quad (6.4)$$

As is the case for the usual univariate factorial moment, the multivariate factorial moments presented above are sensitive to the “tail” of the multivariate multiplicity distribution obtained in an experiment. The limited statistics of an experiment reduce fluctuations measured by means of the high-order factorial moments because of the truncation of the multiplicity distribution [10]. This can exert a negative influence on the behavior of the factorial correlators.

We note another shortcoming of the factorial correlators. As the usual factorial moments, the multivariate definition selects only “spikes”. Dynamical information from “dips”, therefore, is completely lost. This means that we lose important information on bin-bin correlations. As an example, correlations should exist between different bins that contain no particles, i.e.,

$$P_{0,0}^{m,m'}(\delta) \neq P_0^m(\delta)P_0^{m'}(\delta). \quad (6.5)$$

¹Strictly speaking, any statistical dependence between these bins can lead to property (6.1).

According to the definition, the factorial correlator is not able to measure such correlations

The complete information on bin-bin correlations can be obtained, without the bias arising from restricted statistics of an experiment, if one formulates the problem in terms of the bunching parameters [3–6]. The univariate bunching parameters for bin m are defined in terms of the probabilities $P_n^m(\delta)$ as

$$\eta_q^m(\delta) = \frac{q}{q-1} \frac{P_q^m(\delta) P_{q-2}^m(\delta)}{(P_{q-1}^m(\delta))^2}. \quad (6.6)$$

Accordingly, it is possible to construct bivariate bunching parameters in the same way as that used for bivariate factorial moments,

$$\eta_{q,q'}^{m,m'}(\delta) = \frac{qq'}{(q-1)(q'-1)} \frac{P_{q,q'}^{m,m'}(\delta) P_{(q-2),(q'-2)}^{m,m'}(\delta)}{(P_{(q-1),(q'-1)}^{m,m'}(\delta))^2}, \quad q, q' > 1. \quad (6.7)$$

The relation of BPs with usual moments have been found in [3, 5]. For bivariate BPs such a kind of relation can be written as

$$\eta_{q,q'}^{m,m'}(\delta) \simeq \frac{\langle \rho_{m,m'}^{q,q'} \rangle \langle \rho_{m,m'}^{q-2,q'-2} \rangle}{\langle \rho_{m,m'}^{q-1,q'-1} \rangle^2}, \quad \delta \rightarrow 0 \quad (6.8)$$

due to the suppression of Poissonian noise in the limit of small δ .

As is the case for multi-dimensional probabilities, these quantities can be expressed as

$$\eta_{q,q'}^{m,m'}(\delta) = \eta_q^m(\delta) \eta_{q'/q}^{m'}(\delta) = \eta_{q'}^{m'}(\delta) \eta_{q/q'}^m(\delta), \quad (6.9)$$

where $\eta_q^m(\delta)$ is the usual univariate bunching parameter and $\eta_{q'/q}^{m'}(\delta)$ represents a conditional bunching parameter for bin m' constructed from conditional probabilities, i.e., the probability to observe q' particles in bin m' under the condition that q particles have been found in another bin m . Then, the conditional BPs have the form

$$\eta_{q'/q}^{m'}(\delta) = \frac{q'}{(q'-1)} \frac{P_{q'/q}^{m'}(\delta) P_{(q'-2)/(q-2)}^{m'}(\delta)}{(P_{(q'-1)/(q-1)}^{m'}(\delta))^2}, \quad q, q' > 1. \quad (6.10)$$

If the two bins are statistically independent, then the bivariate bunching parameter factorize:

$$\eta_{q,q'}^{m,m'}(\delta) = \eta_q^m(\delta) \eta_{q'}^{m'}(\delta). \quad (6.11)$$

By analogy with the factorial correlators, the bunching correlators can, therefore, be defined as

$$\check{\eta}_{q,q'}^{m,m'}(\delta) = \frac{\eta_{q,q'}^{m,m'}(\delta)}{\eta_q^m(\delta) \eta_{q'}^{m'}(\delta)}. \quad (6.12)$$

As is the case for (6.2), this definition grants unity if the cells m and m' are statistically independent.

The bunching correlators, in general, are not symmetric in q and q' . As is performed in (6.3), we can symmetrize this definition:

$$[\check{\eta}_{q,q'}^{m,m'}(\delta)]_s = \frac{1}{2} (\check{\eta}_{q,q'}^{m,m'}(\delta) + \check{\eta}_{q',q}^{m,m'}(\delta)). \quad (6.13)$$

Defining the distance D between two bins, the bunching correlators can further be averaged over many pairs of equidistant bins. In analogy to (6.3), the problem of bin-bin correlations can be formulated in terms of the bunching correlators

$$\eta_{q,q'}(D) = \frac{1}{(M-k)} \sum_{m=1}^{M-k} [\tilde{\eta}_{q,q'}^{m,m+k}(\delta)]_S \quad (6.14)$$

and their behavior in the limit $D \rightarrow 0$.

According to the above definition of bunching correlators, the second-order bunching correlator contains important extra information *on empty bin-bin correlation* that cannot be extracted by means of factorial correlators. Indeed, if such correlations exist, then, due to (6.5), one obtains

$$\tilde{\eta}_{q,q'}^{m,m'}(\delta) \neq 1 \quad (6.15)$$

for any combination such as $\{2,2\}$, $\{2,3\}$, $\{3,2\}$ etc. For the symmetrized and averaged bunching correlators, this leads to

$$\eta_{q,q'}(D) \neq 1, \quad q = 2, \quad q' = 2, 3, \dots \quad (6.16)$$

On the other hand, if only such (hypothetical) correlations exist, the factorial correlators are equal to one for any higher rank.

6.3 The lowest-order bunching correlator and its behavior

The value of $\eta_{2,2'}(D)$ is affected by events having no particles in both bins and, hence, it incorporates the empty bin-bin correlations that cannot be measured by means of factorial correlators. In this section we shall illustrate the dependence of this quantity on the distance D between the two bins.

For our numerical calculations, we can rewrite the definition of $\eta_{2,2'}(D)$ as follows:

$$\eta_{2,2'}(D) = \frac{1}{M-k} \sum_{m=1}^{M-k} \tilde{\eta}_{2,2'}^{m,m+k}(\delta), \quad (6.17)$$

$$\tilde{\eta}_{2,2'}^{m,m'}(\delta) = \frac{\eta_{2,2'}^{m,m'}(\delta)}{\eta_2^m(\delta)\eta_{2'}^{m'}(\delta)}. \quad (6.18)$$

To define bivariate and univariate BPs, we introduce the following expression as an indicator for the presence of a given spike configuration for a given experimental event t :

$$W_q(m, m', t) = \begin{cases} 1, & \text{if both bins } m \text{ and } m' \text{ contain } q \text{ particles,} \\ 0, & \text{otherwise.} \end{cases} \quad (6.19)$$

Then, we have

$$\eta_2^m(\delta) = 2 \frac{\overline{W}_2(m, m) \overline{W}_0(m, m)}{\overline{W}_1^2(m, m)}, \quad (6.20)$$

$$\eta_{2,2'}^{m,m'}(\delta) = 4 \frac{\overline{W}_2(m,m')\overline{W}_0(m,m')}{\overline{W}_1^2(m,m')}, \quad (6.21)$$

where $\overline{W}_q(m,m')$ is the average of $W_q(m,m',t)$ over N_{ev} experimental events

$$\overline{W}_q(m,m') = \frac{\sum_{t=1}^{N_{\text{ev}}} W_q(m,m',t)}{N_{\text{ev}}}. \quad (6.22)$$

An exact calculation of the statistical error (standard deviation) is always a complex task and requires special attention to any local measurement. Below, we give a sketch of propagation of the standard deviation for (6.17).

The square of the standard deviation for $\overline{W}_q(m,m')$ is given by

$$S_q^2(m,m') = \frac{1}{N_{\text{ev}}(N_{\text{ev}} - 1)} \left[\sum_{t=1}^{N_{\text{ev}}} W_q^2(m,m',t) - N_{\text{ev}} \overline{W}_q^2(m,m') \right]. \quad (6.23)$$

The square of the standard deviation for second-order BPs is given by

$$V_2^2(m,m') = \frac{\overline{W}_0^2}{\overline{W}_1^4} s_2^2 + \frac{4\overline{W}_2^2\overline{W}_0^2}{\overline{W}_1^6} s_1^2 + \frac{\overline{W}_2^2}{\overline{W}_1^4} s_0^2. \quad (6.24)$$

This expression gives us the square of the standard deviation for univariate BPs if

$$\overline{W}_q = \overline{W}_q(m,m), \quad s_q^2 = 4S_q^2(m,m). \quad (6.25)$$

The square of the standard deviation for bivariate BPs can be found from (6.24) if

$$\overline{W}_q = \overline{W}_q(m,m'), \quad s_q^2 = 16S_q^2(m,m'). \quad (6.26)$$

The total statistical error for (6.17) can be found by combining the standard deviations for the univariate and bivariate BPs and averaging the results over all bin pairs.

In Fig. 6.1a, the behavior of $\eta_{2,2'}(D)$ is shown for the case of purely statistical phase-space fluctuations. For our numerical calculations, we simulate the phase-space distribution by a pseudo-random number generator in the “phase space” $0 < x < 1$. The total number of events is 30,000. In this figure we consider the cases in which a total number of particles N in full phase space fluctuates according to full-phase-space fluctuations. We considered the following cases:

- 1) N is fixed for all events ($N=20$);
- 2) N is distributed according to a Poissonian law with mean $\overline{N} = 20$;
- 3) N is distributed according to the JETSET 7.4 PS model [11] simulating e^+e^- -annihilation

at a c.m. energy of 91.2 GeV. Such a distribution is similar to a negative binomial. For this case, we also consider different values of bin size δ .

As expected, the value of the bunching correlator is equal to 1 for the Poisson distribution. We have verified that this result is independent of the mean of the Poisson distribution and of the bin size δ .

For the sample with fixed multiplicity ($N = 20$), there is a negative correlation, since $\eta_{2,2'}(D) < 1$. This kind of correlation is due to the trivial effect that the probability of finding

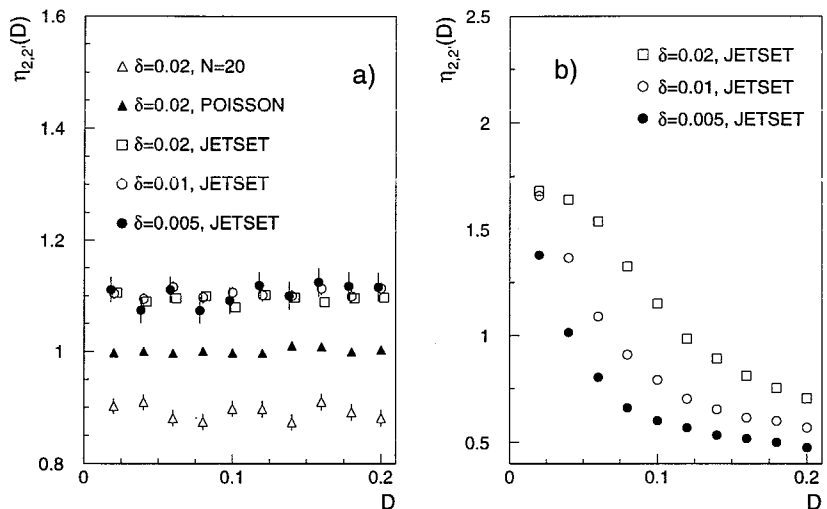


Figure 6.1: Value of $\eta_{2,2}(D)$ as a function of distance D between bins. (a) The behavior in the case of purely statistical fluctuations for different distributions of particles in full phase space. (b) The behavior for the case of dynamical fluctuations (phase-space distribution in azimuthal variable) simulated by the JETSET 7.4 PS model.

a particle in a bin is always less if another particle has already been found in another bin. In the case of no dynamical phase-space correlations, such a negative (pseudo) correlation leads to a D -independent bunching correlator of value smaller than unity.

If particles are distributed according to a distribution broader than Poisson, one should expect a positive correlation. For the case of no phase-space correlations, this again leads to a D -independent bunching correlator, but with a value of $\eta_{2,2'}(D) > 1$.

In Fig. 6.1b we present $\eta_{2,2'}(D)$ for a more realistic situation. Here, N again fluctuates according to JETSET 7.4 PS, but the phase-space distribution is defined in the azimuthal angle with respect to the e^+e^- collision axis. To compare the results with the previous cases, this variable (with full phase-space range 2π) has been transformed to a new variable with unit range. Due to the jet structure of single events, the phase-space distribution in this variable contains dynamical fluctuations. As can be seen from Fig. 6.1b, such fluctuations lead to a bin-bin correlation. The correlation increases for decreasing distance D , from $\eta_{2,2'}(D) < 1$ for large D to $\eta_{2,2'}(D) > 1$ for small D . Moreover, in contrast to Fig. 6.1a, the value of $\eta_{2,2'}(D)$ is affected by the value of the bin size δ .

6.4 Conclusions

In this paper, the bunching-parameter method has been extended to measure bin-bin correlations. This application of the bunching-parameter method has been achieved by considering bunching correlators in analogy to factorial correlators. The method not only allows one to

study fluctuations inside a phase-space bin without experimental bias from finite statistics but also to study correlations between bins separated in phase-space.

One of the remarkable features of the bin-bin correlation study is that the main properties of local fluctuations inside bins, and correlations between the bins can be formulated in a unified manner. Based on our analysis of second-order bunching correlations and on [5], we conclude:

1) For purely statistical phase-space fluctuations, the values of the univariate bunching parameters and those of the bunching correlators are independent of bin size and bin-bin distance. These values are affected by event-to-event multiplicity fluctuations, but are equal to unity for Poisson-distributed particle multiplicity in full phase space;

2) For dynamical phase-space fluctuations, the values of univariate bunching parameters and bunching correlators increase for decreasing bin size δ or distance D between two bins.

Such a similarity in the behavior of these quantities is the result of an intrinsic relation between fluctuation and correlation properties of the local fluctuations.

Finally, from our study, let us note that no universal scaling relation between the local fluctuations and correlations is observed for the azimuthal-angle distribution in JETSET 7.4 PS model, as it follows from the random-cascade model [1, 2], for which the factorial correlators are δ -independent. The analysis of bin-bin correlations based on the bunching correlators clearly shows that the behavior of the second-order correlator is affected by the bin size δ . In fact, this means that realistic intermittent fluctuations cannot be fully described by the scaling indices of the univariate normalized moments as is the case for the random-cascade model. For this reason, the experimental measurement of the correlators is an important complementary part of the fluctuation analysis, which, therefore, cannot be reduced to the investigation of the scaling indices of the local quantities only.

Bibliography

- [1] A.Białas and R.Peschanski, Nucl. Phys. B308 (1988) 857
- [2] A.Białas and R.Peschanski, Nucl. Phys. B273 (1986) 703
- [3] S.V.Chekanov and V.I.Kuvshinov, Acta Phys. Pol. B25 (1994) 1189 (see Chapter 3)
- [4] S.V.Chekanov and V.I.Kuvshinov, J. Phys. G22 (1996) 601 (see Chapter 4)
- [5] S.V.Chekanov, W.Kittel and V.I.Kuvshinov, Z. Phys C74 (1997) 517 (see Chapter 5)
- [6] S.V.Chekanov and V.I.Kuvshinov, Proc. of 5th. Int. Seminar "Non-Linear Phenomena in Complex Systems", Minsk, Belarus 1996, J. Phys. G (in press)
- [7] R.Peschanski, J.Seixas, *Scaling relations between fluctuations and correlations in multiparticle production*, preprint CERN-TH-5903/90, DF/IST-3.90;
NA22 Coll., V.V.Aivazyan et al., Phys. Lett. B258 (1991) 486;
EMC Coll., I.Derado et al., Z. Phys. C54 (1992) 357
- [8] E.A.De Wolf, I.M.Dremin and W.Kittel, Phys. Rep. 270 (1996) 1
- [9] D.Seibert and S.Voloshin, Phys. Rev. D43 (1991) 119
- [10] E.M.Friedlander, Mod. Phys. Lett. A4 (1989) 2457;
W.Kittel, Santa Fe Workshop "Intermittency in high-energy collisions", Ed. F.Cooper et al., (World Scientific, Singapore, 1991) p.83;
P.Lipa et al., Z. Phys. C54 (1992) 115
- [11] T.Sjöstrand, Computer Phys. Commun. 82 (1994) 74

Hadron production in e^+e^- collisions

The main aim of this chapter is to give a short overview of the theoretical and phenomenological approaches to an understanding and interpretation of the final-state hadrons produced in e^+e^- collisions.

7.1 Theoretical description of e^+e^- collisions

Electron-positron scattering is one of the basic experiments to study the fundamental properties of matter. The clean and exactly known initial state of this point-like reaction allows a straightforward test of the Standard Model, the theory describing the interactions between all presently known fundamental particles.

In an e^+e^- collider, the e^+e^- collision takes place in the center of mass system (cms). The main advantage of the cms is that there is no energy loss for center of mass motion: If p and p' are the 4-momenta of the positron and the electron, then the total energy in the cms is $E \equiv \sqrt{s} = (p + p')$.

For a low center of mass energy \sqrt{s} , the process $e^+e^- \rightarrow q\bar{q}$ is dominated by a single virtual photon exchange. When the cms energy of the Z^0 resonance is reached ($\sqrt{s} \simeq 91.2$ GeV), Z^0 exchange becomes the dominating process.

The most probable result of an e^+e^- collision near the Z^0 resonance is multihadron production due to the large branching ratio of $Z^0 \rightarrow q\bar{q}$. Other channels, such as $e^+e^- \rightarrow e^+e^-$ (Bhabha scattering), $e^+e^- \rightarrow \mu^+\mu^-$, $e^+e^- \rightarrow \tau\bar{\tau}$, occur less frequently [1].

The structure of a typical multihadron event in e^+e^- annihilation is shown in Fig. 7.1. In the following, we shall trace the major theoretical ideas on the description of the e^+e^- reaction necessary to understand the next sections.

In a first stage, the e^+e^- pair annihilates into a virtual γ^*/Z^0 resonance according to electroweak theory. The virtual γ^*/Z^0 , in turn, decays into a $q\bar{q}$ pair, also following electroweak theory. Frequently, before the annihilation, bremsstrahlung of a photon (initial-state photon radiation) may occur. This electroweak correction reduces the cms energy of the e^+e^- collision and, therefore, the total effective mass of the hadronic final state.

In a second stage, the initial $q\bar{q}$ may radiate gluons according to the theory of quantum chromodynamics (QCD) [2]. The gluons may radiate other gluons or $q\bar{q}$ pairs, giving rise to a cascade process. This stage is responsible for the formation of hadronic jets. The probability

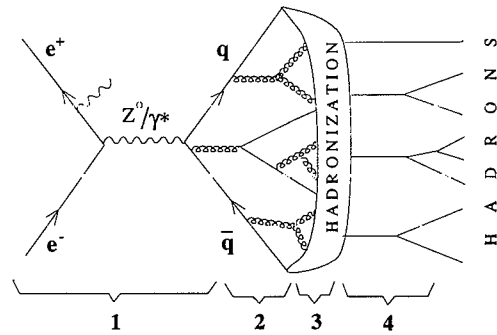


Figure 7.1: A schematic representation of the e^+e^- reaction.

ratio for observing events with a certain number of jets can be written in terms of increasing powers of the strong coupling constant α_s as [3]

$$2 \text{ jets} : 3 \text{ jets} : 4 \text{ jets} = \mathcal{O}(\alpha_s^0) : \mathcal{O}(\alpha_s^1) : \mathcal{O}(\alpha_s^2). \quad (7.1)$$

This means that the majority of the e^+e^- events have a two-jet structure ($\alpha_s < 1$). Because of the small value of α_s at the corresponding virtuality, this stage can be described by perturbative QCD. In this approach, Feynman diagrams are calculated order by order according to the so-called matrix element (ME) method. In principle, these calculations can take into account all interference terms and accurate kinematics. However, such calculations become increasingly difficult in high orders. The calculations have only been carried out up to $\mathcal{O}(\alpha_s^2)$ (i.e., up to four partons in the final state). Since the next-to-leading-order corrections are not known, this means that predictions of perturbative QCD in the framework of the matrix element approach can only be semi-quantitative.

The second possible approach is that of a parton shower (PS). It is based on the leading logarithmic approximation (LLA), where only the leading collinear and soft logarithm terms are taken into account. This approach is formulated in terms of a probabilistic picture. The algorithm is based on an iterative use of the basic branchings, such as $q \rightarrow qg$, $g \rightarrow gg$, $q \rightarrow q\bar{q}$. The probabilities for one of these branchings are given by the Dokshitzer-Gribov-Lipatov-Altarelli-Parisi (DGLAP) evolution equation [4].

In a third stage, the partons fragment into colorless hadrons. Usually, this stage is called hadronization. This process cannot be described as a power expansion in the strong coupling constant, since $\alpha_s > 1$ at the corresponding virtualities. At present, a detailed description of this stage is provided only by models. There are three main types of phenomenological models for hadronization: independent fragmentation, string fragmentation and cluster fragmentation models. All these models are probabilistic and iterative.

The last stage in Fig. 7.1 represents the decay of unstable hadrons into experimental observable particles (mostly pions). This stage includes final Coulomb interaction and Bose-Einstein (BE) interference between identical secondary particles (bosons). The latter effect is a quantum-mechanical phenomenon. However, since there is no complete theory for its description, the BE effect is often modelled as a classical force acting on the like-sign final-state

particles. For the interpretation of physical results presented in the next chapters, the BE effect is a very probable candidate to account for the large local fluctuations at very small phase-space distance. Indeed, it was shown in [5] using two independent phenomenological approaches that the leading contribution to the local intermittent fluctuations may be connected just with the last stage. Unfortunately, there is still a vagueness in the definition of the last stage: In the framework of the cluster models used in [5], it is rather difficult to say to what stage of e^+e^- reactions the last stage of the cluster models may correspond.

7.2 Lund Monte-Carlo generator (JETSET 7.4)

The JETSET Monte-Carlo program is a very successful program to model the process $e^+e^- \rightarrow \gamma^*/Z^0 \rightarrow q\bar{q} \rightarrow \text{hadrons}$, at least up to $\sqrt{s} = m_Z \simeq 91.2$ GeV [6]. This program has its roots in the efforts of the LUND group to understand the hadronization problem. Nowadays, the JETSET program is supplemented with the PYTHIA program. The latter gives access to a variety of hard processes. JETSET and PYTHIA are fully integrated and can together generate not only hadronic final states, but also non-hadronic reactions. Further we shall consider only the JETSET 7.4 program which is formally independent of PYTHIA. A detailed description of both programs can be found in [7].

Quantum mechanics states that all processes in nature have a random character. In order to generate events independently from each other with a random outcome, any Monte-Carlo program uses a pseudo-random generator with uniform distribution. Using (deterministic) functions known from experiment or theory which describe physical processes (such as differential cross sections, fragmentation functions, relevant branching ratios and decay rates), the program, at each step, produces a random outcome from a set of possible outcomes [8]. To model the characteristics of outgoing particles in the process $e^+e^- \rightarrow \text{hadrons}$, such as a list of particle 4-momenta for each event, JETSET factorizes all stages described above into a number of independent components. Each of them can be characterized by a set of functions governing the random outcome.

Let us note that JETSET, like other Monte-Carlo programs, contains a lot of free parameters describing each stage of an e^+e^- reaction. Variation of some of them does not significantly affect the final predictions of this model.

We shall now give a short physical outline of each stage of the process $e^+e^- \rightarrow \text{hadrons}$:

Hard processes in JETSET

The hard process of main interest is $e^+e^- \rightarrow \gamma^*/Z \rightarrow q\bar{q}$. The full interference between γ^* and Z^0 propagators is included. The flavor of the quark in the final state of each event is picked at random, according to the relative couplings. Since initial-state photon radiation may give large corrections to the overall topology of an event, such a process is included in the program.

While the hard electroweak interaction provides a description of the production of a primary $q\bar{q}$ pair, perturbative QCD is responsible for the final-state radiation of quarks and gluons. These high-order QCD corrections can be described in JETSET 7.4 either with the parton shower approach (JETSET 7.4 PS) or with the second-order matrix element (JETSET 7.4 ME). The default of JETSET 7.4 is the parton shower. This option gives a good description of the substructure of jets [6]. However, since this approach is only an

approximation derived by simplifying real dynamics, without a complete form of interference terms, it has limited predictive power for the rate of jets (2 : 3 : 4 -jet composition).

Recently, the JETSET model has been improved by including gluon interference (coherence) in the parton shower. Gluon interference becomes apparent when one goes beyond the LLA. One of the consequences of gluon interference is angular ordering, whereby subsequent partons are emitted at ever decreasing angles with respect to their parent parton [2]. The parton shower in JETSET 7.4 incorporates the coherence effect by requiring a strict ordering in decreasing emission angles (for a parton shower based only on LLA, the emission angles are decreasing in an average sense). This constraint in JETSET 7.4 can be turned off. However, it has been shown that models containing gluon interference agree much better with data than do those without this interference [6].

Besides the parton shower, also the matrix-element option can be used in JETSET 7.4 for the description of corrections in the perturbative process. This program contains options for first-order QCD corrections (describing 3-jet events) and second-order QCD corrections. The latter can describe both the 3-jet events and 4-jet events and predicts final states with up to four hard partons. Since the matrix-element approach takes into account exact kinematics and full interference according Feynman diagrams, JETSET 7.4 ME is more relevant for the prediction of the rates of well-separated jets. However, in contrast to parton showering, the matrix-element description has a restricted predictive power for the description of the full structure of events at high energies (such as average multiplicity, different global distribution of hadrons, *etc.*), because the high-order QCD corrections become sizable at high energies.

Hadronization process in the JETSET model

The basis of the JETSET model is the string hadronization scheme [10]. The physical picture is that, at the end of the perturbative stage, the produced quarks and antiquarks move out in opposite directions, losing energy. The color field between them is supposed to collapse into a string-like configuration (color flux tube) with uniform energy density. The transverse size of the tube is of typical hadronic size (roughly 1 fm). Since the energy per unit length is uniform, this automatically leads to a confinement picture. As the q and \bar{q} move apart, the string may break into two less energetic strings by the production of two colorless systems $q\bar{q}'$ and $q'\bar{q}$. The probability of the production of a pair is taken proportional to a Gaussian fragmentation function $\exp(-m_{\perp}^2)$ ($m_{\perp} = \sqrt{m^2 + p_{\perp}^2}$ is the transverse mass describing a quantum-mechanical tunnel effect). This parameterization thus explains the limited p_{\perp} distribution of particles in the jet as well as the suppression of strange quarks as they are heavier than u and d . The resulting string can break in its turn, until the original string is separated into many short pieces which do not have sufficient energy to break further. The breaking is assumed to stop when the masses of the string pieces reach the hadronic mass scale. Each final $q\bar{q}$ segment of this process is associated with a meson. Baryon production can be introduced by allowing the production of diquark-antidiquark pairs. The process described above is fully probabilistic and iterative.

Another hadronization scheme, the independent fragmentation model [11], is also available in the JETSET program. Initially, the latter model was designed to reproduce the limited transverse momenta and has a great merit of simplicity. In this model, one supposes that each parton fragments into hadrons independently. However, this model cannot be considered as an alternative to the LUND model, since it has been shown that the independent fragmentation model fails to describe a number of experimental data [12].

Production of observable hadrons in the JETSET model

A large number of the particles produced in the hadronization process are unstable and subsequently decay into observable stable hadrons. The decay of short-lived hadrons on this stage is completely described by empirical results, such as branching ratios and masses taken from other experiments. JETSET 7.4 includes several different kinds of decay: strong, electromagnetic and weak decays. Their treatment depends on the nature of the decay.

The Bose-Einstein effect has received some attention in the JETSET 7.4 program. Since the detailed physics is not yet understood, the effect was included in the program as a classical force between final-state identical particles. There are two options in the JETSET: the shape of the correlation function for two pions may be chosen either exponential or Gaussian. Usually, the values of the free parameters in these functions are taken from the experimental study of the BE effect.

7.3 Description of final-state hadrons

7.3.1 Single-particle variables

In this sub-section we shall consider variables defined in an orthonormal system with respect to the beam axis. A detailed description of this system is given at the beginning of Chapter 8.

A produced particle can be characterized by the following variables:

1) Rapidity y :

The rapidity of a charged particle is calculated by the following formula

$$y = \frac{1}{2} \ln \left(\frac{E + p_z}{E - p_z} \right), \quad (7.2)$$

where E is the particle energy assuming the pion mass, p_z the momentum component along the z axis. The rapidity has the important property of being additive with respect to a Lorentz transformation along the z -axis; thus the shape of the distribution remains invariant.

2) Azimuthal Angle φ :

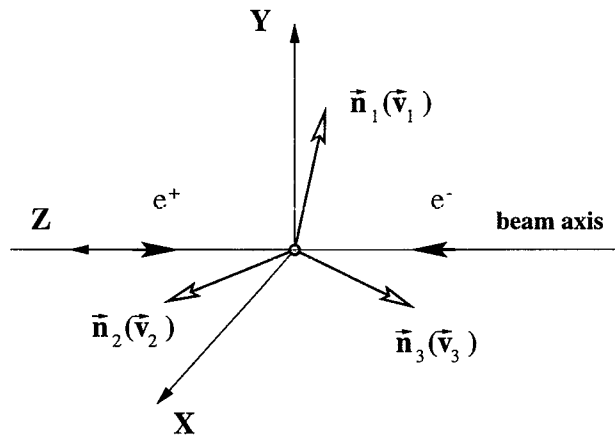
$$\varphi = \arctan \left(\frac{p_y}{p_x} \right). \quad (7.3)$$

Since incoming electron and positron are not polarized, there is no preferred transverse direction for outgoing hadrons and the event averaged distribution in φ is uniform. The variable φ is invariant under Lorentz transformations along the reference axis (z axis). These properties are useful for the study of intermittency.

3) Transverse Momentum p_T :

$$p_T = \sqrt{p_x^2 + p_y^2}, \quad (7.4)$$

is the component of the momentum in the plane transverse to the z axis.

Figure 7.2: Coordinate systems of the e^+e^- collision.

7.3.2 Event-shape variables

To characterize the hadronic event as a whole, we define the so-called event-shape variables. To be calculable in perturbative theory, these variables should be infrared and collinear safe. This means that, if we have a particle a with 3-momentum \vec{p}_a splitting into two new particles b and c with 3-momentum \vec{p}_b and \vec{p}_c , respectively, then the corresponding event-shape variable must be invariant under the following branching

$$\vec{p}_a \rightarrow \vec{p}_b + \vec{p}_c, \quad (7.5)$$

whenever \vec{p}_b and \vec{p}_c are parallel or one of them goes to zero.

The thrust variable, which we shall consider now, meets this requirement.

1) Thrust

The thrust axis, \vec{n}_1 , is defined as the axis along which the projected energy flow is maximized. The value of thrust T_{thrust} and \vec{n}_1 are given by [13]

$$T_{\text{thrust}} = \max \frac{\sum_{i=1} |\vec{p}_i \cdot \vec{n}_1|}{\sum_{i=1} |\vec{p}_i|}, \quad (7.6)$$

where \vec{p}_i is the momentum vector of particle i . The sum \sum_i runs over all final-state particles. The allowed values of T_{thrust} are $1/2 \leq T_{\text{thrust}} \leq 1$, with $T_{\text{thrust}} = 1/2$ for a fully isotropic final state. The value of T_{thrust} approaches unity as the event configuration in the hadron cms becomes more two-jet-like. As the direction on this axis is not defined by (7.6), we use as positive direction of \vec{n}_1 the direction of the most energetic jet.

2) Major

In order to investigate the energy flow in the plane perpendicular to the event thrust axis, a second direction \vec{n}_2 is defined perpendicular to \vec{n}_1 . The major axis is defined in the same way as thrust, but is maximized in the plane perpendicular to the thrust axis [14]

$$T_{\text{major}} = \max \frac{\sum_{i=1} |\vec{p}_i \cdot \vec{n}_2|}{\sum_{i=1} |\vec{p}_i|}, \quad \vec{n}_2 \perp \vec{n}_1. \quad (7.7)$$

3) Minor

The minor axis \vec{n}_3 is defined as orthogonal to both the thrust and the major axes. This gives an orthonormal system for an event (see Fig. 7.2).

Since the event-shape variables are formulated in terms of the three-momentum vectors, none of the variables described above is Lorentz invariant.

4) Sphericity

The disadvantage of thrust is that the maximization process cannot be performed analytically, but has to be done numerically. It takes a lot of computation time. A widely used alternative to thrust is sphericity which can be found analytically. The generalized form of a sphericity tensor is

$$S_r^{\alpha,\beta} = \frac{\sum_{i=1} |\vec{p}_i|^{r-2} p_i^\alpha p_i^\beta}{\sum_{i=1} |\vec{p}_i|^r}, \quad (7.8)$$

where $\alpha, \beta = 1, 2, 3$ correspond to the x, y , and z components of momentum.

For $r = 2$, we get the standard sphericity tensor [15]. By diagonalization of $S_2^{\alpha,\beta}$ one finds three eigenvalues $\lambda_1 \leq \lambda_2 \leq \lambda_3$, $\lambda_1 + \lambda_2 + \lambda_3 = 1$. The value $S = \frac{3}{2}(\lambda_2 + \lambda_3)$ is a measure of jetyness of an event: a 2-jet event corresponds to $S \approx 0$ and an isotropic event to $S \approx 1$. Eigenvectors \vec{v}_i , $i = 1, 2, 3$ can be found corresponding to the three eigenvalues λ_i . This gives an orthonormal coordinate system (Fig. 7.2). The direction of \vec{v}_1 is called the sphericity axis. Let us note that the thrust axis does not necessarily coincide with the sphericity axis.

The coordinate system connected with sphericity has been used for intermittency analysis in [16]. Unfortunately, this choice of coordinate system is rather inconvenient: the sphericity tensor for $r = 2$ is not collinear safe. This means that, in the framework of perturbative QCD, we cannot obtain predictions in terms of the sphericity tensor [17].

For $r = 1$ in (7.8), we can get an infrared and collinear safe sphericity tensor calculable in perturbative theory [18]. Eigenvalues and eigenvectors of it may be defined as before.

For our analysis, we will use the coordinate system connected with the thrust axis. An intermittency analysis has been performed for such a system in [19]. All the three variables y, φ, p_T , where not explicitly stated, are defined in the thrust system. In this system, the z -axis is defined to be along the $\vec{n}_1(\vec{v}_1)$ direction, the x -axis is along $\vec{n}_2(\vec{v}_2)$ and y -axis is along the $\vec{n}_3(\vec{v}_3)$.

Bibliography

- [1] Particle Data Group, *Review of Particle Physics*, Phys. Rev. D54 (1996)
- [2] F.J.Yndurain, "Quantum Chromodynamics: an Introduction to Theory of Quarks and Gluons", Springer, New York, 1983;
Yu.L.Dokshitzer, V.A.Khoze, A.H.Mueller, S.I.Troyan, "Basics of perturbative QCD" Editions Frontieres, 1991
- [3] Z Physics at LEP1, V1, Sect. 19, CERN89-08, eds. G.Altarelli et al., 1989
- [4] V.N.Gribov and L.N.Lipatov, Sov. J. Nucl. Phys. 15 (1972) 438;
G.Altarelli and G.Parisi, Nucl. Phys. B126 (1977) 298;
Yu.Dokshitzer, Sov. Phys. JETP 46 (1977) 641
- [5] S.V.Chekanov, Acta Phys. Pol. B25 (1994) 1583
- [6] I.G.Knowles and T.Sjöstrand (conveners), "QCD Event Generators", Physics at LEP2 CERN-96-01, Vol. 2 (1996) p.103
- [7] T.Sjöstrand, Computer Phys. Commun. 82 (1994) 74
- [8] F.James, "Monte Carlo Theory and Practice", Exp.Tech. in High Energy Phys., ed T.Ferbel, Benjamin-Cummings, 1987
- [9] L3 Coll., M.Acciarri et al., Phys. Lett. B353 (1995) 145;
A.A.Syed, "Particle Correlations in Hadronic Decays of the Z Boson", Ph.D. Thesis Univ. of Nijmegen, The Netherlands 1994
- [10] B.Andersson, G.Gustafson, G.Ingelman, T.Sjöstrand, Phys. Rep. 97 (1983) 31
- [11] R.D.Field and R.P.Feynman, Phys. Rev. D15 (1977) 2590, Nucl.Phys. B138 (1978) 1
- [12] L3 Coll., B.Adeva et al., Z. Phys. C55 (1992) 39 (and references therein)
- [13] E.Fahri, Phys. Rev. Lett. 39 (1977) 1587
- [14] MARK J. Coll., D.P.Barber et al., Phys. Rev. Lett. 43 (1979) 830
- [15] J.D.Bjorken and S.J.Brodsky, Phys. Rev. D1 (1970) 1416
- [16] DELPHI Coll., P.Abreu et al., Nucl. Phys. B386 (1992) 471;
OPAL Coll., Phys. Lett. B262 (1991) 351
- [17] Z.Kunszt and P.Nason, "Z Physics at LEP 1", eds. G.Altarelli et.al., CERN Report CERN-89-08, Vol.1 (1989) 373
- [18] G.Parisi, Phys. Lett. B78 (1978) 65
J.F.Ponoghue, F.E.Low, S.-Y.Pi, Phys. Rev D20 (1979) 2759

- [19] HRS Coll., S.Abachi et al., "Study of Intermittency in e^+e^- Annihilation at 29 GeV", preprint ANK-HEP-CP-90-50 (unpublished), K.Sugano, "Intermittency study in e^+e^- annihilations", in "Intermittency in High Energy Collisions", (World Scientific, Singapore 1991) p.1;
ALEPH Coll., D.Decamp et al., Z. Phys. C53 (1992) 21

L3 Detector and data acquisition

The Large Electron Positron (LEP) Collider of the European Laboratory for Particle Physics (CERN) was designed to produce Z^0 bosons and to study their properties in detail [1]. The LEP Collider is able to accelerate electrons and positrons to a center-of-mass energy of up to 100 GeV in the first phase of operation, and up to nearly 200 GeV in the second phase.

The accelerator is housed in a 26.7 km long tunnel roughly 50 to 150 meters under the surface at the French-Swiss border near Geneva (Fig. 8.1).

After pre-acceleration, the electrons and positrons are concentrated in equidistant bunches running in opposite directions. They collide in the middle of each of the four straight sections to produce Z^0 bosons, which subsequently decay into fermion-antifermion pairs. The decays are observed in the sections that have been equipped with the following detectors: L3, ALEPH, OPAL and DELPHI.

8.1 The L3 Detector

The data used in this analysis were obtained with the L3 detector [2]. The detector was designed to measure the four-momentum of all secondary particles produced in the decay of the Z^0 boson with emphasis on high-resolution measurement of electrons, photons and muons. The detector is installed in a 12m diameter magnet, which provides a uniform field of 0.5T along the beam direction. A perspective view of the L3 detector is shown in Fig. 8.2.

To describe the L3 detector in detail, it is first necessary to define the coordinate system used. The z -direction is defined to be along the beam pipe, in the direction of the electron beam; the x direction is towards the center of the LEP ring, the y axis in the vertical direction pointing upwards (see Fig. 7.2 of Chapter 7). In polar coordinates, θ is the angle from the positive z axis, φ the angle in the $x - y$ plane measured anticlockwise from the positive x -axis and r the absolute distance from the z -axis.

From the interaction point onwards, the following detectors are installed:

1) Silicon Microvertex Detector (SMD)

This detector has been installed inside the central track detector prior to 1994 LEP data taking. It is closest to the beam pipe and provides a good $r - \varphi$ and $r - z$ resolution over the polar-angle range $|\cos\theta| \leq 0.93$ and over the full azimuth.

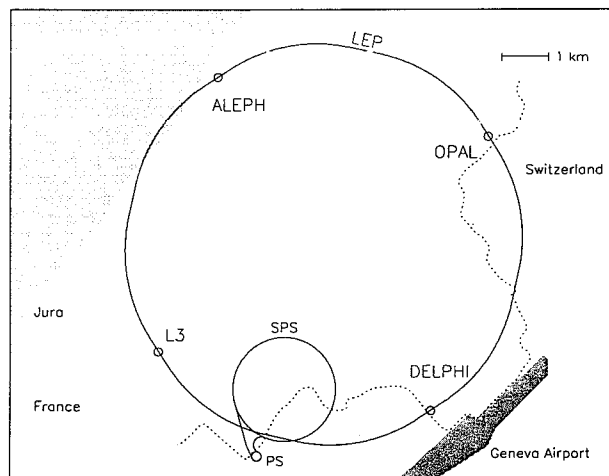


Figure 8.1: *The LEP Storage Ring.*

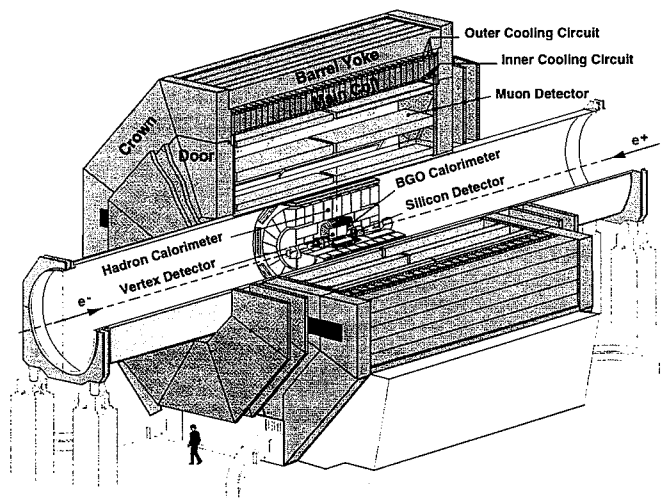


Figure 8.2: *View of the L3 Detector.*

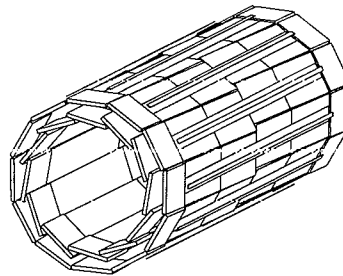


Figure 8.3: *View of the SMD ladders.*

The SMD is built from two cylindrical layers of double sided silicon microstrip detectors, covering 90% of the solid angle. Each layer consists of 12 modules, called ladders (see Fig. 8.3). There are 24 ladders, each of which is built from two separate half-ladders. Each half-ladder is built from two joined double-sided silicon sensors. The junction side of the sensors has implantation strips, which measure an $r - \varphi$ coordinate. There are other strips on the sensor's ohmic side, perpendicular to the junction side strips. They measure the $r - z$ coordinate.

2) Central Tracking Detector

The design purposes of the central tracking detector are:

- 1) to detect charged particles, measure the location and direction of their tracks;
- 2) to reconstruct the interaction point;
- 3) to determine the transverse momentum and the sign of the charge of the particles;
- 4) to reconstruct the decay vertices of particles with lifetimes longer than 10^{-13} sec.

The main part of the central track detector is the time expansion chamber (TEC) (see Fig. 8.4). It is divided radially into an inner and outer chamber. In the TEC chambers, all wires run parallel to the beam pipe. The inner chamber is divided into 12 sectors in φ , the outer chamber into 24 sectors. Each sector contains 8 anode wires (inner chamber) or 54 wires (outer chamber). The chamber is filled with a mixture of 80% CO_2 and 20% iso- C_4H_{10} at a temperature of 291K and a pressure of 1.2 bar. A charged particle passing through the wire chamber causes ionization in the gas of the chamber. The electrons, drifting in a homogeneous electric field of 0.9 kV/cm towards the nearest anode wire, produce a signal (so-called "hit") on this wire (see Fig. 8.5).

The outer TEC chambers are surrounded by the Z-detector needed to improve the z -determination of charged tracks. It consists of two cylindrical multiwire-proportional chambers with cathode-strip readout. The cathode strips are inclined with respect to the z -direction by 69° and 90° for the inner chamber, and by -69° and 90° for the outer chambers. The Z-detector covers a polar-angle range of $45^\circ < \theta < 135^\circ$.

3) Electromagnetic calorimeter (ECAL)

This detector measures photon and electron energies and their directions. To accurately estimate the energy, ECAL has a high stopping power for these particles. It is made of

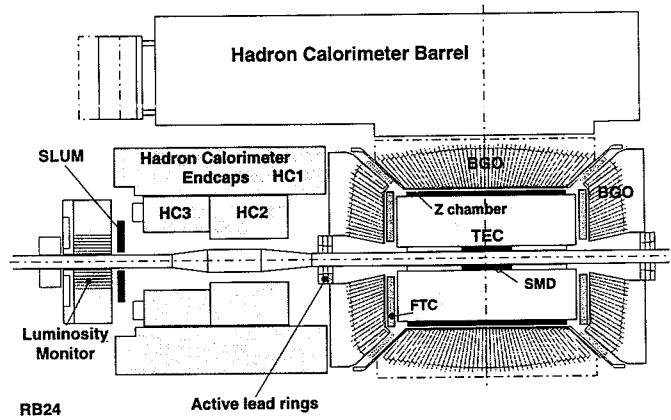


Figure 8.4: Cross section of the L3 detector. The forward direction is shown only on the left side.

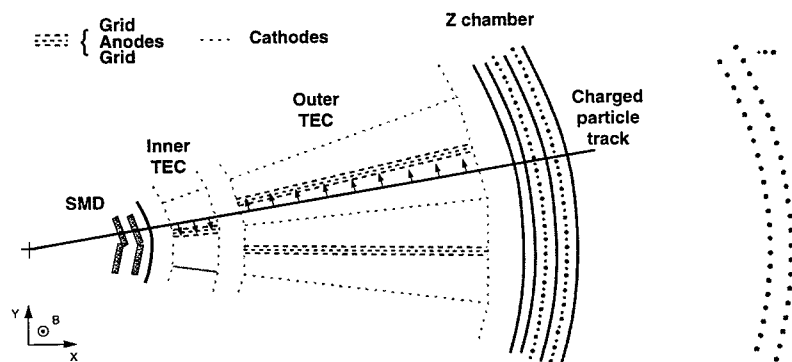


Figure 8.5: TEC viewed in the $x - y$ plane.

Bismuth Germanate (BGO) crystals, which are used both as absorber and scintillator. The calorimeter is sectioned into three main parts, barrel and two endcaps. The barrel surrounds the TEC and covers the polar angle range $42^\circ < \theta < 138^\circ$. The endcaps close the barrel in both sides.

4) Scintillation counter system

The system is located on the outer side of the ECAL barrel. The design purpose of the scintillation counter system is to distinguish genuine dimuon events from the cosmic background. This system consists of 30 single plastic counters and covers the polar angular range $34^\circ \leq \theta \leq 146^\circ$. An azimuthal coverage of 93% is achieved.

5) Hadron calorimeter (HCAL)

The energy of hadrons produced in the e^+e^- collisions is measured by the total-absorption technique in the electromagnetic and hadron calorimeters. The hadron calorimeter (HCAL) is placed just outside the scintillation counter system. It is made of depleted uranium absorber plates interspersed with planar proportional wire chambers and also acts as a filter allowing only non-showering particles to reach the precision muon detector.

The HCAL consists of a barrel and endcaps (Fig. 8.6). The barrel covers the central region ($35^\circ \leq \theta \leq 145^\circ$) and has a modular structure consisting of 9 rings of 16 modules each. The wires in alternating chambers are perpendicular to each other. This gives the possibility of a measurement in both the z and φ direction.

The endcaps cover the polar-angle regions $5.5^\circ \leq \theta \leq 35^\circ$ and $145^\circ \leq \theta \leq 174.5^\circ$ over the full azimuthal range. They extend the coverage of the hadronic calorimeter to 99.5% of 4π .

6) Muon filter

The purpose of an additional muon filter is to add absorption capacity to the hadron calorimeter, to ensure that only non-showering particles can reach the muon detector. The muon filter is divided into eight azimuthal sections, each containing 6 brass absorber plates.

7) Muon detector

Only muons with more than around 3 GeV momentum and neutrinos can reach the muon detector. The detector is built in the form of two ferris wheels, each containing 8 independent units or octants covering the full azimuthal angle and providing measurements in the $x - y$ plane. Each octant contains three layers covering a polar-angular range $45^\circ \leq \theta \leq 135^\circ$. The z -coordinate measurement of the muon track is performed by four layers of Z chambers.

8) Luminosity monitor

The luminosity monitor is designed to measure the LEP beam-beam luminosity inside the detector. The monitor consists of two electromagnetic calorimeters and two sets of proportional wire chambers. These chambers are situated symmetrically on either side of the interaction point. The luminosity is calculated by measuring the rate of small angle Bhabha events.

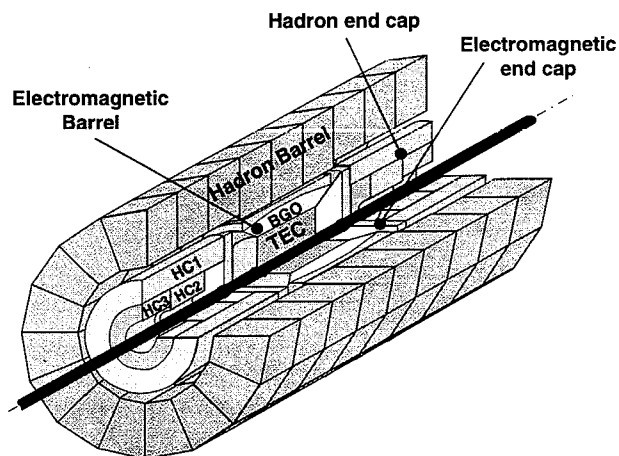


Figure 8.6: *Perspective view of the L3 hadron calorimeter.*

9) Trigger system and data acquisition

In order to maintain a reasonable tape writing rate, a complex trigger and data acquisition system is needed. Each of these systems consists of various logical levels. In the next subsection we shall consider the trigger system in detail.

8.2 Data acquisition and reconstruction

8.2.1 Trigger system

The main goal of the L3 trigger system is to record the detector signals from each beam crossing in which particles have come from the e^+e^- vertex. After each bunch crossing, the system decides whether or not an e^+e^- interaction has taken place. There are three levels of triggers in this system:

Level 1: The purpose of this level is a very fast decision on whether or not the event is interesting for further processing. This level takes the decision within $20 \mu s$. In the case of a positive decision, all the characteristics of an event are stored. A positive decision results in a dead time of $500 \mu s$. Level-1 has components based on the electromagnetic and hadron calorimeters, the luminosity monitors, the scintillation counters, the muon chambers, the SMD and TEC chambers.

Level 2: While the main aim of level-1 is to select interesting events, the level-2 trigger rejects background events selected by level-1. In this stage, an event can be analyzed more thoroughly. On a positive level-2 result, the event is processed to level-3.

Level 3: The level-3 trigger system has more time available than the lower level triggers. It performs more detail and complex calculations. The result of the calculations is a complete set of data from all the detector components.

In the case an event passes all three trigger levels, it is stored onto tape. The event typically demands 40 kB of tape storage.

8.2.2 Event reconstruction

The experimental data are stored in the form of raw information on tapes. To identify the physical content of an event, it is necessary to reconstruct the particles originating from e^+e^- collisions.

The REL3 program is the package used for the reconstruction of the L3 data. It reads and decodes data written by the L3 on-line data acquisition and, then, reconstructs data from each subdetector independently. After that, a special program AXL3 under the control of REL3 performs the global reconstruction. AXL3 creates the following objects representing the final hadrons:

1) Smallest resolvable clusters (SRCs): These objects are obtained by combining the energy deposits in the electromagnetic and the hadronic calorimeters. Usually, the number of SRCs does not coincide with the number of real particles (neutral and charged), since, for example, one SRC may be the result of more than one particle.

2) Tracks: These objects are results of combining signals from SMD and hits found in TEC. The tracks can belong only to charged particles. The information on the charge sign of particles and $\varphi - z$ coordinates of track momentum are available.

Besides, AXL3 performs a jet reconstruction from SRCs, vertex finding and muon candidate reconstruction using information from the muon chambers.

At the end, REL3 writes the reconstructed events on tapes. There are three main types of event format, all of which are in the form of ZEBRA structures [4, 5]:

1) The DRE (Data REconstructed) format. The DRE format contains both the completely reconstructed information (charged tracks, SRCs, jets, *etc.*) and the raw detector information (as TEC hits, channel-by-channel calorimeter data, *etc.*). These data occupy a large tape space (200Kb/event).

2) The DSU (Data SUmmary) format. It is similar to the DRE, except that a lot of the raw detector information is dropped. Besides, the DSU is packed. Once the event is read in, the packed information is automatically expanded in memory. A restricted re-reconstruction of data is still possible from the DSU format.

2) The DVN (Data from the AVNT bank) format corresponds to a small data set (~ 2 kb/event). This format contains only the main information on physical objects. No detector specific information is available any more and no refit of the events is possible. In contrast to the DSU format, the DVN format has the advantage that it may be analyzed extremely quickly. At the same time, this format, in principle, contains all physical information on the events.

In our further analysis, we shall use the data set written in the DVN format. The main reason for this is that all programs for the calculation of local characteristics of a data sample

are rather complicated and demand a lot of computation time when processing a large even sample.

8.2.3 Event simulation

High-precision measurements of LEP experiments require an understanding of the detector response to various signals. This cannot be performed analytically. Computer simulation is therefore, an important part of data analysis which allows us to understand:

- 1) the response of the detector to particle final states;
- 2) various systematic errors;

For this, one resorts to the Monte-Carlo (MC) techniques. The MC program generates the e^+e^- events in the following two steps:

Event generation

The goal of the event generators is to create the characteristics and a list of 4-vectors of outgoing particles according to a physical model of e^+e^- interactions (without detector characteristics). Since quantum mechanics gives us only probabilities for various outcomes independent events are created with the help of weighted pseudo-random numbers. In this thesis we shall use the JETSET event generator. We have given a short description of this generator in Chapter 7 of the thesis.

Event simulation

Ideal detector simulation:

The events created by the event generator are processed through the detector simulation in the same way as the real experimental data. The purpose is to simulate the response of sub-detectors to the generated final particles.

The L3 detector simulation program is called SIL3. It is based on the GEANT3 [3] package. The detector simulation program package GEANT3 contains the details of each subdetector geometry and performs a detailed simulation of all possible interactions of the final-state particles with the materials of the detectors. This simulation program has the element of randomness, because it includes random multiple scattering in random directions, interactions, decays, random noise of the detector, *etc.*

Real detector simulation:

Since the detector imperfections, such as dead cells and BGO crystals, disconnected sectors and inefficient wires vary with time during data taking, one needs to simulate the time-dependent detector to be able to do precise physics measurements. These imperfections are simulated during the reconstruction of the simulated events, by simply ignoring the signals from dead sectors and cells. The real detector simulation gives a better agreement between the data and the predictions from Monte Carlo than does the ideal detector simulation.

The Monte-Carlo events are written in DSU formats. Then, the MC events are usually rewritten in the DVN format. However, considerable amount of the MC information is dropped in the DVN format. Since the re-reconstruction of the MC data is impossible now usually there are two DVN MC sets, one for ideal detector MC and one for the real detector MC simulations.

Bibliography

- [1] LEP Design reports: vol. I "The LEP injector chain", CERN-LEP/TH/83-29 (1983), vol.II, "The LEP main ring", CERN-LEP/TH/84-01 (1984);
I. Wilson and H.Henke, "The LEP Main Ring Accelerating Structure", CERN-89-09 (1989)
- [2] L3 Coll, B.Adeva et al., Nucl. Inst. and Meth. A289 (1990) 35;
L3 Coll, O.Adriani et al., Phys. Rep 236 (1993) 1;
L3 Coll, M.Acciarri et al., Nucl. Inst. and Meth. A351 (1994) 300;
L3 Coll, M.Acciarri et al., Nucl. Inst. and Meth. A360 (1995) 103
- [3] R.Brun et al., "GEANT3", CERN DD/EE/84-1 (Revised), 1987
- [4] R. Brun, J.Zoll, "ZEBRA User's Guide", CERN/DD/EE/84.1, 1984
- [5] J.Swain and L.Taylor, "L3 Computing Guide", preprint of Northeastern University, NUB-3065, Boston, USA 1993

Charged-hadron selection

The investigations presented here are based on a sample of hadronic events at a center of mass energy of $\sqrt{s} \simeq 91.2$ GeV, taken during the 1994 LEP running period. The reconstructed hadronic events are stored in PDVN format (data in DVN format), a data set in which a vast amount of raw detector information has been dropped (see previous chapter). However, to obtain a relatively pure sample of hadronic events, an additional hadronic event selection is needed.

The investigation of multiplicity fluctuations in ever smaller phase-space windows demands a high degree of accuracy on the determination of the particle momentum and a good two-particle resolution. We shall restrict our analysis to charged particles. While neutral particles can only be detected in the calorimeters with lower resolution, charged particles give an additional information both in TEC and SMD.

Hadronic events produced in an e^+e^- reaction are selected by the following two methods:

- 1) Energy deposition in the electromagnetic and hadronic calorimeters.
- 2) Momentum measurement in TEC and SMD.

In the following, we describe, successively, two sets of cuts based on this information.

9.1 Calorimeter-based selection of hadronic events

For the selection of hadronic events on the calorimeter information, we use only SRCs with an energy larger than 100 MeV. After that, we set the following conditions

$$0.6 < E^C/\sqrt{s} < 1.4, \quad (9.1)$$

$$13 < N_{cl} < 75, \quad (9.2)$$

$$E_T/E^C < 0.4, \quad (9.3)$$

$$E_{||}/E^C < 0.4, \quad (9.4)$$

where E^C is the total energy observed in the calorimeters, N_{cl} is the number of calorimeter clusters, E_T is the energy imbalance in the plane perpendicular to the beam direction, $E_{||}$ is that along the beam direction.

The cuts defined above are approximately the same as those used in [1] for the 1993 data. The signature of $Z^0 \rightarrow q\bar{q}$ events is characterized by the total visible energy of hadronic events

which is always around the center-of-mass energy of the e^+e^- collision. Cut (9.1) is applied to reject background events connected with loss of energy in non-sensitive regions of the detector, missing energy due to invisible neutrinos, the two-photon process, and smearing due to the finite resolution of the calorimeters. Fig. 9.1a shows the distribution¹ for visible energy (after application of cuts (9.2) - (9.4)). Cut (9.1) is indicated by arrows. Data are shown by dots and Monte Carlo (MC) by the histogram. The peak on the left of the low-energy cut is caused by $\tau^+\tau^- (\gamma)$ events not simulated by MC [2].

The distribution in the number of SRCs and cut (9.2) are shown in Fig. 9.1b. As in Fig. 9.1a, a small peak to the left of the low-multiplicity cut is caused by $\tau^+\tau^- (\gamma)$ events [2]. Since the number of SRCs is proportional to the number of produced particles, the cut on the minimum number of clusters allowed in an event also rejects non-hadronic events having a low multiplicity. The physical reason of disagreement with MC programs for large N_{cl} is caused by an incorrect description of hadronic showers in BGO crystals of the calorimeter. To obtain better agreement with MC predictions, we apply an additional cut on the maximum number of clusters allowed, not applied in [1]. This cut rejects approximately only 1% of the events.

Since at LEP the laboratory frame coincides with the center of mass frame, hadronic events must be well balanced in energy flow. Hence, cuts (9.3) and (9.4) reject background (uranium noise, beam-gas, beam-wall interaction events) which, have no balanced energy flow (see Figs. 9.2a,b).

In addition to the selection criteria (9.1) - (9.4), events are required to be contained in the barrel region of the calorimeters, i.e. $35^\circ < \theta < 145^\circ$. This is achieved by the following requirement on the polar angle θ_{thr}^c of the event thrust axis determined from calorimeter clusters

$$|\cos \theta_{thr}^c| < 0.74. \quad (9.5)$$

After the calorimeter selection described above, a hadron sample consists of approximately 25% of the raw unselected events stored in the PDVN file.

9.2 Charged-particle selection

Further selection is carried out by means of the information on charged particles from TE and SMD. For this, we require that the direction of the event thrust axis be within the full acceptance of the central tracking chamber ($45^\circ < \theta < 135^\circ$). This cut automatically takes into account the acceptance of SMD, since it covers the polar angle range $21^\circ < \theta < 158^\circ$. Hence, we set the following condition on a hadronic event candidate

$$|\cos \theta_{thr}^T| < 0.7, \quad (9.6)$$

where θ_{thr}^T is the polar angle of the thrust axis determined from charged tracks only.

As in the previous section, each cut presented below is performed on a sample of data after application of all other cuts.

¹After the application of all other cuts to be discussed below, the total number of events N_{tot} is not identical for the various distributions presented here. To avoid N_{tot} -dependence, all distributions are normalized to one.

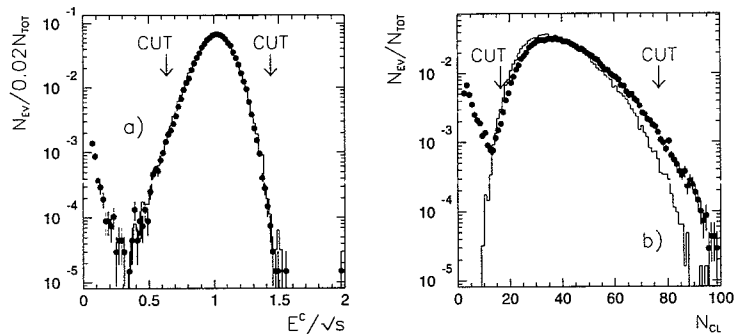


Figure 9.1: **(a)**: Visible-energy distribution (closed symbols) compared with the corresponding MC predictions. **(b)**: Cluster-multiplicity distribution with corresponding MC predictions. Data are represented by dots and MC by the histogram. All other cuts have been applied.

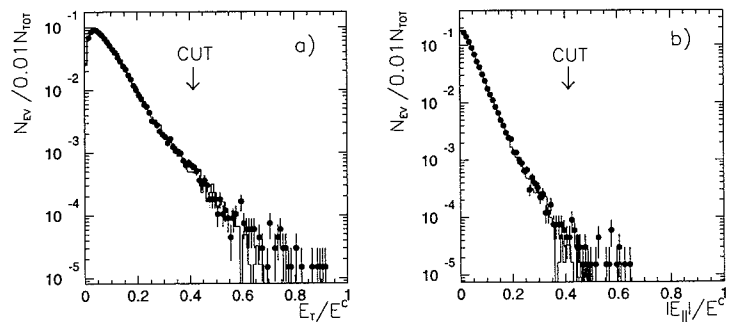


Figure 9.2: Transverse **(a)** and longitudinal **(b)** energy-imbalance distributions (closed symbols) compared with MC predictions (histogram). All other cuts have been applied.

9.2.1 Cuts on full events

The primary goal of the charged-particle cuts on full events is to further reduce background arising from beam-gas, beam-wall interaction events and from $e^+e^- \rightarrow l^+l^-(\gamma)$ processes, where l denotes a charged lepton (e, μ, τ).

1) Total-momentum cut

Fig. 9.3 shows the distribution of the total momentum sum of the charged-particle tracks, normalized to \sqrt{s} . Here, we set the following condition

$$\frac{P_{\text{tot}}}{\sqrt{s}} \equiv \frac{\sum_i |\vec{p}_i|}{\sqrt{s}} > 0.15, \quad (9.7)$$

where the sum runs over all tracks of an event, \vec{p}_i represents the momentum of particle i . Cut (9.7) is indicated in Fig. 9.3.

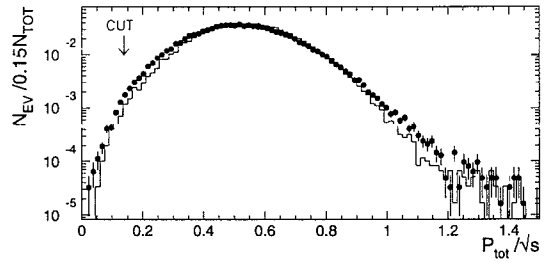


Figure 9.3: Total-momentum distribution for charged-particle tracks compared with MC. All other cuts have been applied.

2) Transverse and longitudinal-momentum cuts

As mentioned before, a hadronic event has to have a well balanced energy flow, and, hence, a well balanced sum of momentum components of tracks, perpendicular to and along the beam axis. We can reject different contaminations that do not have a balanced momentum sum if we set the following conditions (see Fig. 9.4)

$$\frac{P_{\parallel}}{P_{\text{tot}}} \equiv \frac{\sum_i |p_{\parallel i}|}{\sum_i |\vec{p}_i|} < 0.75, \quad \frac{P_{\perp}}{P_{\text{tot}}} \equiv \frac{|\sum_i \vec{p}_{T i}|}{\sum_i |\vec{p}_i|} < 0.75. \quad (9.8)$$

To avoid total-momentum dependence, the quantities P_{\parallel} , P_{\perp} are normalized to P_{tot} .

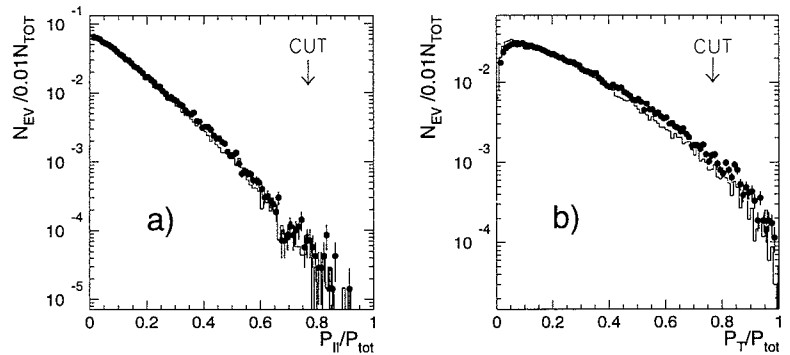


Figure 9.4: Longitudinal (a) and transverse (b) momentum imbalance distributions.

3) Cut on multiplicity of charged tracks

The charged-particle multiplicity N_{ch} distribution is presented in Fig. 9.5. Leptonic and two-photon events have a low multiplicity. To remove these, the requirement $N_{\text{ch}} \geq 5$ is applied. Good agreement between data and MC is observed.

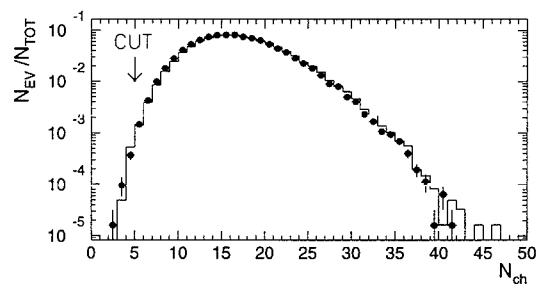


Figure 9.5: *Charged-track multiplicity distribution and the corresponding MC prediction.*

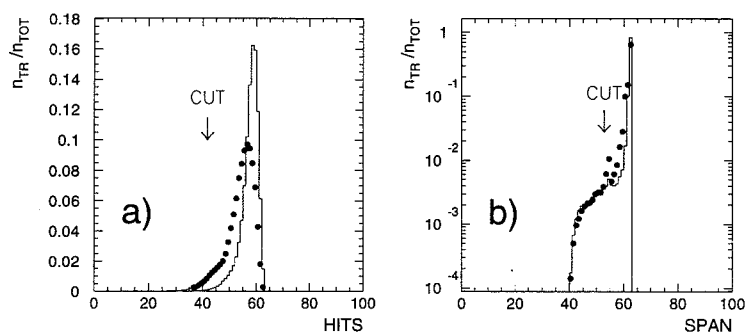


Figure 9.6: *Distribution for: (a) number of hits; (b) number of span.*

9.2.2 Selection of charged tracks

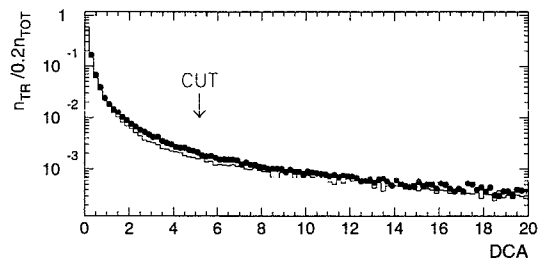
In this sub-section we consider selection procedures for tracks within an event already selected by the cuts described in the previous sections. The aim is to reject badly reconstructed tracks.

1) Selection on the number of hits

A charged particle passing through a wire chamber causes ionization in the gas of the chamber. The electrons, drifting to the nearest anode wire, produce a signal (“hit”) on this wire. Since TEC contains 62 wires (8 in the inner sector and 54 in the outer), the charged particle can produce a maximum of 62 hits. A charged track candidate is regarded to have at least 40 hits (Fig. 9.6a). As for previous years, a discrepancy between MC and data remains due to an underestimation of missing hits in the inner sector of TEC.

2) Selection on span

A particle track is reconstructed by combining hits. It can happen that the reconstruction program combines a track from hits belonging to different particles. In general, the misreconstructed track has a smaller length than that from a true particle. The length of a

Figure 9.7: *Distribution of DCA.*

track in terms of hits is the so-called span. It is defined as

$$\text{Span} = W_{\text{out}} - W_{\text{in}} + 1, \quad (9.9)$$

where W_{out} is the wire number of the outermost hit and W_{in} that of the innermost hit. The requirement for a track to have a span of at least 50 helps to reject mis-reconstructed tracks (see Fig. 9.6b).

3) *Cut on distance of closest approach*

Hadrons directly produced by Z^0 decay have to originate from the interaction vertex. A track can be extrapolated back to the vertex. The distance of closest approach (DCA) for the track is defined as the distance of the track to the interaction point in the plane perpendicular to the beam direction. The requirement of the DCA to be less than 5mm helps to correctly identify hadrons produced in the given reaction (Fig. 9.7). There are small discrepancies between data and MC which are not yet understood.

3) *Cut on transverse momentum*

A cut on the transverse momentum of a track with respect to the beam direction is applied because tracks with low transverse momentum cannot be measured accurately in TEC and cannot enter the calorimeter. To avoid any reconstruction error, each track is required to have a measured transverse momentum larger than 100 MeV/c.

4) *Cut on the azimuthal angle φ_2 between two neighboring tracks*

According to MC simulation [3, 4], hadrons resulting from τ decays in $e^+e^- \rightarrow \tau^+\tau^-$ reactions have a large value of angle φ_2 between two neighboring tracks in the $R - \varphi$ plane. By accepting events with φ_2 less than 170° , the background from τ decays is suppressed (see Fig. 9.8a).

5) *Cut on the polar production angle θ*

One of the features of the 1994 data stored in PDVN is the presence of small symmetric peaks at small forward and backward production angle θ (see Fig. 9.8b). These peaks are present also on the detector level of the MC program. Such a behavior of the distribution is expected from a shortcoming in the reconstruction programs for SMD where two hit

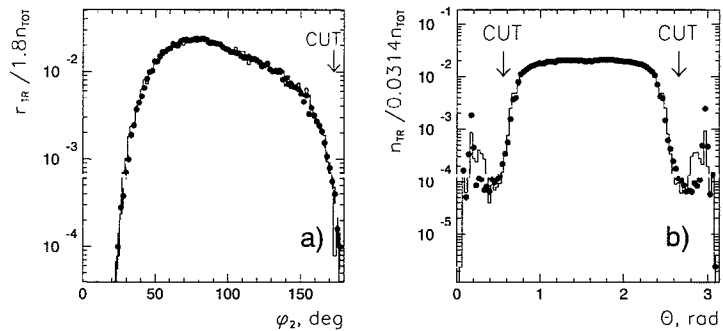


Figure 9.8: Distribution in: (a) azimuthal angle between two neighboring tracks; (b) the polar angle θ with respect to the beam axis.

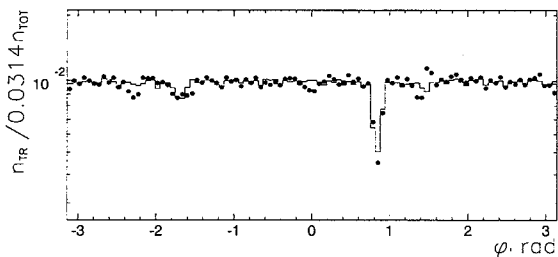


Figure 9.9: Distributions in the azimuthal angle φ with respect to the beam axis.

belonging to different particles are considered as one track almost parallel to the beam axis [5]. Since we use the PDVN data set for hadronic events, in which the detector information is very limited, the following cut is applied to eliminate these mis-reconstructed tracks

$$|\cos \theta| < 0.88. \quad (9.10)$$

It should be noted that we, of course, also reject real tracks. However, the number of such tracks is very small (less than one per cent) and the cut is applied for the data and MC.

6) Cut on azimuthal angle φ

During the 1994 run, the fourth outer sector of TEC had a limited efficiency (see the dip near $\varphi = 1$ rad in Fig. 9.9). To obtain a good agreement with the MC results, we included this dip in the simulation. Since we used the PDVN event format, we have done this *a posteriori*, randomly rejecting a corresponding fraction of tracks in the sector $0.7 < \varphi < 1.0$ rad. Analogously, we have simulated a small dip in the sector $-2.0 < \varphi < -1.6$ rad, which is also a result of bad efficiency in the corresponding TEC sector.

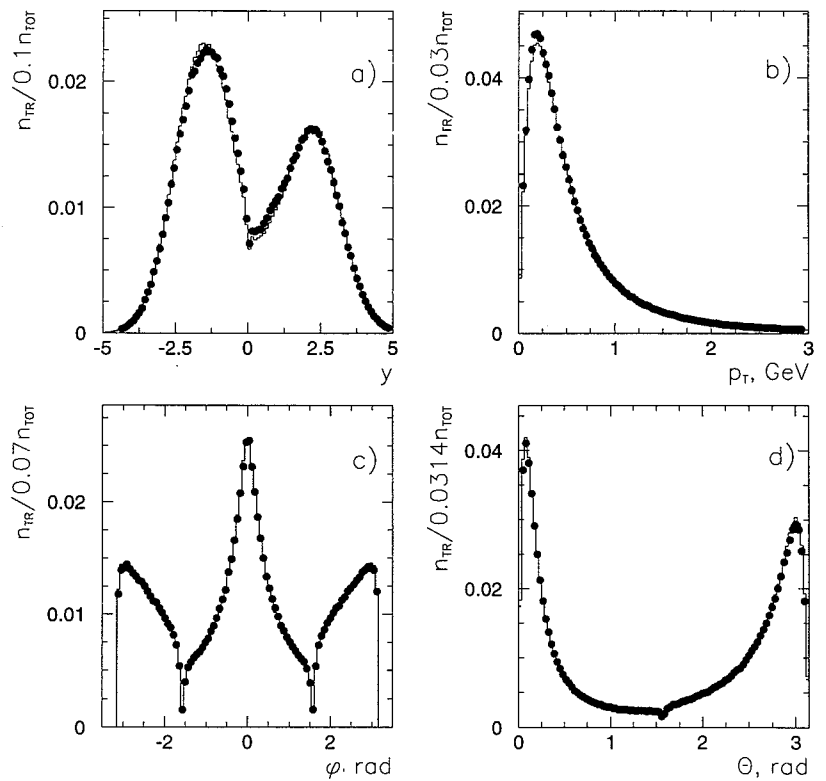


Figure 9.10: *Inclusive distributions for different variables measured with respect to the thrust axis.*

9.3 Inclusive distributions

Before the study of local properties of distributions, let us consider single-particle inclusive distributions. A comparison between the inclusive distributions for uncorrected data and detector-level MC provides the first test of the validity of the selection procedure described above. The event-thrust axis calculated for final-state hadrons is used as the event axis for the calculation of y , p_T , φ , θ .

The inclusive phase-space distributions for the given variables are presented in Fig. 9.10. The data are represented by full symbols. All distributions agree well with the MC or detector level. Only a slight systematic shift is seen for the rapidity distribution. It causes no systematic error for the calculation of local characteristics of the sample, since both MC and data distributions will be transformed to flat distributions. The asymmetry in Figs. 9.10a,d is due to the definition of the positive axis direction.

Bibliography

- [1] L3 Collaboration, M.Acciarri et al., Phys. Lett. B353 (1995) 145
- [2] F.Filthaut, "Hadronic Cross Section Measurements on the Z Resonance with the L_3 Detector", Ph.D. Thesis, Univ. of Nijmegen 1993, The Netherlands
- [3] A.A.Syed, "Particle Correlations in Hadronic Decays of the Z Boson", Ph.D. Thesis, Univ. of Nijmegen 1994, The Netherlands
- [4] L3 Collaboration, B.Adeva et al., Phys. Lett. B265 (1991) 451
- [5] H.De Boeck, private communication. I am indebted to this member of the L3 Collaboration for bringing this explanation to my attention.

Resolution

A measurement of local multiplicity fluctuations involves counting particles in small phase-space bins according to a given algorithm. To avoid systematic bias arising from limited detector resolution, one should find, first of all, the resolution of the L3 detector. The knowledge of this quantity will help to choose a minimum bin size for our study of local fluctuations.

For the determination of the resolution in the various variables used in our analysis, we use the Monte-Carlo technique [1]. Let X be the true value of a variable calculated from an event generated by Monte Carlo (MC). After generation according to present theoretical knowledge (generator level of MC), all tracks resulting from this event are processed through a simulation of detector properties (detector level of MC). In this stage, the program SIL3, based on the GEANT3 package, corrects the event for particle interactions with the detector material, limited resolution and acceptance of the detector and various detector imperfections. After the detector simulation, the MC event is reconstructed in the same way as a real LEP event. Thus, we obtain reconstructed MC events, which can be used for the calculation of the same variable after distortion by detector effects. Let X' be the value of this variable obtained from the event on the detector level of MC. Then, for a given event, one can find the difference

$$\delta X = X' - X. \quad (10.1)$$

All δX are histogrammed for a sufficiently large sample of MC events to grant a distribution for the resolution.

The resolution, obtained as described above, was investigated for the 1993 data in [1], when the SMD was not yet installed inside the TEC. Providing $r - \varphi$ and $r - z$ coordinate measurements over the polar-angle range $|\cos \theta| < 0.93$ and over the full azimuth, the SMD is expected to improve the resolution for the 1994 data. As we shall see below, this leads to a better resolution for all variables used in our analysis. In the following, we will describe the resolution in various variables, compared to those obtained for 1993 in the earlier study.

10.1 Resolution of variables with respect to the beam axis

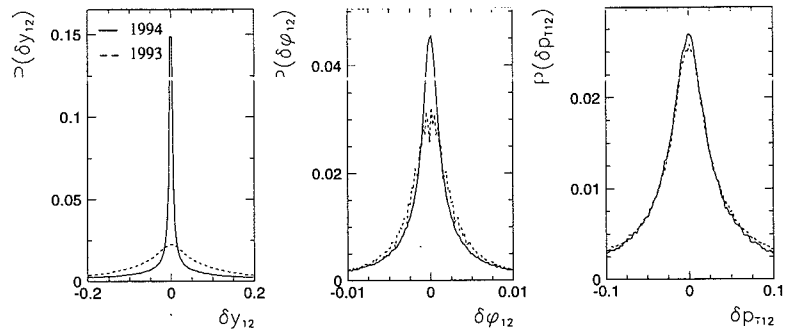


Figure 10.1: The resolution of various distance measures calculated with respect to the beam axis. The dashed lines show the 1993 MC, the solid lines represent the 1994 MC.

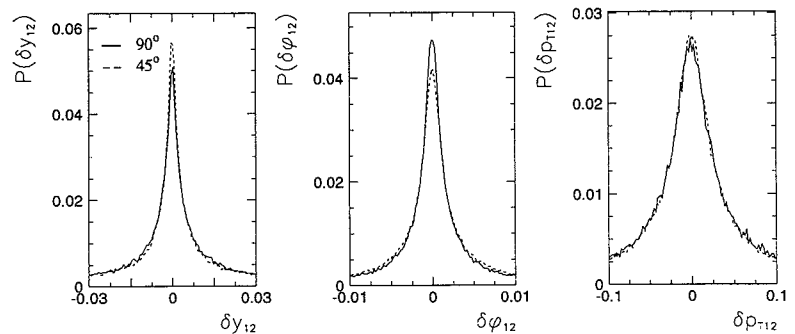


Figure 10.2: The resolution for distance measures calculated with respect to the beam axis. The solid lines show the histograms for a track pair with $1.46 \text{ rad} < \theta < 1.66 \text{ rad}$ (approximately perpendicular to the beam direction). The dashed lines show the histograms for track pairs with θ in the ranges $0.5 \text{ rad} < \theta < 0.9 \text{ rad}$ and $2.1 \text{ rad} < \theta < 2.5 \text{ rad}$.

For our analysis, we will use the following two-particle distance-measure variables:

- 1) rapidity difference $y_{12} = |y_1 - y_2|$ between two tracks;
- 2) azimuthal angle $\varphi_{12} = |\varphi_1 - \varphi_2|$ between two tracks;
- 3) transverse momentum difference $p_{T12} = |p_{T1} - p_{T2}|$ between two tracks.

Each of these variables is calculated, first using the generator-level MC sample (this gives the value of X in (10.1)), and then using the detector-level MC (the value X' in (10.1)). The differences δX are histogrammed after a run through 50,000 hadronic events of the JETSET 7.4 PS model. Fig. 10.1 shows the histograms obtained for the three variables. Since the histograms are normalized to unity, they represent, in fact, the probability density $P(\delta X)$ of a deviation δX from X after the L3 detector simulation. The dashed lines represent the histograms for the 1993 data, the solid lines those for the 1994 data. All histograms have lar

tails. Except for these tails, we assume that all these distributions, at least approximately, have Gaussian form, i.e. they result from a large number of independent contributions (the Central Limit Theorem). The value of half-width at half-maximum (HWHM) H_2 , which approximately equals the variance σ of the Gaussian distribution ($H_2 = 1.18\sigma$), can be used as a characteristic of the resolution.

It can clearly be seen from Fig. 10.1 that the resolution is better for 1994 than for 1993, in particular for y_{12} , but also for φ_{12} ¹. The HWHM values obtained for these variables from Fig. 10.1 are listed in Tab. 10.1. The statistical errors were estimated using three samples with equal number of events.

It should be pointed out that the resolution obtained above is an average, since the value of HWHM for each variable is affected both by the values of the distance measure and the position of the pair in the corresponding phase-space covered by TEC. As an example, Fig. 10.2 shows the dependence of double-track resolutions on the angle θ defining the position of a track pair in TEC. The resolution for rapidity is slightly better for pairs emitted at an angle $\theta \sim 45^\circ$ to the beam line, than perpendicular to the beam. For azimuthal-angle resolution, the situation is opposite. The resolution for transverse momentum is found to be almost θ -independent.

10.2 Resolution of variables with respect to the thrust axis

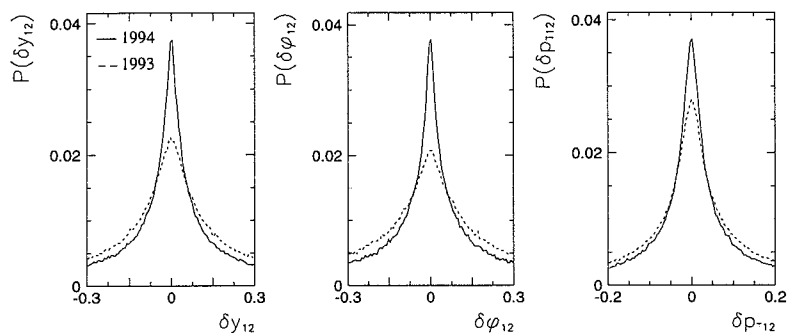


Figure 10.3: Resolution of distance measures calculated with respect to the thrust axis. The dashed lines represent the 1993 MC, the solid lines show the 1994 MC.

Since our main goal is to study fluctuations inside jets, we will pay more attention to the resolution of variables calculated with respect to the thrust axis.

Fig. 10.3 shows the histograms for the resolution of the variables used in Fig. 10.1, but now defined with respect to the thrust axis. The last two lines of Table 10.1 give the HWHM

¹To avoid a bias connected with different statistics and selection procedure for the 1993 and 1994 runs, we have repeated the calculations for the two-track resolutions for 1993 using the same cuts as for 1994. Our results are rather close to those obtained in [1]. The difference is mainly due to the smaller number of MC events (2500) used in [1].

values of these histograms. As we can see, the resolution is worse for the variables with respect to the thrust axis than for those defined with respect to the beam axis. Moreover, in contrast to the resolution calculated with respect to the beam, the HWHM values are rather similar for all distance measures. This is mainly due to the fact that this resolution involves the knowledge of the resolution in all three variables calculated with respect to the beam axis. Besides, the systematic uncertainties in the determination of the event thrust may affect the resolution.

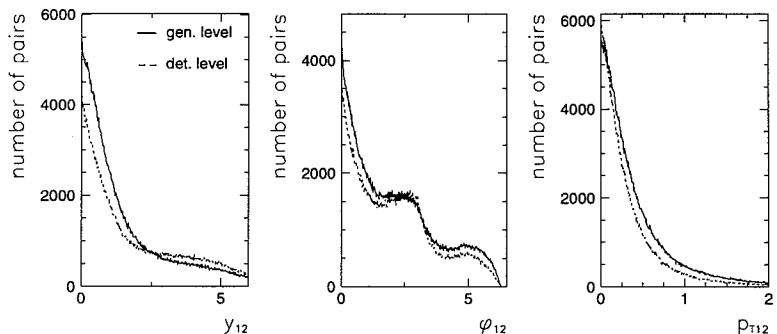


Figure 10.4: *Two-particle distance measures calculated with respect to the thrust axis on generator level (solid lines) and detector level (dashed lines) of MC. The total number of events is the same for both cases (50.000 MC events). The histograms are presented without normalization to unity.*

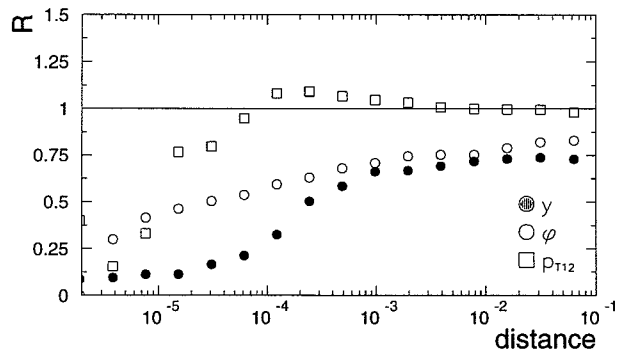


Figure 10.5: *Ratio of the distance measures on detector-level MC to generator-level MC as a function of distance between two tracks (50.000 MC events).*

Fig. 10.4 represents the number of pairs as a function of the distance measures y_{12} , φ_{12} , p_{T12} obtained on generator-level MC (solid lines) and on detector-level MC (dashed lines). The number of events for both distributions is 50.000. As we see, distortions of the two-particle distances from JETSET 7.4 are visible and have a quite complicated character.

To study distortions from two-track separation after detector simulation for a small value of the distance measures, let us consider the ratio R of the number of pairs on detector-level

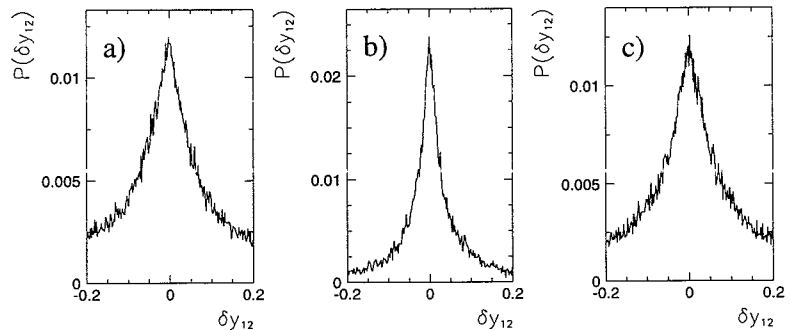


Figure 10.6: Resolution of rapidity difference defined with respect to the thrust axis for the three domains of y (on generator level of MC): **a)** $-2.2 < y < -1.8$, $H_2 = 0.060(5)$; **b)** $-0.2 < y < -0.2$, $H_2 = 0.025(7)$; **c)** $1.8 < y < 2.2$; $H_2 = 0.045(5)$.

to generator-level MC. Fig. 10.5 shows the value of R as a function of the distance between tracks y_{12} , φ_{12} , p_{T12} . For all distance measures, with the exception of large p_{T12} , $R < 1$, since the number of tracks on the detector level of MC is smaller than that on the generator level. For all distance measures, the value of R decreases with decreasing distance between tracks, because the detector suffers from a limited two-track separation and this experimental bias increases with decreasing distance between tracks.

From the last line of Table 10.1 we deduce that the resolution of the distance measure is 0.05 for y_{12} and above 0.03 for the other two variables. Of course, the smallest bin size in the analysis of fluctuations will have to be larger than this resolution. From Fig. 10.5 we can see that track losses are still acceptable and can be correctable.

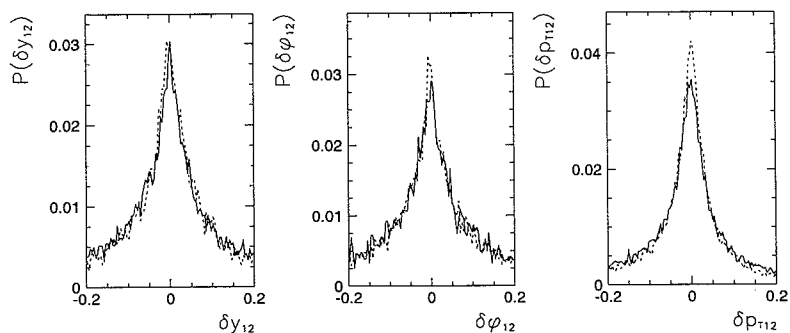


Figure 10.7: Resolution of distance measures calculated with respect to the thrust axis. The solid lines show the histograms for $|\cos \theta_{\text{thr}}| < 0.1$, the dashed lines correspond to $|\cos \theta_{\text{thr}}| > 0.6$.

The HWHM obtained in such an approach are averages, because the value of δX depends

	y	φ, rad	$p_T, \text{GeV}/c$
	with respect to the beam axis		
1993 data	0.07 ± 0.01	$(0.25 \pm 0.05) \cdot 10^{-2}$	0.028 ± 0.002
1994 data	0.01 ± 0.01	$(0.10 \pm 0.05) \cdot 10^{-2}$	0.025 ± 0.002
	with respect to the thrust axis		
1993 data	0.10 ± 0.02	0.12 ± 0.01	0.045 ± 0.005
1994 data	0.05 ± 0.02	0.03 ± 0.01	0.031 ± 0.005

Table 10.1: H_2 for different variables calculated both from 1993 and 1994 MC events.

on the variable value in the corresponding phase space covered by TEC. The dependence of the HWHM is not very strong, but still visible. As an illustration, we present in Fig. 10.6(a) the resolution of rapidity calculated with respect to the thrust axis for different rapidity domains (1994 MC). Fig. 10.6(b) shows the distribution with the smallest value of HWHM. This figure corresponds to the central region of the rapidity distribution, i.e. to the broad valley in the single-particle density ($-0.2 < y < 0.2$).

Furthermore, the HWHMs weakly depend on the value of the distance measures y , φ_{12} and p_{T12} . Table 10.2 shows the HWHM for various cuts on the distance measures. These results were obtained in one measurement, so the values of HWHM are given without statistical errors, but these are expected not to be very large.

Moreover, the HWHM obtained are affected by the direction of the thrust axis in individual events. In Fig. 10.7, we present two possible situations, when the thrust axis is almost perpendicular ($|\cos \theta_{\text{thr}}| < 0.1$) and at an angle ($|\cos \theta_{\text{thr}}| > 0.6$) to the beam line. The resolution of φ_{12} and p_{T12} is better for the second case. This is due to construction of TEC, in which wires are stretched parallel to the beam direction.

We recall that, initially, the L3 collaboration has optimized its detector for the best precision on electrons, muons and photons. As we see now, the resolution of rapidity defined with respect to the thrust axis is quite similar to that for the DELPHI detector, where two tracks could be resolved if their rapidities differed by more than 0.04 units [2]. This means that, using the SMD for the 1994 run, the L3 detector has become a good tool to measure accurately charged hadronic tracks.

10.3 Resolution of the squared four-momentum difference

For the study of local fluctuations to be presented below, it is also necessary to find the resolution for the squared four-momentum difference Q_{12}^2 between two tracks. This Lorentz invariant variable is defined as

$$Q_{12}^2 = -(p_1 - p_2)^2, \quad (10.1)$$

	$y_{12} < 0.1$	$0.1 < y_{12} < 0.5$	$0.5 < y_{12} < 1.5$
y_{12}	0.04	0.035	0.045
φ_{12}	0.035	0.025	0.035
p_{T12}	0.031	0.030	0.030

	$p_{T12} < 0.1$	$0.1 < p_{T12} < 0.5$	$0.5 < p_{T12} < 1.5$
y_{12}	0.04	0.05	0.06
φ_{12}	0.035	0.03	0.03
p_{T12}	0.03	0.035	0.07

	$\varphi_{12} < 0.1$	$0.1 < \varphi_{12} < 0.5$	$0.5 < \varphi_{12} < 1.5$
y_{12}	0.035	0.025	0.04
φ_{12}	0.04	0.03	0.04
p_{T12}	0.03	0.03	0.03

Table 10.2: H_2 for variables with respect to the thrust axis for various cuts on distance measures calculated on generator-level MC.

with p_1 and p_2 being the four-momentum of particles 1 and 2, respectively. The histogram for δQ_{12}^2 in Fig. 10.8 shows that the resolution for the 1994 MC run is better than that for 1993. The HWHM is equal to $0.011 \pm 0.003 \text{ GeV}^2/c^2$ for 1994 ($0.020 \pm 0.003 \text{ GeV}^2/c^2$ for 1993).

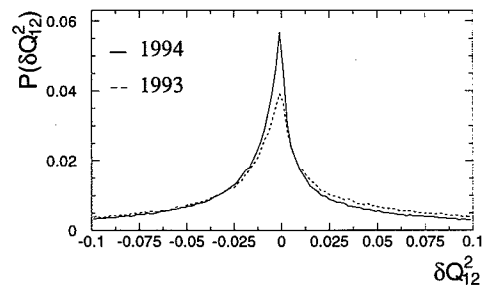


Figure 10.8: Resolution of the squared four-momentum difference Q_{12}^2 .

The obtained HWHM are an average characteristic of the resolution of the squared four-momentum difference. In contrast to the distance measures defined with respect to the

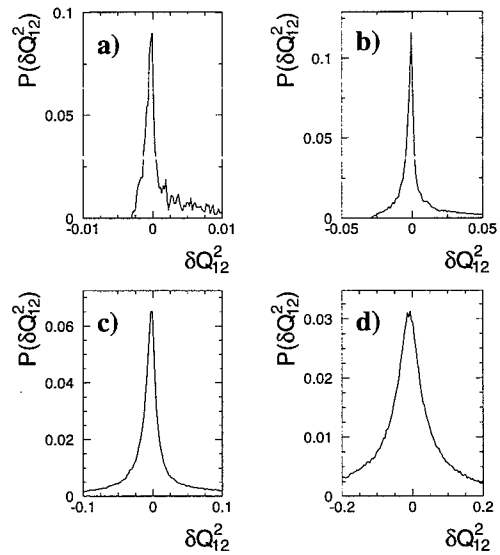


Figure 10.9: *Two-track resolution for the squared four-momentum difference for different cuts on Q_{12}^2 calculated on generator-level MC: a) $Q_{12}^2 < 3 \cdot 10^{-3}$; b) $3 \cdot 10^{-3} < Q_{12}^2 < 0.03$; c) $0.03 < Q_{12}^2 < 0.3$; d) $Q_{12}^2 > 0.3$ (in units of GeV^2/c^2).*

thrust axis, this value strongly depends on the value of Q_{12}^2 , itself. In Fig. 10.9, we present the dependence of the resolution for Q_{12}^2 on the value of Q_{12}^2 . The best resolution is obtained for small values of Q_{12}^2 . The corresponding HWHM are given in Table 10.3. Note, that an asymmetry of the distributions increases with decreasing of Q_{12}^2 .

	H_2
$0 < Q_{12}^2 < 3 \cdot 10^{-3}$	$(0.5 \pm 0.3) \cdot 10^{-3}$
$3 \cdot 10^{-3} < Q_{12}^2 < 0.03$	$(0.25 \pm 0.6) \cdot 10^{-2}$
$0.03 < Q_{12}^2 < 0.3$	$(0.70 \pm 0.04) \cdot 10^{-2}$
$0.3 < Q_{12}^2$	$(0.40 \pm 0.04) \cdot 10^{-1}$
all Q_{12}^2	$(0.11 \pm 0.03) \cdot 10^{-1}$

Table 10.3: H_2 as a function of Q_{12}^2 calculated on generator-level Monte Carlo, in units GeV^2/c^2 .

As we have seen, the distance between the two tracks on the detector level is not the same as that on the generator level; for Gaussian smearing of track parameters, the prob-

bility for distance measures to be distorted by less than one HWHM is approximately 0.8. In practice, this probability is less than 0.8 due to non-Gaussian tails in the resolution. However, if the distance between two tracks is smaller than some value (which is much less than the corresponding HWHM), then the two tracks are interpreted as one track and we completely lose the information on fluctuations. Hence, it is important to know the smallest distance between two-tracks, i.e., two-track separation at which the two particles can still be distinguished by the detector.

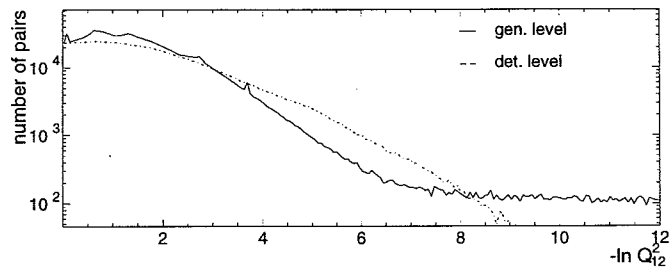


Figure 10.10: Number of pairs as a function of the squared four-momentum difference for the generator level of MC (solid line) and for the detector level of MC (1994). Both histograms are presented without normalization to unity.

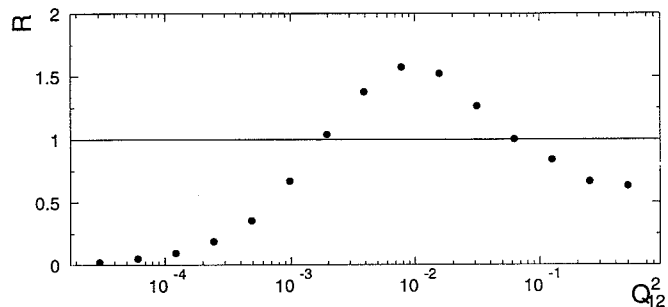


Figure 10.11: Ratio of pairs on detector-level to generator-level MC as a function of Q_{12}^2 .

To find the smallest distance for Q_{12}^2 , we present in Fig. 10.10 the number of pairs as a function of $-\ln Q_{12}^2$ for the generator level of MC (solid line) and the same distribution on the detector level of MC (dashed line) for 1994. The number of events is the same ($1.5 \cdot 10^4$) for both cases. For $-\ln Q_{12}^2 > 8$, the number of particle pairs becomes smaller on the detector level than on the generator level. Then, the distribution on detector-level MC goes to zero as the value of $-\ln Q_{12}^2$ increases. The value of two-track separation, therefore, is equal to $-\ln Q_{12}^2 = 9$ or $Q_{12}^2 = 1.2 \cdot 10^{-4} \text{ GeV}^2/c^2$.

The peaks presented on the histogram of the generator level of JETSET 7.4 PS model are found to be a consequence of resonance decay. Due to the detector smearing, such peaks are too small to be visible on the detector level.

Fig. 10.11 shows the ratio R of the number of two-particle tracks on detector-level to generator-level Monte Carlo as a function of Q_{12}^2 . In contrast to y_{12} and φ_{12} in Fig. 10.5 the distribution has a tendency to increase with decreasing Q_{12}^2 for not very small Q_{12}^2 and then drops very rapidly when Q_{12}^2 becomes too small. Note that the p_{T12} distance measure has the same feature (see Fig. 10.5).

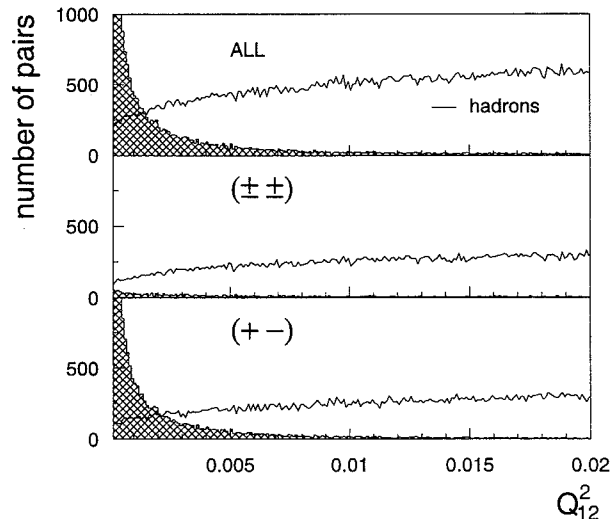


Figure 10.12: *The number of pairs for different charged-particle combinations as a function of Q_{12}^2 . The lines represent the number of hadronic pairs, the hatched areas indicate the contributions of electrons and positrons. The total number of events is 300k (generator level) of JETSET 7.4 PS.*

To define the minimum value of Q_{12}^2 to be used for the study of local fluctuations, we shall use the HWHM corresponding to the region $0.03 < Q_{12}^2 < 0.3$. This value is therefore chosen to be 0.007. The reason for this is that the smallest value of Q_{12}^2 has to be large enough to ensure that the contribution to the local fluctuations from the Dalitz e^+e^- pairs is small. To illustrate this point, Fig. 10.12 shows the JETSET 7.4 PS predictions for the number of hadronic pairs (solid lines) and e^+e^- pairs (hatched areas). The figure indicates that e^+e^- Dalitz decay products are the major source of the observed signal in the region $Q_{12}^2 < 0.005 - 0.007 \text{ GeV}^2/c^2$. Hence, our measurements will not be affected by this effect if we require $Q_{12}^2 \geq 0.007 \text{ GeV}^2/c^2$. In addition, this cut reduces possible contaminations from photon conversion not correctly reproduced in the simulation.

10.4 Determination of the smallest bin size

	H_2	H_3	H_4	H_5
y_{12}	0.05 ± 0.02	0.07 ± 0.03	0.09 ± 0.03	0.10 ± 0.04
φ_{12}, rad	0.03 ± 0.01	0.04 ± 0.01	0.05 ± 0.02	0.06 ± 0.02
θ_{12}, rad	0.013 ± 0.001	0.018 ± 0.01	0.022 ± 0.002	0.026 ± 0.002
$p_{T12}, \text{GeV}/c$	0.031 ± 0.005	0.043 ± 0.007	0.054 ± 0.008	0.062 ± 0.01

Table 10.4: H_i of the variables defined with respect to the thrust axis (1994 MC).

To reduce possible systematic bias arising from limited detector resolution, one needs to estimate the minimum bin size for the study of local fluctuations. Since the calculations of the NFMs and BPs involve the knowledge that many particles are in the same bin, we need to know the *many-particle* resolution. We restrict ourselves to not more than a 5-track resolution. In fact, this is enough for the determination of the smallest bin size for the fifth-order bunching parameters. We will also use such a 5-track resolution for the calculation of normalized factorial moments. However, strictly speaking, one should remember that an exact calculation of even the lowest order of NFMs involves the knowledge of the resolution for more than five particles.

The easiest way to estimate the resolution of many tracks is again to assume a Gaussian form of the resolution functions for two tracks. If we have i independent random variables distributed with an equal variance σ_1 according to the Gaussian law, then the distribution for the sum of these variables has the following variance

$$\sigma = \sqrt{i} \sigma_1^2. \quad (10.3)$$

According to this property of Gaussian distributions, the HWHM H_i for i -particle resolution has the following form

$$H_i \simeq \sqrt{(i-1)H_2^2}. \quad (10.4)$$

The values of H_i are given in Table 10.4.

The value of H_5 obtained for a given variable gives us the smallest bin size to be used for further calculations. In addition to the variables studied before, in Table 10.4 we also give the resolution of θ_{12} defined with respect to the thrust axis.

Bibliography

- [1] A. A. Syed, "Particle Correlations in Hadronic Decays of the Z Boson", Ph.D. Thesis
Univ. of Nijmegen 1994, The Netherlands
- [2] DELPHI Coll., P.Abreu et al. Nucl. Phys. B386 (1992) 471

11

Transformation of variables

11.1 Motivation

In the ideal limit, when the results of the analysis are independent of the total number of experimental events and the phase-space interval δ tends to zero, the choice of a particular variable to study local fluctuations is irrelevant. In practice, however, it is necessary to consider a restricted number of events and a non-zero interval δ . In this case, the experimental results strongly depend on the shape of the single-particle spectrum [1]. In this section, we begin with an explanation of the reason for this to occur.

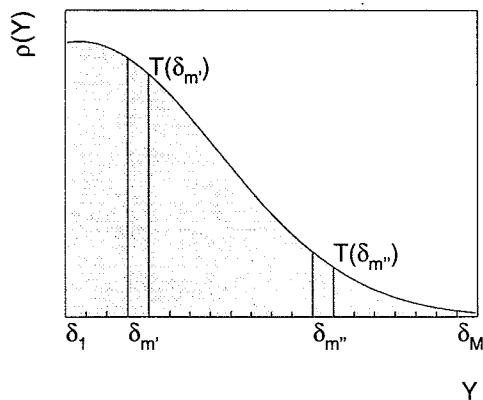


Figure 11.1: *Bin-splitting measurement of local fluctuations for a non-flat single-particle density*

Let us consider some characteristic $T(\delta_m)$ of local fluctuations in the small phase-space interval δ_m of a particular variable Y . The index $m = 1, \dots, M$ defines a given bin, with M representing the total number of such bins (see Fig. 11.1). In general, the phase space of the variable Y can be non-uniformly populated by particles. This means that the single-particle distribution (or inclusive density)

$$\rho(Y) = \frac{1}{N_{\text{ev}}} \frac{dn}{dY} \quad (11.1)$$

(N_{ev} is the total number of events in the sample, n is the number of particles) in Y can be any function of Y .

Let us consider the simplest choice, $T(\delta_1) = T(\delta_2) = \dots = T(\delta_M)$, i.e., $T(\delta_m)$ is independent of the position of the bin considered. This case corresponds, for example, to factorial moments with bin-dependent local (“vertical”) normalization $F_q = \langle n_m^{[q]} \rangle / \langle n_m \rangle^q$, because these quantities are approximately independent of the average multiplicity in the bin m . In practice, of course, the values of $T(\delta_m)$ do not agree exactly for different bins m due to experimental errors. Traditionally, to obtain the most probable value, one averages over all bins m of equal size $\delta_m = \delta$

$$T(\delta) = \frac{1}{M} \sum_{m=1}^M T(\delta_m). \quad (11.2)$$

If we assume that the measurements for different bins $T(\delta_m)$ are independent¹, then the statistical error (variance) for $T(\delta)$ can be estimated as follows

$$\Delta T(\delta) = \frac{1}{M} \sqrt{\sum_{m=1}^M [\Delta T(\delta_m)]^2}, \quad (11.3)$$

where $\Delta T(\delta_m)$ is the statistical error of $T(\delta_m)$.

Obviously, we can perform an experimental calculation of $T(\delta_m)$ only for events which contain at least two particles in the bin δ_m . Because of the limited statistics, the number of events to be used for our calculation of the $T(\delta_m)$ varies with the position of the bin. For example, for the calculation of $T(\delta_{m''})$, we can use only a small fraction of the total events, while the calculation of $T(\delta_{m'})$ involves a much large number of events. Hence, the statistical error for $T(\delta_{m''})$ is larger than that for $T(\delta_{m'})$. Clearly, this affects the final calculation of the statistical error of $T(\delta)$, and the total statistical error $\Delta T(\delta)$ may be rather large.

The problem becomes even more acute when one studies the behavior of quantities which are affected by the shape of the phase-space density. For example, the usual factorial moments $\langle n_m^{[q]} \rangle$ without local normalization depend on the average local multiplicity $\langle n_m \rangle$ in the given bin, and, hence, on the shape of the inclusive density. Then, the expression $T(\delta_1) = T(\delta_2) = \dots = T(\delta_M)$ is not correct, even on the theoretical level. In this case, the method (11.2) of increasing statistics by bin averaging cannot be meaningful: both $T(\delta)$ and $\Delta T(\delta)$ strongly influenced by the form of the single-particle inclusive density.

Our conclusion is that the best choice of a variable for the experimental calculation of local properties of the sample is one having a flat phase-space distribution. Since most variables of interest to us have non-flat single-particle densities, we have to resort to a transformation of these variables to new “cumulative” variables with a flat single-particle spectrum.

11.2 One-dimensional cumulative variable

A method of transformation of any one-dimensional variable Y into a cumulative variable $X(Y)$ with the desired flat one-particle phase-space distribution has been proposed independently by Ochs [2] and by Białas and Gazdzicki [3].

¹This is a rather strong assumption, since, as a rule, there are correlations between different bins.

Let us assume that the single-particle density in a variable Y is measured and given by the inclusive distribution $\rho(Y)$. Then, the cumulative variable is defined as

$$X(Y) = C^{-1} \int_{Y_{\min}}^Y \rho(Y') dY', \quad C = \int_{Y_{\min}}^{Y_{\max}} \rho(Y') dY', \quad (11.4)$$

where Y_{\min} and Y_{\max} are the lower and upper phase-space limits of the variable Y .

The variable $X(Y)$ has a flat density for any Y by construction, since

$$\rho(Y)dY = \rho(Y(X)) \left| \frac{\partial Y}{\partial X} \right| dX = \rho(Y(X)) \left| \frac{\partial X}{\partial Y} \right|^{-1} dX = CdX, \quad (11.5)$$

i.e. $\rho(X) = C = \text{const.}$ From the definition (11.4) it follows that

$$0 \leq X(Y) \leq 1. \quad (11.6)$$

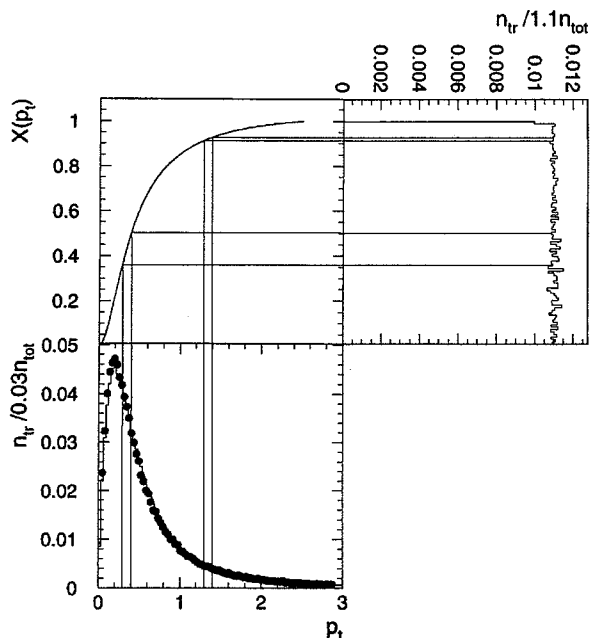


Figure 11.2: *One-dimensional Bialas-Gazdzicki-Ochs transform for the inclusive p_T distribution calculated with respect to the thrust axis. The distribution in the corresponding cumulative variable is shown only for MC.*

In Fig. 11.2 we illustrate this method for the inclusive p_T distribution obtained from MC events. As we can see, transformation (11.4) stretches the highly populated phase-space intervals of the original variable and squeezes scarcely populated intervals. For our calculation of $\rho(p_T)$, we use 10^4 bins in the original variable Y .

Fig. 11.2 illustrates that the method is not perfect. Though the distribution in variable $X(p_T)$ is relatively flat, it contains fluctuations. The fluctuations are larger for high particle density in the original variable, since a relatively small number of bins in Y variable contributes and the effect of non-matching bin boundaries is strong there.

11.3 Multi-dimensional transformation

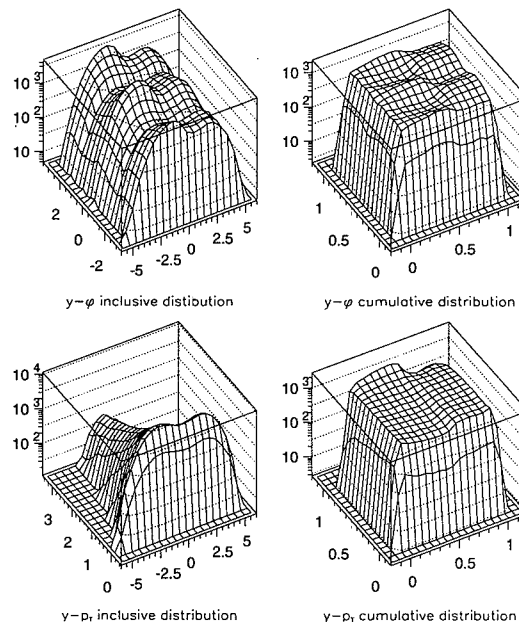


Figure 11.3: *Two-dimensional Ochs transform.*

When increasing the number of dimensions, the problem of non-uniformity of the phase space distribution becomes of primary importance. The method described above can be naturally extended to multi-dimensional phase space. To find cumulative variables $X_1(y)$, $X_2(p_T)$, $X_3(\varphi)$ for which $\rho(X_1, X_2, X_3)$ is constant, Biała and Gazdzicki proposed to perform the transformation according to the following algorithm [3]

$$(y, p_T, \varphi) \rightarrow (X_1, p_T, \varphi) \rightarrow (X_1, X_2, \varphi) \rightarrow (X_1, X_2, X_3), \quad (11.7)$$

each time using the density of particles in the corresponding set of variables.

From an experimental point of view, such a method is rather difficult to carry out due to computer memory limitations. This is because, first of all, we should find the three-dimensional inclusive distribution $\rho(y, p_T, \varphi)$ calculated in a very fine grid. This can be done by means of a three-dimensional array. To obtain stable results on the normalized factoria

moments and bunching parameters, each dimension of this array must be considerably larger than the total number of bins used for the calculations of the local fluctuations.

However, if the three-dimensional inclusive density factorizes, i.e.,

$$\rho(y, p_T, \varphi) = \rho(y) \rho(p_T) \rho(\varphi), \quad (11.8)$$

then the one-dimensional definition (11.4) can be applied separately to the independent variables y , p_T , φ (Ochs method [2]). This (rather strong) assumption leads to the following three independent transformations

$$\rho(y) \rightarrow \rho(X_1), \quad \rho(p_t) \rightarrow \rho(X_2), \quad \rho(\varphi) \rightarrow \rho(X_3). \quad (11.9)$$

The methods of Ochs and Białas - Gazdzicki have been compared in [4]. It has been found that both lead to approximately the same results for the behavior of the NFM. So, in view of its simplicity, we will only use the Ochs method here.

As an example of the Ochs transformation, we consider the two-dimensional transformations for the variables y , p_T , φ with respect to the thrust axis. Fig. 11.3 shows the corresponding two-particle distributions before (left figures) and after the Ochs transformation (right figures). In the latter, the two-dimensional distributions are almost flat. Nevertheless, some residual structure due to correlations between the variables is visible in the transformed distributions. This effect can exert a substantial negative influence in a higher-dimensional case. Further, for the three-dimensional study, we shall therefore only use quantities which do not require bin splitting and the Ochs transformation.

As a final remark, note that after the Białas-Gazdzicki-Ochs transformation, the definition of the smallest bin size according to two-track resolution becomes a non-trivial task. If one splits the transformed distribution into bins with equal size, the actual bin size of the original variable will be smaller for large single-particle density and larger for small density. To reduce possible systematic bias arising due to insufficient detector resolution for a large single-particle density of the original variable, we will use the five-particle resolution instead of the two-particle one.

Bibliography

- [1] K.Fiałkowski, B.Wosiek and J.Wosiek, Acta Phys. Pol. B20 (1989) 639
- [2] W.Ochs, Z. Phys. C50 (1991) 339
- [3] A.Białas and M.Gazdzicki, Phys. Lett. B252 (1990) 483
- [4] F.P.M.Botterweck, "Density Fluctuations in π^+ / K^+ p Interaction at 250 GeV/c, Ph.D Thesis. Univ. of Nijmegen, 1992, The Netherlands

Experimental Analysis of Local Fluctuations

In this chapter, we present an experimental investigation of local fluctuations in the final-state hadron system produced in Z^0 decays at $\sqrt{s} \simeq 91.2$ GeV. The final-state hadrons were recorded with the L3 detector during the 1994 LEP running period. The calculations are based on approximately 810k hadronic events selected by the procedure described in Chapter 9.

For comparison with the experimental data, two Monte-Carlo (MC) samples of multihadronic events are generated with JETSET 7.4 PS with initial-state photon radiation. The first sample contains all charged final-state particles with a lifetime larger than 10^{-9} s (generator-level sample). The second, detector-level sample, includes distortions due to detector effects, limited acceptance, finite resolution, long-lived resonances decaying within the detector and the event selection. The events are processed with the same reconstruction program as used for the experimental data. Both generator-level and detector-level MC samples have the same statistics (810k hadronic events).

In the experimental analysis, we shall use both normalized factorial moments (NFM) and bunching parameters (BPs). A corrected NFM or BP is found by means of the following correction procedure

$$D_q^{\text{cor}} = C_q D_q^{\text{raw}}, \quad C_q = \frac{M_q^{\text{gen}}}{M_q^{\text{det}}}. \quad (12.1)$$

Here, M_q^{gen} and M_q^{det} symbolize an NFM or BP of order q calculated from the generator-level and detector-level MC samples, respectively. D_q^{raw} represents an NFM or BP calculated directly from the raw data, D_q^{cor} those corrected by C_q . The same correction procedure has been used in [1–3].

12.1 Motivation

Experimentally, local fluctuations in e^+e^- processes have already been studied by the TASSO [4], HRS [5], CELLO [6], OPAL [3], ALEPH [7], DELPHI [1, 2] and L3 [8] Collaborations. The data do exhibit a power-like rise of NFMs with decreasing δ , especially in two and three dimensional variables. The conclusion has been reached that such a phenomenon

is a consequence of the multi-jet structure of events, i.e., groups of particles with similar angles resulting in spikes of particles as seen in selected phase-space projections. It has been found that for the statistics used at that time (ALEPH - 80k, DELPHI - 78k, OPAL - 140k, L3 - 248k) current MC models can adequately describe the data, even without additional tuning. Important exceptions have, however, been found by OPAL [3] (in rapidity defined with respect to the sphericity axis) and DELPHI [2] (for restricted charge-multiplicity and p_T regions). A direct measurement of the multiplicity distribution $P_n(\delta)$ in restricted rapidity intervals δ has been undertaken by ALEPH [9] using a sample of 300k hadronic events. The JETSET 7.3 PS model is found to describe the data, though the model produces a slightly broader multiplicity distribution for small δ . The predictions of HERWIG 5.6 model significantly disagree with the data.

Recently, it has been realized, however, that the factorial-moment method poorly reflects the information context of the local fluctuations, since the NFM of order q contains a trivial contamination from lower-order correlation functions [10]. As a result, rather different event samples can exhibit a very similar power-law behavior of the NFMs. The fact that subtle details in the behavior of $P_n(\delta)$ are missing, together with the small statistics used at that time, may partly explain why MC models can reasonably describe the local fluctuations.

Cumulants are a more sensitive statistical tool (see [10] and references therein). However, their measurement is rather difficult and was rarely attempted. Besides, the cumulants are expected to be influenced by the statistical and systematical biases to even larger degree than the NFMs, since they are constructed from the factorial moments of different orders.

To study the local multiplicity fluctuations in more detail, in addition to the NFMs, we shall use the BPs which are more sensitive to variations in the shape of the local multiplicity distribution $P_n(\delta)$ with decreasing δ . The higher sensitivity of the BPs is due to the ability of BPs to resolve $P_n(\delta)$ without the redundant information from the overall shape of the distribution. Moreover, they are not affected by the statistical bias from finite event samples and the systematical bias due to insufficient resolution. As we have noted in Chapter 11, the latter bias becomes even more acute for the Białas-Gazdzicki-Ochs transformation adopted throughout this thesis.

12.2 Experimental definitions

In order to increase the statistics and to reduce the statistical error on the observed local quantities when analyzing the experimental data, we use the bin-averaged NFMs and BPs.

1) Horizontal NFMs:

The NFM of order q is given by the standard definition widely used in high-energy physics

$$F_q(\delta) = \frac{1}{M} \sum_{m=1}^M \frac{\langle n_m^{[q]} \rangle}{\langle \bar{n} \rangle^q}, \quad n_m^{[q]} = n_m(n_m - 1) \dots (n_m - q + 1), \quad (12.1)$$

where n_m is the number of particles in bin m , $\langle \bar{n} \rangle = \bar{N}/M$, \bar{N} is the average multiplicity for the full phase space, $M = \Delta/\delta$ is the total number of bins, and Δ represents the full phase-space volume.

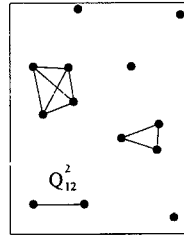


Figure 12.1: Example of the Grassberger-Hentschel-Procaccia counting topology for squared four-momentum variable Q_{12}^2 .

2) *Horizontal BPs:*

We shall use the following definition of the horizontal BPs [11, 12]:

$$\eta_q(\delta) = \frac{q}{q-1} \frac{\bar{N}_q(\delta)\bar{N}_{q-2}(\delta)}{\bar{N}_{q-1}^2(\delta)}, \quad \bar{N}_q(\delta) = \frac{1}{M} \sum_{m=1}^M N_q(m, \delta), \quad (12.3)$$

where $N_q(m, \delta)$ is the number of events having q particles in bin m and M has the same meaning as it has for the NFMs.

Both quantities (12.2) and (12.3) are equal to unity for purely independent particle production following a Poissonian multiplicity distribution in restricted bins.

Note that the definitions presented above can be used in practice for a flat single-particle density distribution. To be able to study non-flat distributions, we have to carry out a transformation from the original phase-space variable to one in which the underlying distribution is approximately uniform (see Chapter 11).

3) *Generalized integral BPs:*

The bin-splitting method of local-fluctuation measurement considered above suffers from the following shortcomings:

- a) Using this method, we lose information on spikes that happen to be divided by bin boundaries.
- b) Not all variables can be used for such calculations. For example, the squared four-momentum difference $Q_{12}^2 = -(p_1 - p_2)^2$ cannot be used in the bin-splitting method.
- c) For high-dimensional calculations, the statistics actually used is very limited.

Recently, a new type of bunching parameter has been proposed that makes use of the interparticle distance-measure technique [12]. To study fluctuations of spikes, we shall consider the generalized integral BPs using the pairwise squared four-momentum difference $Q_{12}^2 = -(p_1 - p_2)^2$. In this variable, the definition of the BPs is given by

$$\chi_q(Q_{12}^2) = \frac{q}{q-1} \frac{\Pi_q(Q_{12}^2)\Pi_{q-2}(Q_{12}^2)}{\Pi_{q-1}^2(Q_{12}^2)}, \quad (12.4)$$

where $\Pi_q(Q_{12}^2)$ represents the number of events having q spikes of size Q_{12}^2 , irrespective of how many particles are inside each spike. To define the spike size, we shall use the so-called

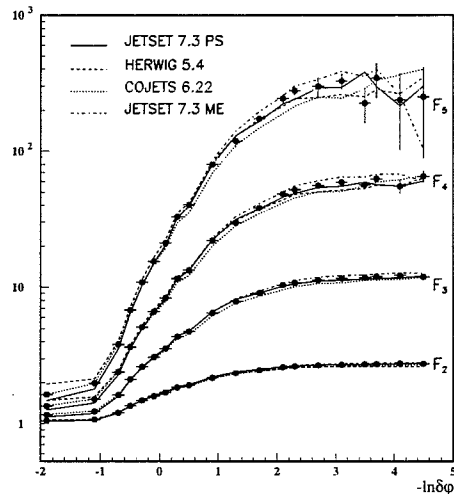


Figure 12.2: *NFMs of order 2 to 5 as a function of $-\ln \delta\phi$. The dots represent the data and the lines are the predictions of MC models [8].*

Grassberger-Hentschel-Procaccia (GHP) counting topology [13], for which a g -particle hypertube is assigned a size $\epsilon = Q_{12}^2$ corresponding to the maximum of all pairwise distances (see Fig. 12.1). For purely independent production, with the multiplicity distribution characterized by a Poissonian law, the BPs (12.4) are equal to unity for all q .

4) Generalized differential BPs:

The main advantage of using (12.4) is that, in contrast to the bin-splitting definition (12.3), local fluctuations can be studied in the squared four-momentum difference $Q_{12}^2 = -(p_1 - p_2)^2$ between two particles. However, for large Q_{12}^2 , the generalized integral BPs have the following shortcoming: they are strongly influenced by the global structure of multi-jet events [12]. Since we are interested in the spike fluctuations inside jets, this effect distorts the information content to be revealed with the help of the integral BPs.

For sufficiently large experimental statistics, such a drawback can be largely avoided by making use of the generalized differential BPs. The generalized differential BPs have been introduced for a selective study of multiplicity fluctuations of spikes with a well-defined fixed particle content. For two-particle spikes, the generalized differential BPs can be written as follows

$$\chi_q(Q_{12}^2, 2) = \frac{q}{q-1} \frac{\Pi_q(Q_{12}^2, 2) \Pi_{q-2}(Q_{12}^2, 2)}{\Pi_{q-1}^2(Q_{12}^2, 2)}, \quad (12.5)$$

where $\Pi_q(Q_{12}^2, 2)$ represents the number of events having q two-particle spikes of size Q_{12}^2 .

It is important to realize, however, that for $Q_{12}^2 \rightarrow 0$, the definitions (12.4) and (12.5) lead to the same result, i.e.,

$$\chi_q(Q_{12}^2) \rightarrow \chi_q(Q_{12}^2, 2). \quad (12.6)$$

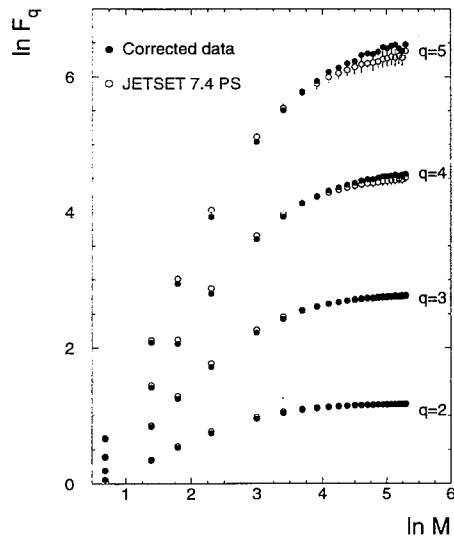


Figure 12.3: *NFMs* as a function of the number M of bins in azimuthal angle φ defined with respect to the beam axis.

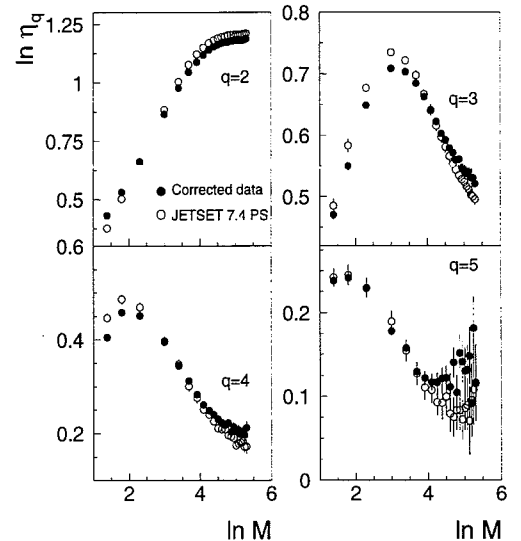


Figure 12.4: *BPs* as a function of the number M of bins in azimuthal angle φ defined with respect to the beam axis.

Moreover, note that all counting topologies (GHP, “star” and “snake”) discussed in [12] become equivalent for $\chi_q(Q_{12}^2, 2)$.

12.3 In the detector frame

12.3.1 Factorial-moment method

The current analysis extends the previous L3 studies [8, 14] based on the 1991 L3 data. In that study, the azimuthal angle φ defined with respect to the beam axis was chosen as the phase-space variable. The reason was that for the 1991 - 1993 data the resolution of the L3 detector in azimuthal angle was much better than that for other variables defined with respect to the beam axis (see Chapter 10). Since the event-averaged distribution in φ is uniform, the Białas-Gazdzicki-Ochs transformation described in Chapter 11 is not necessary for this case.

The behavior of the horizontal NFMs (12.2) as a function of bin-size $\delta\varphi = 2\pi/M$ for the 1991 data [8, 14] is reproduced in Fig. 12.2. For the given statistics of that time (248k), MC predictions show good agreement with the data.

We repeated this analysis using the higher statistics available from 1994 (five times higher than that used in [8, 14]). Moreover, we use the information on charged tracks from SMD which largely improves the resolution. Fig. 12.3 shows the horizontal NFMs (12.2) as a function of the number $M = 2\pi/\delta\varphi$ of partitions of the full angular interval 2π , where $\delta\varphi$ denotes the bin size in azimuthal angle defined with respect to the beam axis. In Fig. 12.3, the

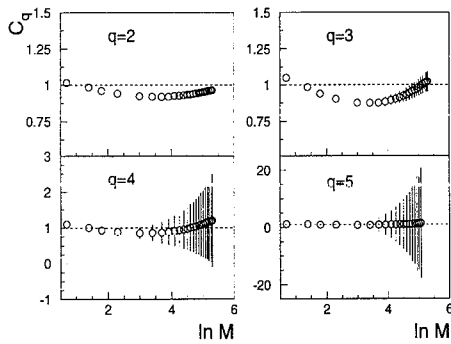


Figure 12.5: *The correction factors applied to the NFMs in azimuthal angle defined with respect to the beam axis.*

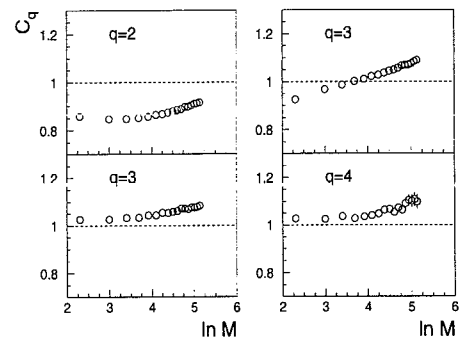


Figure 12.6: *The correction factors applied to the BPs in azimuthal angle defined with respect to the beam axis.*

corrected data are shown by full symbols, the generator-level of JETSET 7.4 PS as tuned by the L3 Collaboration on single-particle and event-shape distributions [15] by open symbols. Here and below, the smallest bin size is estimated from the MC study of the charged-track resolution of the L3 detector with SMD in the particular variable (see Chapter 10).

The statistical errors on the data are derived from the covariance matrix of the horizontally averaged factorial moments. They include the statistical error on the correction factor C_q defined in (12.1). To combine the statistical error on the correction factor, we assume that the statistical errors for the generator-level and detector-level Monte Carlo's are independent. This conservative assumption leads to an upper limit of the error derived for C_q .

A small systematic uncertainty for the correction factor C_q exists due to the generator-level dependence of MC. This uncertainty was estimated by computing the correction factor from HERWIG 5.8 [16] model. The systematic error on the C_q is given as half of the difference between the JETSET and HERWIG correction factors. It was found that in most cases this uncertainty is negligible and largest for different charged particle combinations (see below). The error bars on the corrected data are given as the quadratic sum of the statistical and the systematical errors.

The error bars on the MC predictions include both statistical and systematical errors. The systematical errors were estimated by varying, by one standard deviation, the parameter b (PARJ(42)) of the LUND fragmentation function, the width of the Gaussian p_x and p_y hadronic transverse momentum distribution, σ (PARJ(21)), and the Λ value used for α_s in parton showers (PARJ(81)).¹ For the statistics used, the errors on the MC results are dominated by the systematical errors, so that the open symbols represent the values of NFM with the L3 default and the error bars indicate the maximum and minimum values obtained after the parameter variations.

Fig. 12.3 shows that the MC predictions slightly oscillate around the corrected data, but reasonably reproduce the experimental data (see also [17]).

¹The value of these parameters have been tuned by the L3 Collaboration to reproduce the single-particle spectra and the global shape distributions.

The correction factors C_q shown in Fig. 12.5 tend to reduce the measured NFMs. The corrections applied have a non-linear behavior and become larger for high-order moments. A similar behavior of the correction factors (applied to the NFMs) has been found by the OPAL collaboration [3].

The same variable is used to calculate the horizontal type of BPs (12.3). The behavior of $\ln \eta_q(M)$ as a function of $\ln M$ is presented in Fig. 12.4. Being more sensitive to the structure of fluctuations, the BPs show that JETSET 7.4 PS slightly overestimates the increase of the second-order BP and oscillates around the third-order BP calculated from the data. The MC predictions reproduce the higher-order BPs reasonably well. Fig. 12.6 shows the correction factors applied to the BPs.

In contrast to the behavior of the NFMs, a striking difference is found between the second-order BP and all higher-order ones ($q = 3, 4, 5$). While the second-order BP increases (bunching effect), all higher-order ones decrease with increasing M . The observed decrease of the high-order BPs with increasing M reflects a particle anti-bunching of the order $q > 2$ due to jet structure, i.e., particles are bunched together inside each jet, but there are empty phase-space intervals between the bunches due to energy-momentum conservation [17].

The dependence of BPs on M indicates not only that the width of the multiplicity distribution grows, but also that its shape changes significantly for ever larger M . The rise of $\eta_2(M)$ for increasing M and $\eta_2(M) > 1$ can be understood as follows: For small δ (large M), $P_0(\delta) \rightarrow 1$, so that the decrease of $P_2(\delta)$ has to be smaller than that of $P_1^2(\delta)$ (see (2.25) in Chapter 2). The condition $P_2(\delta) > P_1^2(\delta)$ is an obvious consequence of positive correlations between particles. However, the behavior of higher-order BPs depends strongly on the interplay between the values of the ratios of probabilities $P_n(\delta)/P_{n-1}(\delta)$ and $P_{n-1}(\delta)/P_{n-2}(\delta)$.

If we adopt the assumption that all high-order BPs at large M can be expressed via the the second-order BP as follows [11]

$$\eta_{q>2}(M) \propto \eta_2^r(M), \quad \eta_2(M) \propto M^{\phi_2}, \quad (12.7)$$

where r is the so-called degree of multifractality, then, for large M , the corresponding anomalous fractal dimensions (AFDs) have the form [11]

$$d_q = d_2(1 - r) + r d_2 \frac{q}{2}. \quad (12.8)$$

Qualitatively, the only way to use expression (12.7) for the description of the experimental curves shown in Fig. 12.4 is to assume that

$$r < 0. \quad (12.9)$$

Hence, the AFDs decrease with increasing moment order q and even can become negative for large q . This observation means that the corresponding high-order NFMs decrease as the phase-space interval is reduced. Clearly, in this case, the hadronic system under consideration cannot be considered a fractal one any more, since the inverse power-law behavior of NFMs ceases to be valid. Note that for decreasing high-order BPs, the violation of the inverse-power laws for high-order NFMs can be seen from a more general relation between the NFMs and BPs for $\delta \rightarrow 0$ (see [11, 12]).

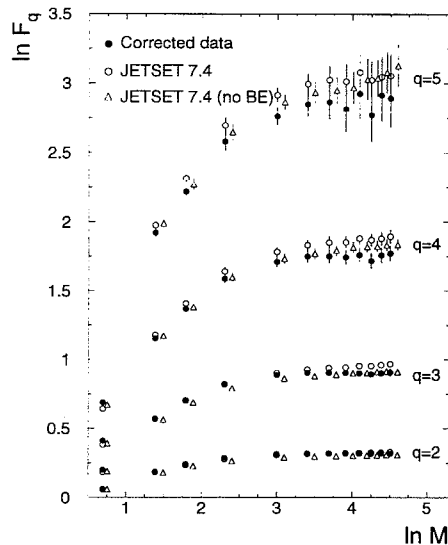


Figure 12.7: *NFMs as a function of the number M of bins in rapidity y defined with respect to the thrust axis.*

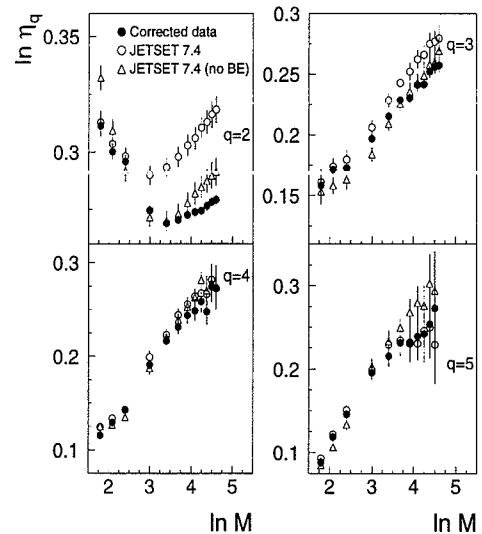


Figure 12.8: *BPs as a function of the number M of bins in rapidity y defined with respect to the thrust axis.*

12.4 In the event frame

12.4.1 All charge combinations

With the above observation in mind, it is obvious that the NFMs and BPs calculated so far are strongly influenced by the jet structure of events. Hence, in order to study genuine fluctuations inside jets, one needs to use a variable defined with respect to the jet axis, rather than the beam axis. In most investigations, the NFMs have been measured in rapidity y defined with respect to the thrust axis [5, 7] or the sphericity axis [2, 3].

The improved two-track resolution of the 1994 run allows us to use the rapidity defined with respect to the thrust axis for the present analysis. The analysis for this variable is performed in the full rapidity range $|y| \leq 5$. Since the distribution in rapidity is non-uniform (see Section 9.3), we carry out the Białas-Gadzinski-Ochs transformation described in Chapter 11. The NFMs as a function of the number of bins in (transformed) rapidity y are shown in Fig. 12.7. The predictions of JETSET 7.4 PS tuned by the L3 Collaboration are presented by open circles. The correction factors applied to the NFMs are shown in Fig. 12.9.

The behavior of the NFMs shows the same trend as that of the azimuthal angle φ defined with respect to the beam axis. The signal observed, however, is much smaller for the present calculations. As we see, JETSET 7.4 PS overestimates the intermittency effect for large M . This discrepancy increases with rising moment order q .

Fig. 12.8 shows the results for the horizontally normalized BPs (12.3) in rapidity y defined with respect to the thrust axis, after the Białas-Gadzicki-Ochs transformation. Fig. 12.1

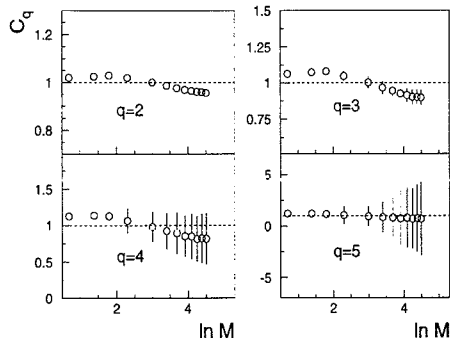


Figure 12.9: The correction factors applied to the NFMs in y defined with respect to the thrust axis.

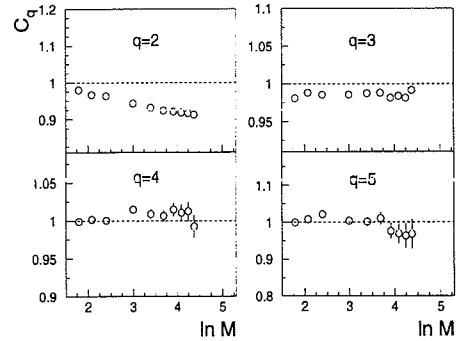


Figure 12.10: The correction factors applied to the BPs in y defined with respect to the thrust axis.

presents the correction factors. A disagreement with the MC predictions is observed for $q = 2, 3$, while higher-order BPs are described well by the model. In contrast to the case of φ defined with respect to the beam axis (see Fig. 12.4), all high-order BPs show a power-law increase with increasing M , indicating that the fluctuations in this variable are of a *multifractal type*. Indeed, in this case, the high-order BPs can be approximated by the relation (12.7), but now with a *positive non-zero* constant r . Hence, the AFDs in the form (12.8) always have positive values and the inverse power law of the NFMs is valid for all moment orders q investigated. Note that the conclusion on the multifractal type of the fluctuations becomes possible without the necessity to calculate intermittency indices. In contrast, to reveal multifractality with the help of the NFM-method, one first needs to carry out fits of the NFMs by a power law.

From a physical point of view, the multifractality observed is a consequence of the cascade nature of parton branching, hadronization, resonance decays and Bose-Einstein correlations. Recently, several authors considered the possibility that Bose-Einstein (BE) correlations could be responsible for the intermittency effect at small Q_{12}^2 . The influence of BE correlations on a quantity depends strongly on the type of quantity (such as NFMs, BPs, *etc.*) and the variable (y , φ , p_T , *etc.*) used. Obviously, BE correlations are a typical candidate for the origin of local fluctuations in 3-momentum phase space, that also can lead to a rise of fluctuations in one-dimensional rapidity phase space. The influence of the BE correlations using JETSET has been studied by DELPHI [2]. However, no visible influence of the BE correlations on the behavior of NFMs has been found there.

To demonstrate the BE effect, Figs. 12.7 and 12.8 also show a comparison of the JETSET 7.4 PS model without BE interference (open triangles) to the data. Indeed, the model expectations without the BE effect shown in Fig. 12.7 have a smaller rise of the NFMs than those with the BE effect.

It is quite remarkable how clearly the influence of BE correlations on the local fluctuations in JETSET can be seen in the second-order BP (see Fig. 12.8). This is due to the fact that the BE effect is implemented in JETSET on the level of two-particle correlations, which

are strictly related to the second-order BP (NFM). (In fact, the form of the second-order BP $\eta_2(\delta) \sim P_2(\delta)/P_1^2(\delta)$ is similar to that of the correlation function used in Bose-Einstein analysis).

The predictions of the JETSET 7.4 PS model deviate from the data for second-order BP in the region $\delta y < 1.0$ ($\ln M > 2.3$). However, good agreement is observed for large rapidity intervals $\delta y > 1.0$. In this region, the predictions of the model without BE correlations included deviate significantly from the data, but they lead to a better agreement for small δy . This indicates that JETSET without BE correlations would in fact require a re-tuning to reduce discrepancies for large phase-space intervals.

The BE correlations of charged pions have been studied in e^+e^- -annihilation at the Z mass by the DELPHI, OPAL and ALEPH Collaborations. Using a mixed-track reference sample, it has been found that the Gaussian parameterization can describe the data with $\lambda = 0.35 \pm 0.04$ and $r = 0.42 \pm 0.04$ [18,19].² These results were obtained from all pion pairs including pions from long-lived particles (K^0, D, B). Consequently, these values are mean values for all identical pions. Similar values were obtained by ALEPH [20]. A study of $\pi^0\pi^0$ correlations by the L3 Collaboration has shown that a fit with the Gaussian parameterization yields $\lambda = 0.37 \pm 0.12$ and $r = 0.40 \pm 0.16$ [21] (errors include both systematical and statistical errors). Based on those findings, it is reasonable to assume that λ and r have smaller values than those used by the L3 collaboration in the JETSET 7.4 model. Here we do not pursue the aim to obtain a good agreement between the data and the MC predictions by variation of the BE parameters, since the parameters should be obtained from a direct measurement of the correlations between like-charged particles. This has not yet been done by the L3 Collaboration so far.

12.4.2 Like-charged and unlike-charged particle combination

To study the disagreement between the data and JETSET in more detail, we split $\eta_2(\delta y)$ into two BPs for the two charge combinations ($\pm\pm$) and ($+ -$):

$$\eta_2(\delta y) = \eta_2^{(\pm\pm)}(\delta y) + \eta_2^{(+ -)}(\delta y). \quad (12.10)$$

Here $\eta_2^{(\pm\pm)}(\delta y)$ is defined by (12.3) with $N_2(m, \delta) = N_2^{(\pm\pm)}(m, \delta y)$, where $N_2^{(\pm\pm)}(m, \delta y)$ is the number of events having only like-charged two-particle combinations inside bin m of size δy . Analogously, $\eta_2^{(+ -)}(\delta y)$ is constructed from the number of events $N_2^{(+ -)}(m, \delta y)$ having only unlike-charged two-particle combinations. Note that due to a combinatorial reason $\eta_2^{(\pm\pm)}(\delta y) < \eta_2^{(+ -)}(\delta y)$, however they stay independent of δy in the case of independent production.

From a comparison of the behavior for ($\pm\pm$) in the left part of Fig. 12.11 and that for ($+ -$) in the right, we can deduce that the initial decrease of $\ln \eta_2(\delta y)$ in Fig. 12.10 with increasing $\ln M$ is solely due to the decrease of $\eta_2^{(+ -)}(\delta y)$. On the other hand, the increase of $\ln \eta_2(\delta y)$ for $\ln M > 3.5$ is due to a similar tendency in the behavior of $\eta_2^{(\pm\pm)}(\delta y)$ at intermediate values of δy and the rise of $\eta_2^{(+ -)}(\delta y)$ at small rapidity interval. The MC overestimates the fluctuations both for like-charged and unlike-charged particle combination at small δy .

²These values were obtained using corrections for Coulomb interaction.

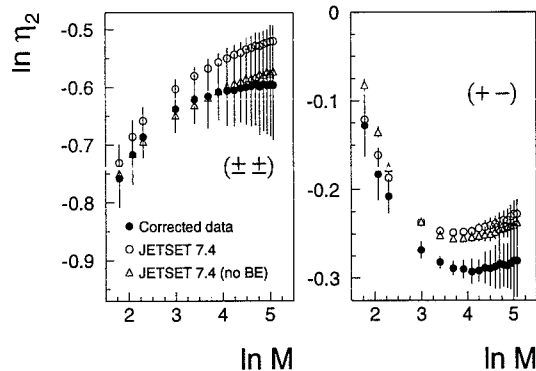


Figure 12.11: The second-order BP for like-charged and unlike-charged particle combinations.

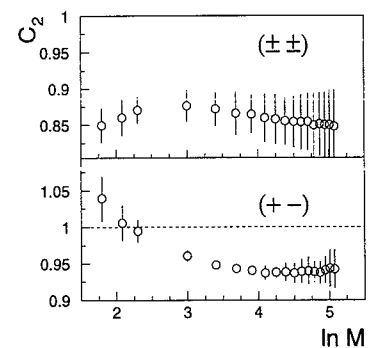


Figure 12.12: The correction factors applied to $\eta_2^{(\pm\pm)}$ and $\eta_2^{(+-)}$.

The BE modeling strongly affects the absolute value of $\eta_2^{(\pm\pm)}(\delta y)$, but the δy -dependence of $\eta_2^{(\pm\pm)}(\delta y)$ seems to be due to parton showers and hadronization. The large (systematic) errors on $\eta_2^{(\pm\pm)}(\delta y)$ calculated from MC mainly come from the uncertainty on the JETSET parameter PARJ(21) responsible for the width of the Gaussian hadronic transverse momentum distribution in the LUND model. This observation stresses the importance of fragmentation for the local quantity measured. The variation of fragmentation parameters does not affect the unlike-charged particle fluctuations, while the BE interference has a significant influence on the unlike-charged particles for $\ln M < 2.3$ ($\delta y > 1.0$).

The strong anti-bunching tendency is seen for $\eta_2^{(\pm\pm)}(\delta y)$ for $\ln M < 3.5$ ($\delta y > 0.3 - 0.5$) can be attributed to resonance decays and to chain-like charge-ordered particle production along the thrust axis, as expected from the QCD-string model [22]. The latter effect leads to local charge conservation with an alternating charge structure along the rapidity defined with respect to the thrust axis. Evidence for this effect was recently observed by DELPHI [23]. As a result, there is a smaller rapidity separation between unlike-charged particles than between like-charged. Having correlation lengths $\delta y \sim 0.5 - 1.0$ in rapidity, the resonance and the charge-ordering effects, however, become smaller with decreasing δy and this leads to the fast decrease of $\eta_2^{(\pm\pm)}(\delta y)$ with decreasing δy . For very small δy ($\ln M > 5$), the BP is affected by the π^0 Dalitz decay ($\pi^0 \rightarrow e^+e^-\gamma$) and γ conversion.

Note that to distinguish the NFMs calculated for different charge combinations in the bin-splitting method is difficult due to insufficient sensitivity of this tool and a purely combinatorial reason. For example, $F_2^{(+)}(\delta)$ may follow the same behavior as $F_2^{(\pm\pm)}(\delta)$ since the high-multiplicity tail of $F_2^{(+)}(\delta)$ is affected by like-charged particles. The comparison of one-dimensional NFMs for like-sign particles with all charged combinations did not show differences [1]. A study of the charge dependence of two- and three-dimensional NFMs in e^+e^- -processes at 91.5 GeV generated with JETSET 7.4 was undertaken in [24]. The $F_2^{(+)}(\delta)$ shows a similar trend as $F_2^{(\pm\pm)}(\delta)$, but, for very small two- and three-dimensional bins, $F_2^{(+)}(\delta)$ rose more rapidly than $F_2^{(\pm\pm)}(\delta)$ which had a clear plateau. The inclusion of

the BE option had only a small influence on the δ -dependence of the NFM.

As a final remark of this section, we remind that also the OPAL Collaboration in fact observed a difference between the MC and the data in rapidity calculated with respect to the sphericity axis [3]. The explanation given there was that the exact details of the determination of the sphericity axis may affect the final result. However, such an explanation cannot clarify why this effect yields different results for data and MC.

12.5 In the four-momentum difference

A suitable variable to measure fluctuations by means of the generalized distance-measure technique is the squared four-momentum difference $Q_{12}^2 = -(p_1 - p_2)^2$ between two charged particles. This is because of the fact that such a variable incorporates the 3-dimensional analysis. Indeed, Q_{12}^2 is related to the frequently used variables y , φ and p_T as follows [25]

$$Q_{12}^2 \simeq m^2 \left[\alpha^2 \delta\varphi^2 + (1 + \alpha^2) \delta y^2 + \frac{\alpha^4 \delta x^2}{(1 + \alpha)^2} \right], \quad (12.11)$$

where $\alpha = p_T/m$ and $\delta x = \ln(p_{T1}/p_{T2})$. Hence, a small 3-dimensional bin defined in y , φ and p_T corresponds to a small distance in Q_{12}^2 (the opposite is not true). In addition, the squared four-momentum difference Q_{12}^2 is a Lorentz invariant variable.

12.5.1 Generalized integral BPs

Fig. 12.13 shows the behavior of the generalized BPs χ_q (12.4) as a function of Q_{12}^2 . The statistical errors for data and MC are derived according to the expression for the standard deviation obtained in [12]. The error bars shown in Fig. 12.13 are evaluated using the procedure discussed in subsection 12.3.1. The corresponding correction factors are shown in Fig. 12.15.

The solid lines ($\chi_q = 1$) represent the behavior of the integral BPs in the Poissonian case. In contrast, all BPs obtained from data and MC rise with decreasing Q_{12}^2 (increasing $-\ln Q_{12}^2$). The anti-bunching effect ($\chi_q(Q_{12}^2) < 1$) for small $-\ln Q_{12}^2$ is caused by the energy-momentum conservation constraint.

As observed in the one-dimensional study above, JETSET overestimates the local fluctuations. A similar discrepancy has been found in [14] using density-strip integrals in Q_{12}^2 .

To learn more about the mechanism of multiparticle fluctuations in Q_{12}^2 , we present in Fig. 12.14 the behavior of the second-order BP as a function of Q_{12}^2 for multiparticle hyper-tubes (spikes) made of like-charged and that of unlike-charged particles, separately. A large difference is observed between these two samples. For like-charged particle combinations (i.e., for spikes with a maximum charge), a linear increase is seen for all values of $-\ln Q_{12}^2$. However, the bunching is much smaller and even disappears at large $-\ln Q_{12}^2$ for unlike-charged particle combinations. This effect can be explained by resonance decays, when decay products of short-lived resonances tend to be separated in phase space.

The resonance effect is much weaker for like-charged combinations. In addition, the BE correlations affect the like-charged particle combinations. JETSET 7.4 PS leads to a strong rise of $\chi_2^{(\pm\pm)}(Q_{12}^2)$ for like-charged particle combinations, even without BE interference.

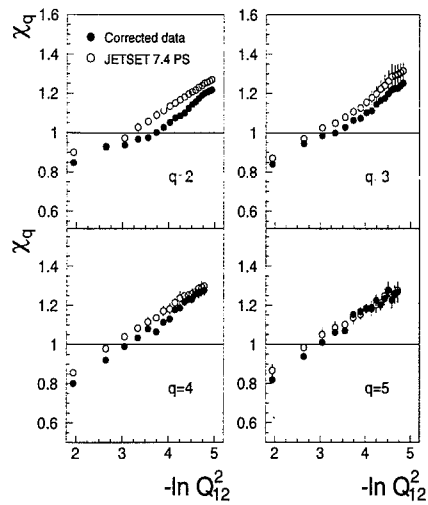


Figure 12.13: *Generalized integral BPs as a function of the squared four-momentum difference Q_{12}^2 between two charged particles.*

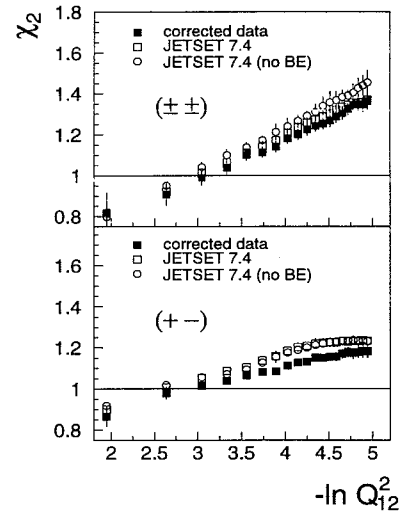


Figure 12.14: *Generalized second-order BP as a function of the squared four-momentum difference Q_{12}^2 between two charged particles.*

It is interesting to observe in Fig. 12.14 that the BE correlations do not strongly affect the behavior of the generalized BPs, while the BPs presented in Fig. 12.8 are very sensitive to the BE effect. Let us give an interpretation of this observation: The behavior of any conventional local quantity (such as NFM or BP) calculated in a selected phase-space bin reflects a *bunching of particles* in spikes. The stronger the bunching effect is, the larger is the local quantity. Mathematically, this means that this quantity is influenced by the average number of spikes per event. In terms of the multiplicity distribution $P_N(\epsilon)$ of observing N spikes of size ϵ (see [12]), this means that the conventional local quantity is a function of the average number of spikes per event,

$$\sum_{N=1}^{\infty} N P_N(\epsilon). \quad (12.12)$$

In JETSET the BE effect is implemented on the level of the two-particle correlation function. The model moves like-charged particles closer to each other in the $\epsilon = Q_{12}^2$ variable. Actually this leads to an enhancement of the number of multiparticle spikes. Hence, the value of (12.12) increases. As a result, the NFMs and BPs evaluated in the bin-splitting technique are larger than those calculated in JETSET without BE interference.

Now let us come back to the generalized BPs shown in Fig. 12.14. According to definition (12.4), the BPs $\chi_q(Q_{12}^2)$ measure the deviation of $P_N(\epsilon)$ from a Poissonian distribution. Clearly, such a kind of measurement has little to do with the measurement of the average spike multiplicity (12.12). Even if BE interference as implemented in JETSET increases the bunching of particles, the shape of $P_N(\epsilon)$ (and, hence, the *bunching of spikes*) may be the same or only change slightly. Fig. 12.14 shows that the treatment of BE correlations in

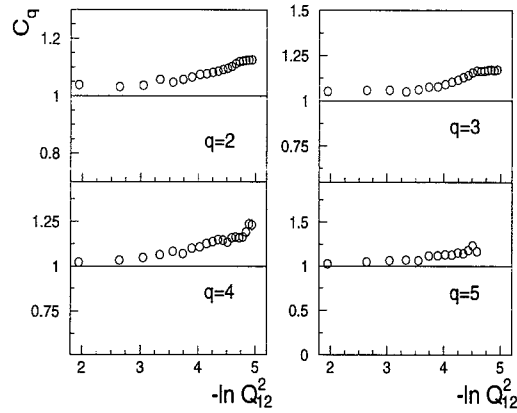


Figure 12.15: *The correction factors applied to the generalized integral BPs.*

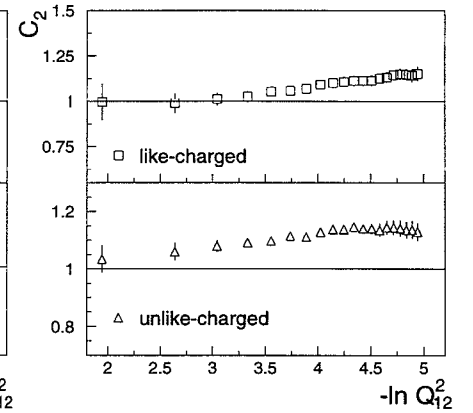


Figure 12.16: *The correction factors applied to the generalized second-order BP.*

JETSET mainly increases the probability $P_1(\epsilon)$ of observing a single spike. This leads to a small *decrease* of $\chi_2(Q_{12}^2)$ for like-charged particles. The unlike-charged particles are not affected by BE correlations. Generally, a realistic BE effect may change both the bunching of particles and the bunching of spikes. The latter effect should be visible from the study of $\chi_q(Q_{12}^2)$.

JETSET 7.4 PS overestimates the data for like-charged and unlike-charged combinations. As an additional verification, the default tuning of JETSET 7.4 PS has been compared to the data. The same kind of the disagreement is found (not shown).

The disagreement for the unlike-charged particle combinations in Q_{12}^2 and in rapidity probably has a common reason. Probable shortcomings of JETSET 7.4 PS leading to the discrepancies found are the simulation of hadronization³ and the BE effect. As an example the residual distortion of the decays of short-lived resonances by BE correlations not yet implemented in the JETSET 7.4 PS model may be a good candidate for an explanation of such a discrepancy. The importance of the latter effect was realized recently, when a significant mass shift of ρ^0 was observed by OPAL and DELPHI [27, 28].

The production rate of $f_0(975)$ and $f_2(1270)$ measured by DELPHI [28] is another challenge for the JETSET model. In this respect, it is not improbable that a much larger fraction of the observed final-state hadrons results from resonance decays than is usually assumed. In this case, the negative correlations should be larger, and a better agreement with the data for the intermediate values of Q_{12}^2 would be achieved for unlike-charged particles. Indeed we have found that a realistic small variation of the production of resonances (ρ , ω , η , η') responsible for the unlike-charged particle fluctuations in the JETSET 7.4 PS can lead to a better agreement. This is not likely to improve the discrepancy fully, however, since the

³For $2.5 < -\ln Q_{12}^2 < 5.0$, our calculations show a large sensitivity of the results obtained to the parameterization of LUND fragmentation, since the large systematic errors for this domain of Q_{12}^2 come mainly from the variation of the LUND fragmentation parameters PARJ(42) and PARJ(21) by one standard deviation

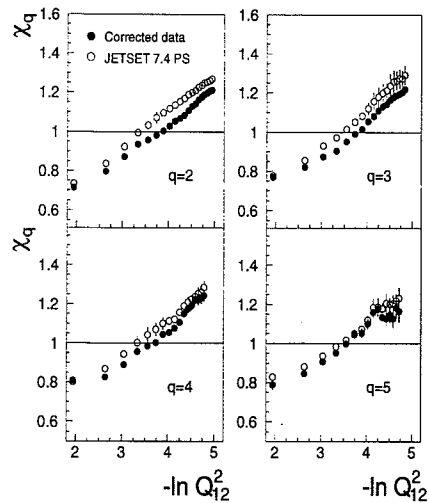


Figure 12.17: *Generalized differential BPs for two-particle spikes.*

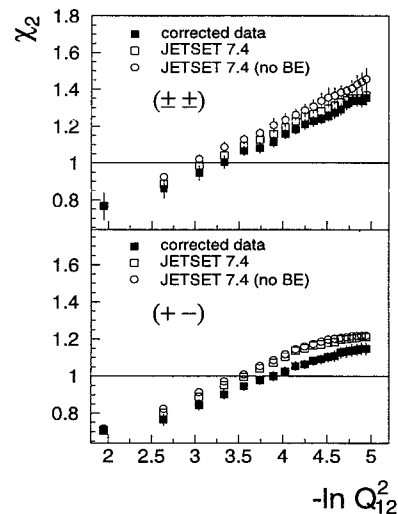


Figure 12.18: *Generalized second-order BP for two-particle spikes.*

JETSET 7.4 PS tuned by the L3 Collaboration shows a reasonable agreement with the production rates of the main resonances [15], so that the variation of the parameters should not be large.

Of course, the disagreement for the unlike-charged particle combinations in Q_{12}^2 (and, hence, for the all-charged combinations shown in Fig. 12.13) can also lead to the disagreement between the JETSET 7.4 PS and the data in the case of the one-dimensional variables φ and y presented in Section 12.4.

12.5.2 Generalized differential BPs

To be complete, we present in Figs. 12.17, 12.18 the behavior of the differential BPs (12.5) as a function of Q_{12}^2 between two charged particles. The corresponding correction factors applied to $\chi_q(Q_{12}^2, 2)$ are shown in Figs. 12.19 and 12.20. As we see, the only difference between Figs. 12.13, 12.14 and Figs. 12.17, 12.18 is faster rise of the second-order differential BP (for not too large $-\ln Q_{12}^2$) than of the integral one. As we have already indicated in [12], the reason for this behavior is that only the two-jet events with the same number of particles can contribute to $\chi_q(Q_{12}^2, 2)$.

12.6 Discussion

For the first time, local multiplicity fluctuations of experimental data have been studied by means of bunching parameters. Using this method, fluctuations in rapidity defined with respect to the thrust axis and in the four-momentum difference Q_{12}^2 are found to exhibit a multifractal behavior. The multiplicity distributions in these variables, therefore, cannot be described by conventional distributions (Poisson, geometric, logarithmic, positive-binomial,

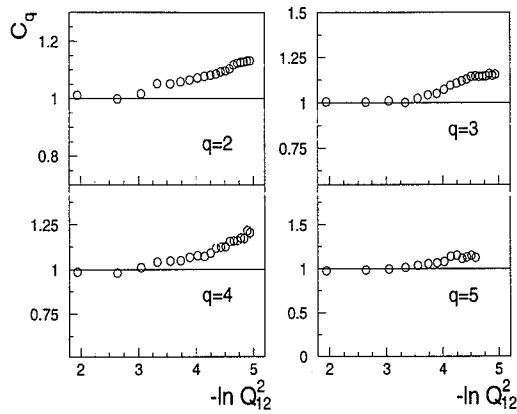


Figure 12.19: *The correction factors applied to the generalized differential BPs.*

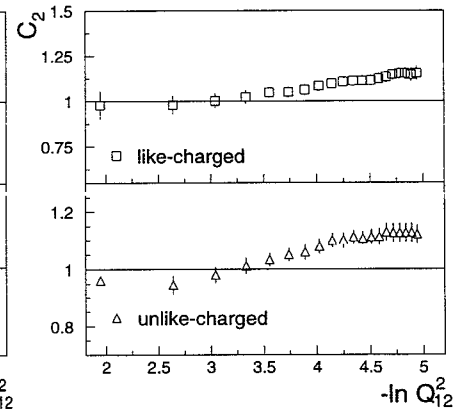


Figure 12.20: *The correction factors applied to the differential second-order BP.*

negative-binomial), which have δ -independent high-order BPs. More general multiplicity distributions with power-like high-order BPs have been considered in Chapter 4. Such types of distributions, therefore, appear to be more relevant to the situation observed. However, a phenomenological description of these distributions can, only to a slight extent, provide a physical explanation of the nature of multifractal behavior.

For e^+e^- interaction, one can be confident that, at least on the parton level of the reaction, perturbative QCD can give a hint for the understanding of the problem. Analytical calculations based on the double-log approximation of perturbative QCD show that the multiplicity distribution of partons in ever smaller opening angles is inherently multifractal [29]. Qualitatively, this is consistent with our results. Of course, the choice of variable can affect the observed signal. Hence, the final conclusion on an agreement between QCD and the data can only be derived after the calculation of local quantities in angular variables that are defined with respect to the thrust (or sphericity) axis.

We have shown that the increase of the second-order BP is mainly due to like-charged particles. JETSET 7.4 PS shows the same power-law trend even without BE effect. This means that the intermittency observed for like-charged particle combinations appears to be a largely consequence of parton showers and hadronization. The latter phenomenon is found to have a large influence on the local quantities, since the variation of JETSET fragmentation parameters can significantly change the simulated signal.

A noticeable disagreement is found between JETSET and the data. To some extent this discrepancy may be due to the way the JETSET 7.4 PS model was tuned by the L3 Collaboration. The tuning of the model was performed to provide a good description of global shape distributions and inclusive particle spectra [15]. Our analysis indicates that such commonly used tuning is not enough to give a good description of the local observable. Besides, a large systematic uncertainty in the definition of the fragmentation parameters for JETSET makes it difficult to compare of the local fluctuations observed with the model predictions.

The problem of the discrepancy observed, however, is more complicated, and an additional study of JETSET itself is necessary: It has been shown that JETSET 7.4 PS overestimates fluctuations of unlike-charged particles both in rapidity defined with respect to the thrust axis and in the four-momentum-difference variable. The variation of JETSET parameters cannot fully reduce the discrepancy observed. Thus, it appears that some important points in the simulation of hadronization, resonance production and BE effect are missing in the present version of JETSET and further modifications of the model are needed.

Furthermore, from the discrepancies observed for like-charged combinations it becomes clear that the treatment of BE correlations has to be improved. A similar conclusion has been deduced in [25], where it has been shown that JETSET fails to reproduce the multiplicity dependence of the intermittency index ϕ_2 . Recently, progress has been made to incorporate the BE correlations directly into the Lund model [30]. In this new method, the BE interference is taken into account on the level of string fragmentation. Hence, one can expect that BE correlations can significantly affect unlike-charged combinations as well, and there may be a chance that the disagreement obtained between JETSET and the data will be reduced.

Bibliography

- [1] DELPHI Coll., P.Abreu et al., Phys. Lett. B247 (1990) 137;
A.De Angelis, Mod. Phys. Lett. A5 (1990) 2395
- [2] DELPHI Coll., P.Abreu et al., Nucl. Phys. B386 (1992) 471
- [3] OPAL Coll., M.Z.Akrawy et al., Phys. Lett. B262 (1991) 351
- [4] TASSO Coll., W.Braunschweig et al., Phys. Lett. B231 (1989) 548
- [5] K.Sugano (HRS Collab.), Proc. Santa Fe Workshop "Intermittency in High-Energy Collisions", Eds: F.Cooper et al. (World Scientific, Singapore, 1991) p.1
- [6] CELLO Coll., H.J.Behrend et al., Phys. Lett. B256 (1991) 97
- [7] ALEPH Coll., D.Decamp et al., Z. Phys. C53 (1992) 21
- [8] L3 Coll., B. Adeva et al., Z. Phys. C55 (1992) 39
- [9] ALEPH Coll., D.Buskulic et al., Z. Phys. C69 (1995) 15
- [10] E.A.De Wolf, I.M.Dremin and W.Kittel, Phys. Rep. 270 (1996) 1
- [11] S.V.Chekanov and V.I.Kuvshinov, Acta Phys. Pol. B25 (1994) 1189 (see Chapter 3);
S.V.Chekanov, W.Kittel and V.I.Kuvshinov, Acta Phys. Pol. B26 (1996) 1739 (see Chapter 6)
- [12] S.V.Chekanov, W.Kittel and V.I.Kuvshinov, Z. Phys. C74 (1997) 517 (see Chapter 5)
- [13] P.Grassberger, Phys. Lett. A97 (1983) 227;
H.Hentschel and I.Procaccia, Physica D8 (1983) 43
- [14] A. A. Syed, "Particle correlations in hadronic decays of the Z Boson", Ph.D. Thesis, Univ. of Nijmegen 1994, The Netherlands
- [15] J.Casaus, L3 Note 1946, PPE Div., CERN, 1996;
Sunanda Banerjee and Swagato Banerjee, L3 Note 1978, PPE Div., CERN, 1996;
I.G.Knowles and T.Sjöstrand (conveners), "QCD Event Generators", Physics at LEP, CERN-96-01, Vol. 2 (1996) p.103
- [16] G.Marchesini and B.R.Webber, Nucl. Phys. B310 (1988) 461;
G.Marchesini et al., Comp. Phys. Comm. 67 (1992) 465
- [17] S.V.Chekanov, Proc. of 7th Int. Workshop on Multiparticle Production "Correlations and Fluctuations", Nijmegen, The Netherlands 1996, Eds: R.C.Hwa et al. (World Scientific, Singapore, 1997) p.192
- [18] DELPHI Coll., P.Abreu et al., Phys. Lett. B286 (1992) 201
- [19] DELPHI Coll., P.Abreu et al., Z. Phys. C63 (1994) 17

- [20] ALEPH Coll., D.Decamp et al., Z. Phys. C54 (1992) 75
- [21] E.A.De Wolf, Proc. of 24 Int. Symp. on Multiparticle Dynamics 1994, Eds: A.Giovannini et al., (World Scientific, Singapore, 1995) p.15
- [22] B.Andersson, G.Gustafson, G.Ingelman, T.Sjöstrand, Phys. Rep. 97 (1983) 31
- [23] J.W.Lamsa, ICHEP'96, Conf. pa01-094; DELPHI Note 96-72
- [24] J.Rameš, Proc. of 24 Int. Symp. on Multiparticle Dynamics, Vietri sul Mare (Italy) 1994, Eds: A.Giovannini et al. (World Scientific, Singapore, 1995) p.104
- [25] K.Fiałkowski, Proc. of 24 Int. Symp. on Multiparticle Dynamics, Vietri sul Mare (Italy) 1994, Eds: A.Giovannini et al., (World Scientific, Singapore, 1995) p.85
- [26] S.V.Chekanov, Talk presented at L3 General Meeting (Berlin, 1996)
- [27] OPAL Coll., P.D.Acton et al., Z. Phys. C56 (1992) 521
- [28] DELPHI Coll., P.Abreu et al., Z. Phys. C65 (1995) 548
- [29] W.Ochs and J.Wosiek, Phys. Lett. B305 (1993) 144;
Yu.Dokshitzer and I.M.Dremin, Nucl. Phys. B402 (1993) 139;
Ph.Brax, J.-L.Meunier and R.Peschanski, Z. Phys. C62 (1994) 649
- [30] B.Andersson, Proc. of 7th Int. Workshop on Multiparticle Production "Correlations and Fluctuations", Nijmegen, The Netherlands 1996, Eds: R.C.Hwa et al. (World Scientific, Singapore, 1997) p.86

Test of Analytical QCD Predictions

13.1 Introduction

Local multiplicity fluctuations have been studied for many years in terms of a variety of phase-space variables, but only recently has substantial progress been made to derive analytical QCD predictions for these observables [1–3]. Attempts have already been undertaken by the DELPHI Collaboration [4] to compare the analytical QCD predictions [1] with the experimental data for angular intermittency measured in hadronic Z^0 decay. The authors have mainly concentrated on the study of correlation functions, cumulants and multiplicity moments of orders $q = 2, 3$ derived in the Double Leading Log Approximation (DLLA) of QCD. The analytical predictions tend to underestimate the correlations between particles in small angular windows if one uses a $\Lambda \sim 0.1 - 0.2$ GeV for the QCD dimensional scale. However, a reasonable agreement is achieved for an effective $\Lambda \sim 0.04$ GeV, significantly smaller than theoretical QCD estimates [5].

As shown in the previous chapter, the local fluctuations inside jets are of multifractal type, which is qualitatively consistent with the QCD predictions. In this chapter we extend this study and present a first quantitative comparison of the theoretical QCD predictions [2, 3] with the L3 data, emphasizing the behavior of normalized factorial moments of orders $q = 2, \dots, 5$ in angular phase-space intervals.

13.2 Analytical predictions

QCD predictions have been obtained [2, 3] for normalized factorial moments (NFM) $F_q(\Theta)$, which have the following behavior

$$F_q(\Theta) \equiv \frac{\langle n(n-1)\dots(n-q+1) \rangle}{\langle n \rangle^q} \propto \left(\frac{\Theta_0}{\Theta} \right)^{(D-D_q)(q-1)}, \quad (13.1)$$

where, for the one-dimensional case ($D = 1$), Θ_0 is the opening angle of a cone around the jet-axis, Θ is the angular half-width window of rings around the jet-axis centered at Θ_0 (see Fig. 13.1), n is the number of particles in these rings and $\langle \dots \rangle$ is the average over all events. The analytical QCD expectations for the Rényi dimension D_q are as follows [2, 3]:

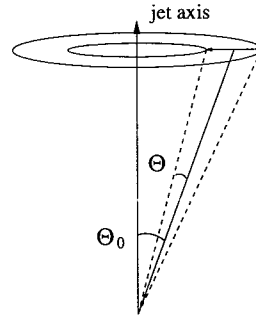


Figure 13.1: A schematic representation of the measurements of the local fluctuations in the polar angle around jet axis ($D = 1$).

- 1) In the fixed coupling regime, for moderately small angular bins,

$$D_q = \gamma_0(Q) \frac{q+1}{q}, \quad (13.2)$$

where $\gamma_0(Q) = \sqrt{2C_A\alpha_s(Q)}/\pi$ is the anomalous QCD dimension calculated at $Q \simeq E\Theta$, $E = \sqrt{s}/2$, and $C_A = N_c = 3$ is the gluon color factor.

- 2) In the running-coupling regime for small bins, the Rényi dimension becomes a function of the size of the angular ring due to the running coupling effect ($\alpha_s(Q)$ increases with decreasing Θ). It is useful to introduce a new scaling variable [3],

$$z = \frac{\ln(\Theta_0/\Theta)}{\ln(E\Theta_0/\Lambda)}.$$

In terms of this phase-space variable, the maximum possible phase-space region ($\Theta = \Theta_0$) corresponds to $z = 0$.

There are two approximate expressions derived in DLLA which will be tested:

- a) According to [2], the D_q have the form

$$D_q \simeq \gamma_0(Q) \frac{q+1}{q} \left(1 + \frac{q^2+1}{4q^2} z \right). \quad (13.3)$$

- b) Another approximation has been suggested in [3]:

$$D_q \simeq 2\gamma_0(Q) \frac{q+1}{q} \left(\frac{1-\sqrt{1-z}}{z} \right). \quad (13.4)$$

In [2], an expression for D_q has also been obtained in the Modified Leading Log Approximation (MLLA). In this case, (13.3) remains valid, except that $\gamma_0(Q)$ is replaced by an effective $\gamma_0^{\text{eff}}(Q)$ depending on q :

$$\gamma_0^{\text{eff}}(Q) = \gamma_0(Q) + \gamma_0^2(Q) \frac{b}{4C_A} \left[-B \frac{q-1}{2(q+1)} + \frac{q-1}{2(q+1)(q^2+1)} + \frac{1}{4} \right], \quad (13.5)$$

$$b = \frac{11C_A}{3} - \frac{2n_f}{3}, \quad B = \frac{1}{b} \left[\frac{11C_A}{3} + \frac{2n_f}{3C_A^2} \right],$$

where n_f is the number of flavors ($n_f = 5$ at LEP1).

For our comparison of the data with the theoretical predictions quoted above, we will use the following parameters

$$\Theta_0 = 25^\circ, \quad \Lambda = 0.16 \text{ GeV}.$$

The first parameter is free. Its value is chosen to make our study comparable with the DELPHI analysis [4]. A larger value of Θ_0 would allow a larger range of values of the variable z to be studied, but the statistics available would be smaller at larger z . On the other hand, a smaller value of Θ_0 would reduce the range of z to be tested due to detector resolution. Only weak dependence of the correlation functions on Θ_0 has been found at LEP energies [4], in agreement with the analytical QCD predictions.

The value of Λ chosen is that found in tuning the JETSET 7.4 PS program [7] on L3 data [8] and in our most recent determination of $\alpha_s(m_Z)$ [9].

The effective coupling constant is evaluated at $Q \simeq E\Theta_0$, which gives $\alpha_s(E\Theta_0) \simeq 0.17$ according to the first-order QCD expression for $\alpha_s(Q)$. This value leads to $\gamma_0(E\Theta_0) \simeq 0.57$.

13.3 Experimental procedure

In this paper, we present an experimental investigation of local fluctuations in the final-state hadron system produced in Z^0 decays at $\sqrt{s} = 91.2$ GeV. The sphericity axis is used as the jet axis. The final-state hadrons were recorded with the L3 detector during the 1994 LEP running period. The calculations are based on approximately 810k selected hadronic events. They are selected by the standard L3 selection procedure, based on energy deposition in the electromagnetic and hadronic calorimeters and momentum measurement of charged tracks in the Central Tracking Detector including the Silicon Microvertex Detector. From these events, good tracks are selected to calculate the NFM's. The entire selection procedure is described in more detail in Chapter 9.

To carry out a correction procedure, a Monte-Carlo sample of multihadronic events is generated with JETSET 7.4 PS [7] including initial-state photon radiation. On the first level (generator level), the sample generated directly from the JETSET model contains all charged final-state particles with a lifetime larger than 10^{-9} s. On the second level (detector level), it includes distortions due particle interactions with the detector material, limited resolution, multi-track separation, acceptance of the detector, event selection and various detector imperfections. The Monte-Carlo events were processed with the same reconstruction program as used for the experimental data.

A corrected NFM is found by means of the following correction procedure

$$F_q^{\text{cor}} = C_q F_q^{\text{raw}}, \quad C_q = \frac{F_q^{\text{gen}}}{F_q^{\text{det}}}. \quad (13.6)$$

Here, F_q^{gen} and F_q^{det} symbolize an NFM of order q calculated from the generator level and detector level of JETSET 7.4 PS model, respectively. F_q^{raw} represents the same quantity calculated directly from the data.

Using the same method, the data are further corrected for the occurrence of Bose-Einstein correlations, initial-state photon radiation and Dalitz decays. For this, additional Monte Carlo samples are used. The first one is the default JETSET 7.4 sample, which does not include the initial-state photon radiation and Bose-Einstein correlations. F_q^{def} is calculated from this sample. Then, the correction factor

$$C_q^{(1)} = \frac{F_q^{\text{def}}}{F_q^{\text{gen}}}$$

corrects the data for initial-state photon radiation or Bose-Einstein correlations, since these effects are not included in the analytical QCD calculations. Since the Bose-Einstein correlations are simulated in JETSET model essentially as final-state interactions between pairs of identical pions, such an implementation was shown cannot correctly reproduce the local multiplicity fluctuations (see Chapter 12). Therefore, in addition to the data corrected with $C_q^{(1)}$, below we show the data without this correction procedure.

To correct the data for the occurrence of Dalitz decays of the π^0 , the following correction factor

$$C_q^{(2)} = \frac{F_q^{\text{Dz}}}{F_q^{\text{def}}}$$

is used. Here, F_q^{Dz} is obtained from the default-parameter JETSET, but without Dalitz pairs.

The corrections including $C_q^{(1)}$ and $C_q^{(2)}$ are of the order of $\sim 10\%$ for the second-order NFM and approximately $\sim 15\%$ for the fifth-order NFM.

The resolution of the L3 detector for a number of relevant variables has been estimated in Chapter 10. The resolution of polar angle defined with respect to the thrust axis is found to be approximately 0.013 radians. For higher orders NFMs, the minimum angle Θ is chosen according to the many-particle resolutions studied in Chapter 10.

13.4 Analysis

Fig. 13.2 shows the experimental result on the behavior of the NFMs as a function of the scaling variable z . The corrected data (full circles) were obtained by using the three correction factors C_q , $C_q^{(1)}$ and $C_q^{(2)}$ discussed above. The error bars show only statistical errors and include the statistical errors on the correction factors under the conservative assumption that all statistical errors on each correction factor are independent. To increase statistics we evaluated the NFMs in each sphericity hemisphere of an event and averaged the results assuming that the local fluctuations in each jet are independent.

The open symbols show the predictions of the JETSET 7.4 PS model for hadronic (open circles) and partonic (open triangles) levels. The open circles show the JETSET 7.4 PS default, without initial-state photon radiation, Bose-Einstein correlations and Dalitz decays. The data and the hadronic level of the JETSET model have a slope much steeper than that for the partonic level. The Monte-Carlo prediction for hadrons gives a reasonable description of the fluctuations for $z < 0.4$ ($\Theta > 0.03$), but overestimates the data for very small angular intervals ($z > 0.4$).

It has been suggested in [3] that it is instructive to consider the ratio $F_q(z)/F_q(0)$ in order to reduce hadronization effects on the actual behavior of the NFMs. In addition, this

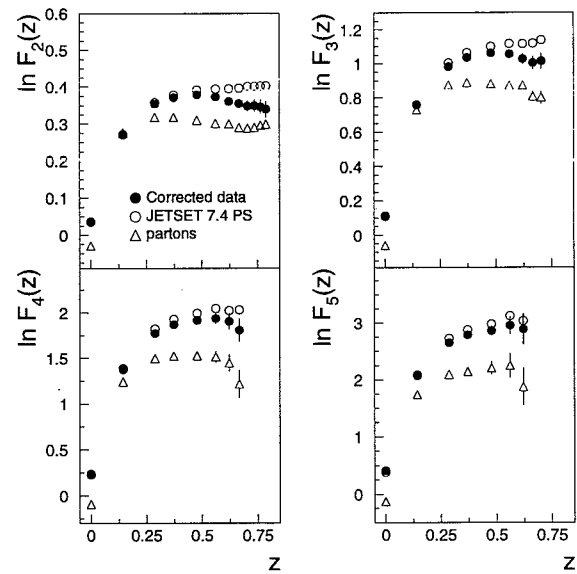


Figure 13.2: $NFMs$ ($q = 2, \dots, 5$) as a function of the scaling variable z and JETSET 7.4 PS predictions, on the partonic and hadronic levels. Data are corrected for initial-state photon radiation, Bose-Einstein correlations and Dalitz decays.

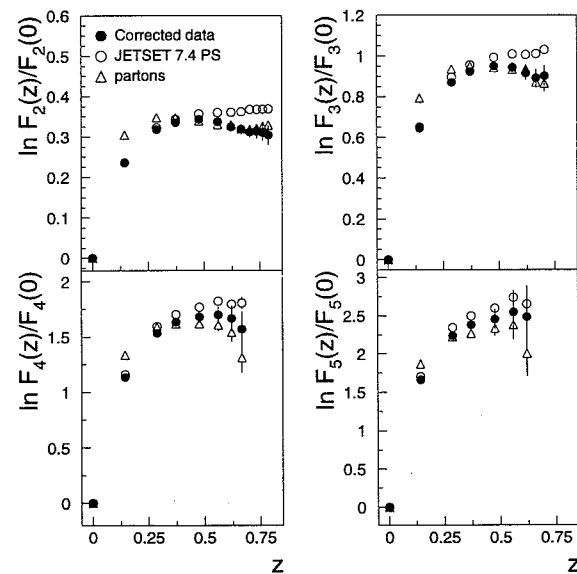


Figure 13.3: The behavior of $F_q(z)/F_q(0)$ ($q = 2, \dots, 5$) and JETSET 7.4 PS predictions, on the partonic and hadronic levels. Data are corrected for initial-state photon radiation

reduces a theoretical ambiguity for the evaluation of NFMs in full phase space ($z = 0$) that renders the comparison of the data with the analytical predictions uncertain. In terms of $F_q(z)/F_q(0)$, the power law (13.1) can be rewritten as

$$\ln \frac{F_q(z)}{F_q(0)} = z(1 - D_q)(q - 1) \ln \frac{E\Theta_0}{\Lambda}. \quad (13.7)$$

The behavior of the $\ln(F_q(z)/F_q(0))$ as a function of z is shown in Fig. 13.3. The partonic level of JETSET is indeed much closer to the data, though a significant difference between the slopes for the data and the partonic level of JETSET is still present.

The comparison of the analytical QCD predictions (13.2)-(13.5) for $\Lambda = 0.16$ GeV to the corrected data is shown in Fig. 13.4. Here we also show data (full triangles) which are not corrected for Bose-Einstein correlations. These data were obtained by using only two correction factors C_q and $C_q^{(2)}$. Since the contribution of initial-state photon radiations is relatively small, full triangles essentially represent the data with Bose-Einstein correlation between identical pions. Predictions (13.3)-(13.5) lead to the saturation effects seen in the data, but significantly underestimate the observed signal, especially for $q = 2$. The reason for the saturation effect seen on the QCD predictions is the dependence of $\alpha_s(Q)$ on Θ . The fixed coupling regime (see (13.2) and solid lines in Fig. 13.4) approximates the running coupling regime for small z , but does not exhibit the saturation effect seen in the data. The MLLA predictions do not differ significantly from the DLLA result (13.3) (Fig. 13.4).

Agreement of the QCD predictions for the second-order NFM with the data can be achieved by decreasing the value of Λ . A similar observation has been made by DELPHI [4] in a study according to parameterization derived in [1]. As an example, Fig 13.5 shows the case of $\Lambda = 0.04$ GeV. Such an effective value makes the coupling constant smaller and thus can expand the range of reliability of the perturbative QCD calculations (for $\Lambda = 0.04$ GeV $\alpha_s(E\Theta_0) \simeq 0.13$, $\gamma_0(E\Theta_0) \simeq 0.50$). However, this leads to a large disagreement between the QCD predictions and the data for higher-order NFMs at large z . We have varied Λ in the range of 0.04 – 0.25 GeV and found that there is no value of Λ in this range which produces agreement for all orders of NFMs.

Note also that the disagreement for the second-order NFMs can also be reduced by considering the second-order expression for $\alpha_s(Q)$ or by replacing $n_f = 3$, instead of $n_f = 5$. This leads to a decrease of the $\gamma_0(E\Theta_0)$. In this case, however, again no good agreement can be reached for all higher-orders of the NFMs.

13.5 Conclusion

The predictions of the DLLA and MLLA of perturbative QCD are shown to be in disagreement with the local fluctuations as observed for hadronic Z^0 decay. This conclusion is valid for relatively large values of Λ ($\Lambda = 0.16$ GeV) as well as for small values ($\Lambda = 0.04$ GeV). In the latter case, a reasonable estimate for the second-order NFM can be reached, consistent with the DELPHI conclusion [4]. However, our analysis shows that, in this case, the theoretical higher-order NFMs strongly overestimate the data.

In the theoretical predictions discussed above, energy-momentum conservation in triparton vertices is not embedded. A recent study [10] of this effect shows that the energy conservation constraint is sizeable and leads to a stronger saturation effect. Hence, energy-momentum conservation is not the reason for the disagreement observed for $F_2(z)/F_2(0)$.

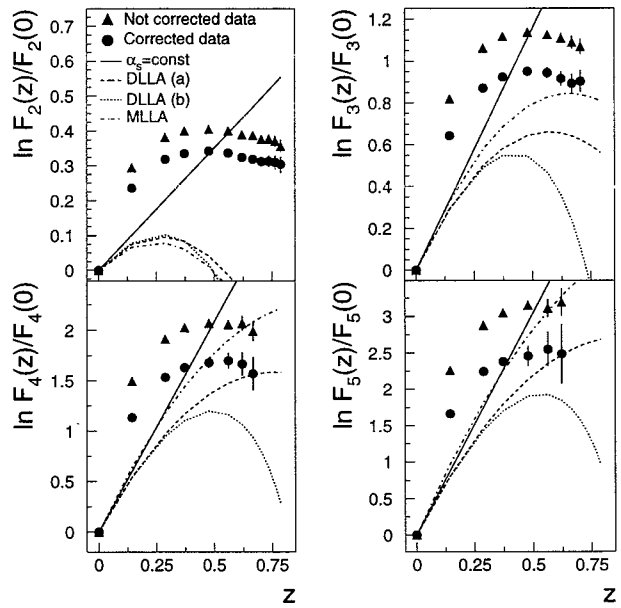
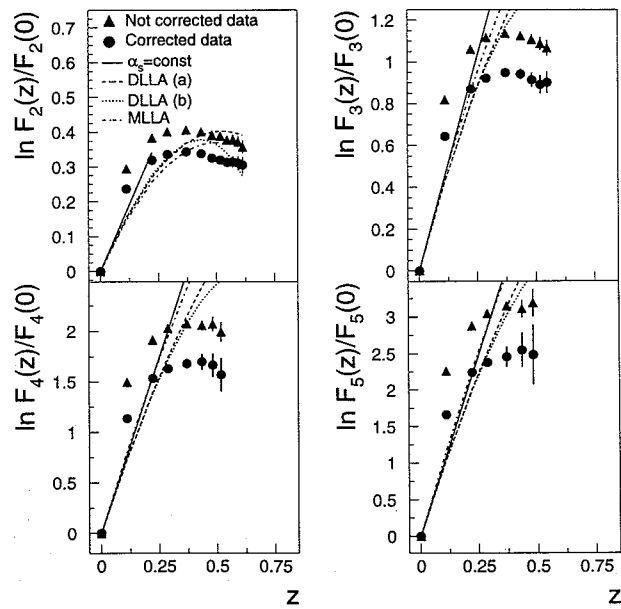


Figure 13.4: The analytical QCD predictions for $\Lambda = 0.16$ GeV: 1) $\alpha_s = \text{const}$ (13.2); 2) DLLA (a) (eq. (13.3)); 3) DLLA (b) (eq. (13.4)); 4) MLLA (eqs. (13.3) and (13.5)). The corrected data (full circles) obtained by using correction factors C_q , $C_q^{(1)}$ and $C_q^{(2)}$. Full triangles show the data corrected only with C_q and $C_q^{(2)}$.



As has been commented in [2], the most probable reason for the disagreements with experimental data is the asymptotic character of the QCD predictions, corresponding to an infinite number of partons in an event. Another contribution to the failure of the predictions can lie with the local parton-hadron duality hypothesis, which is used to justify comparison of the predictions of perturbative QCD. The predictions are for partons, but the experimental results are calculated from data on particles. The non-perturbative domain of QCD may have a large influence on the values of the NfMs.

Bibliography

- [1] W.Ochs and J.Wosiek, Phys. Lett. B289 (1992) 152; B305 (1993) 144; Z. Phys. C68 (1995) 269
- [2] Yu.Dokshitzer and I.M.Dremin, Nucl. Phys. B402 (1993) 139
- [3] Ph.Brax, J.-L.Meunier and R.Peschanski, Z. Phys. C62 (1994) 649
- [4] F.Mandl and B.Buschbeck (DELPHI Coll.), Proc. 24 Int. Symp. on Multiparticle Dynamics, September 1994, Salerno, Italy, Eds. A.Giovannini et al. (World Scientific, Singapore, 1995) p.52;
B.Buschbeck and F.Mandl, ICHEP'96 Ref. pa01-028;
B.Buschbeck, P.Lipa, F.Mandl (DELPHI Coll.), Proc. 7th Int. Workshop on Multiparticle Production "Correlations and Fluctuations", Nijmegen, The Netherlands 1996, Eds: R.C.Hwa et al. (World Scientific, Singapore, 1997) p.175
- [5] Particle Data Group, *Review of Particle Physics*, Phys. Rev. D54 (1996) 83
- [6] S.V.Chekanov, Proc. 7th Int. Workshop on Multiparticle Production "Correlations and Fluctuations", Nijmegen, The Netherlands 1996, Eds: R.C.Hwa et al. (World Scientific, Singapore, 1997) p.192
- [7] T.Sjöstrand, Comp. Phys. Comm. 82 (1994) 74
- [8] S.Banerjee, D.Duchesneau, S.Sarkar, L3 Note 1818 (1995);
J.Casaus, L3 Note 1946 (1996);
L3 Coll., B.Adeva et al. Z. Phys. C55 (1992) 39
- [9] A.Buytenhuijs, "QCD Gluon Radiation Studies Using the L3 Detector", Ph.D. Thesis, Univ. of Nijmegen 1996, The Netherlands
- [10] J.-L.Meunier and R.Peschanski, Z. Phys. C72 (1996) 647

14

Summary

This thesis is based on two separate but mutually complementary sources. First, it contains theoretical studies of local multiplicity fluctuations of final-state hadrons observed in all types of high-energy processes. The results are outlined in subsection 2.4 and at the end of each paper reproduced in this thesis. Below we summarize in short the main results:

- We developed a new method for a precise measurement of local multiplicity fluctuations, the so-called bunching-parameter method. The method opens up the possibility to study local fluctuations without the trivial contamination arising from the finite size of the event-sample. In moving to ever smaller phase-space intervals, this is a big advantage over the previously used tools, such as normalized factorial moments and normalized cumulant moments.
- It was shown that the method is able to reveal local fluctuations in more detail than the conventional normalized-factorial moment method. Hence, the method proposed can be used to obtain a refined insight into various production mechanisms.
- The method can be generalized to examine bin-bin correlations and admits the use of the interparticle distance-measure technique as the next step in the direction of maximal utilization of the information provided by experiments.
- Based on the fact that the bunching parameters have a more direct link to the structure of the multiplicity distribution inside a small phase-space interval, we suggest a possible form of multifractal distribution which is more relevant to the observed fluctuations than the commonly used negative-binomial distribution.

The second part of this thesis describes an experimental application of the approach developed in the first part. Local multiplicity fluctuations of charged particles produced in Z^0 decay are analyzed from the data collected in 1994 by the L3 Collaboration at CERN. The main results are:

- The resolution of the L3 detector was determined for the different variables and data taking periods. It was found that the resolution is sufficient for the precision analysis in the case of the 1994 data taking period, but not in the case of that of 1993.

- Using the method proposed, we analyzed the behavior of the bunching parameter for charged final-state particles in different phase-space variables. The results confirm that the bunching-parameter method is particularly sensitive to the structure of local fluctuations.
- A strong multifractal structure of the fluctuations was observed inside jets, while the calculations in the variables defined with respect to the beam axis did not show such a trend. This new result was achieved entirely with the help of the method developed and described in the theoretical part of this thesis.
- The JETSET 7.4 PS model tuned by the L3 Collaboration cannot reproduce the details of the fluctuations. For the one-dimensional analysis, better agreement may be achieved by further tuning of the model parameters and by improving the Bose-Einstein modeling. However, the problem of the discrepancy found for unlike-particle combinations is more complicated, and further improvement of the model itself is necessary.
- A significant disagreement was found between the analytical perturbative QCD predictions for angular intermittency and the data. This discrepancy suggests large contributions to the local multiplicity fluctuations in small angular regions from high-order perturbative QCD and from non-perturbative effects.

An understanding of the intermittency phenomenon in various high-energy processes is still insufficient. If one believes that Quantum Chromo Dynamics is the best candidate for the theory of Strong Interactions, one should expect that it provides a suitable framework for the description of the local fluctuations. A big step has already been made to actually derive the intermittency in perturbative QCD for the simplest e^+e^- -annihilation processes. However, there is a long way to go toward the understanding and analytical description of contributions to the local fluctuations from the non-perturbative regime of QCD, as well as from resonance decays and Bose-Einstein interference.

Samenvatting

Dit proefschrift berust op twee afzonderlijke, maar elkaar aanvullende onderzoeken. Ten eerste bevat het een theoretische studie naar lokale schaalinvariante vertakkingsfluctuaties, die in de afgelopen jaren zijn waargenomen in de hadronische eindtoestanden van alle soorten hoge-energieprocessen. De resultaten hiervan worden beschreven in subsectie 2.4 en aan het einde van elk van de in dit proefschrift opgenomen publicaties. In het kort zijn de voornaamste resultaten de volgende:

- We hebben een nieuwe methode ontwikkeld voor een precisiemeeting van de lokale vertakkingsfluctuaties, de samenbundelingsparametermethode. Deze methode maakt het mogelijk om lokale fluctuaties te bestuderen zonder hinder van de triviale verstoring, die het gevolg is van de eindige omvang van de verzameling gevallen. Bij het bestuderen van voortdurend kleinere faseruimte-intervallen is dit een groot voordeel ten opzichte van eerder gebruikte middelen zoals genormaliseerde factoriële momenten of genormaliseerde cumulatieve momenten.
- Er wordt aangetoond, dat met deze methode in meer detail naar lokale fluctuaties kan worden gekeken, dan met de conventionele genormaliseerde factoriële momenten. Daarom is de voorgestelde methode geschikt om een verfijnd inzicht te krijgen in de verschillende productieprocessen.
- De methode kan worden veralgemeend om interval-interval correlaties te bestuderen. Ze staat toe een afstandsmaat tussen de deeltjes te introduceren als een volgende stap naar het optimaal gebruik van de informatie, die door de experimenten wordt geleverd.
- Op grond van het feit, dat de samenbundelingsparameters directer verbonden zijn met de structuur van de vertakkingsverdeling binnen een klein faseruimte interval stellen we een multifractale distributie voor, die meer vertelt over de waargenomen fluctuaties, dan een negatief binomiaal verdeling.

Het tweede deel van dit proefschrift is de toepassing in een experiment van de benadering ontwikkeld in het eerste deel. Lokale vertakkingsfluctuaties van geladen deeltjes afkomstig uit het verval van Z bosonen zijn geanalyseerd in gegevens uit 1994, afkomstig van de L3 samenwerking in CERN. De voornaamste resultaten zijn:

- Een bepaling van het oplossend vermogen van de L3 detector voor verschillende variabelen in enkele opnameperiodes. Het oplossend vermogen bleek voldoende voor een precisiestudie voor de gegevens uit de periode 1994, maar niet voor die uit 1993.
- Met behulp van de voorgestelde methode hebben we het gedrag van de samenbundelingsparameters bestudeerd voor de verschillende faseruimtevariabelen van deeltjes in de eindtoestand. De resultaten bevestigen dat samenbundelingsparameters bijzonder gevoelig zijn voor de structuur van lokale fluctuaties.
- We nemen een sterke multifractale structuur waar in de fluctuaties binnen de uitgaande deeltjesbundels, terwijl deze ontbreekt in de berekeningen gedaan ten opzichte van de inkomende bundelas. Dit is een nieuw resultaat volledig voortkomend uit de hier ontwikkelde methode.
- Het door de L3 samenwerking afgeregeld JETSET 7.4 PS model kan de details van de fluctuaties niet voorspellen. Voor een een-dimensionale analyse kan betere overeenstemming worden bereikt door de modelparameters bij te stellen en de Bose-Einstein effecten te verbeteren. Niettemin, de afwijking gevonden voor ongelijk geladen deeltjesparen is ingewikkelder en een verdere verbetering van het model is noodzakelijk.
- Analytische QCD storingsberekeningen voor de hoekcorrelaties wijken significant van de data. Dit doet vermoeden, dat grote bijdragen tot lokale fluctuaties afkomstig zijn van perturbatieve QCD van hogere orde en van niet-perturbatieve verschijnselen in het kleine hoek gebied.

Een volledig begrip van de correlaties in de verschillende hoge energie reacties is nog ver weg. Wie gelooft in Quantum Chromo Dynamica als beste kandidaat voor een theorie van de sterke wisselwerking zou mogen verwachten, dat dit ook een goede basis zou verschaffen voor de beschrijving van lokale fluctuaties. Een grote stap voorwaarts is al gemaakt door het feitelijk afleiden van de correlaties met QCD-storingsrekening voor de eenvoudigste e^+e^- annihilatieprocessen. Toch ligt er nog een lange weg naar begrip en analytische beschrijving van de bijdrage aan lokale fluctuaties van het niet-storingsbeschreven deel van QCD, van de resonantie vervallen en van de Bose-Einstein-interferentie.

Curriculum Vitae

Sergei Chekanov

The author of this thesis was born on June 9, 1969 in Minsk (Republic of Belarus, then USSR). In 1986 he finished secondary school and was accepted to the Physical Department of the Byelorussian State University the same year. He was called up for military service in the Soviet army in 1987 and continued his university education in 1989. He graduated in theoretical physics with honors in 1993. After graduation, he was offered a post-graduate training in theoretical physics at the Theoretical Department of the Academy of Science of Belarus under the supervision of Prof. Dr. V.I.Kuvshinov and he passed all post-graduate courses in the Belarus Academy of Science during 1993-1995. In 1995, he continued his Ph.D. research at the High Energy Physics Institute Nijmegen (University of Nijmegen, Nijmegen, The Netherlands) under the supervision of Prof. Dr. E.W.Kittel. Here, the author carried out the theoretical and experimental investigations of correlations/fluctuations in hadron systems produced in Z decay as a member of the L3 Collaboration in CERN (Geneva).

He took part in 4th Int. School on Theory of Elementary Particles in 1992 (Dubna, Russia), 7th and 8th Annual Joint Belgian-Dutch-German graduate schools of particle physics in 1995 (Cul-des Sarts, Belgium) and in 1996 (Rolduc, The Netherlands). He was participant of: 1) 1st, 2nd, 3d, 4th, 5th, 6th Int. Seminar "Nonlinear Phenomena in Complex Systems" (1992-1997, Polatsk-Minsk, Belarus); 2) Int. Conference "Quantum Systems: New Trends and Methods" (1994, Minsk, Belarus); 3) 10th Int. Workshop on High Energy Physics and Quantum Field Theory (1994, Zvenigorod, Russia); 4) L3 Int. General Meeting (1996, Berlin, Germany); 5) 7th Int. Workshop on Multiparticle Production (1996, Nijmegen, The Netherlands); 6) Dutch Phys. Society Annual Meeting (1996, ECN Petten, The Netherlands); 7) 32nd Int. Conf. "QCD and High-Energy Hadronic Interactions" (1997, Moriond, France).

List of Publications

1. S.V.Chekanov and V.I.Kuvshinov,
Phenomenological Properties of Hadronization and Anomalous Fractal Dimension Behavior,
“Non-Linear Phenomena in Complex Systems”, Proc. 1st Int. Seminar, Polatsk, Belarus 1991, Eds: V.I.Kuvshinov et al., (Polatsk, Belarus, 1992) p.186-191
2. S.V.Chekanov and V.I.Kuvshinov,
Multifractal Properties of Hadronization,
“Non-Linear Phenomena in Complex Systems”, Proc. 2nd Int.Seminar, Polatsk, Belarus 1992, Eds: V.I.Kuvshinov and D.W.Serow (St.Petersburg, Russia, 1993) p.159-170
3. S.V.Chekanov,
Bunching Parameter and Multifractal Structure of Multiplicity Distributions in High-Energy Collisions,
“Non-Linear Phenomena in Complex Systems”, Proc. 3d Int. Seminar, Eds: V.I. Kuvshinov et al. (Polatsk, Belarus, 1994) p.170-176
4. S.V.Chekanov,
Local Fluctuations and Intermittency in Hadronization Process,
“Quantum Systems: New Trends and Methods”, Proc. 1st Int Conf, Minsk, Belarus, 1994, Eds. Y.Shir et al. (World Scientific, Singapore, 1995) p.367-374
5. S.V.Chekanov and V.I.Kuvshinov,
Contributions to Intermittency From Different Stages of Cluster Models,
Proc. 9th Int. Workshop on High Energy Physics and Quantum Field Theory, Zvenigorod, Russia, 1994 (World Scientific, Singapore, 1995)
6. S.V.Chekanov and V.I.Kuvshinov,
Bunching Parameters and Intermittency in High-energy Collisions,
Acta Phys. Pol. B25 (1994) p.1189-1197
7. S.V.Chekanov,
Intermittency in Cluster Models; Correlations and Fluctuation Approaches,
Acta Phys. Pol. B25 (1994) p.1583-1594
8. S.V.Chekanov and V.I.Kuvshinov,
Multifractal NBD-Like Multiplicity Distribution in Bunching Parameter Analysis,
“Non-Linear Phenomena in Complex Systems”, Proc. 4th Int. Seminar, Minsk 1995, Eds: V.Kuvshinov and G.Krylov, (Minsk, Belarus, 1996) p.43-50

9. S.V.Chekanov, D.V.Klenitsky and V.I.Kuvshinov,
*Properties of Multiplicity Distributions Derived From QCD Konishi-Ukawa-Venezian
Evolution Equations*,
“Non-Linear Phenomena in Complex Systems”, Proc. 4th Int. Seminar, Minsk 1993
Eds: V.Kuvshinov and G.Krylov, (Minsk, Belarus, 1996) p.51-58
10. S.V.Chekanov and V.I.Kuvshinov,
Multifractal Multiplicity Distribution in Bunching-Parameter Analysis,
J. Phys. G22 (1996) p.601-610
11. S.V.Chekanov and V.I.Kuvshinov,
On the Role of Multiparticle Clusters in Intermittent Fluctuations,
“Non-Linear Phenomena in Complex Systems”, Proc. 5th Int. Seminar, Minsk 1995
Eds: G.Krylov et al. (Minsk, Belarus, 1997) (in press)
12. S.V.Chekanov, W.Kittel and V.I.Kuvshinov,
*Generalized Bunching Parameters and Multiplicity Fluctuations in Restricted Phase
Space Bins* ,
HEN-391, Z. Phys. C74 (1997) p.517-529
13. S.V.Chekanov, W.Kittel and V.I.Kuvshinov,
Bin-Bin Correlation Measurement by the Bunching-Parameter Method,
HEN-392, Acta Phys. Pol. B27 (1996) p.1739-1748
14. S.V.Chekanov and V.I.Kuvshinov,
Multiparticle Clusters and Intermittent Fluctuations,
Nijmegen preprint, HEN-398 J. Phys. G (in press)
15. S.V.Chekanov (for the L3 Collaboration),
Local Multiplicity Fluctuations in Z decay,
preprint HEN-394, Presented at 7th International Workshop on Multiparticle Production
“Correlations and Fluctuations”, Nijmegen, The Netherlands 1996, Eds: R.C.Hofstadter
et al. (World Scientific, Singapore, 1997) p.192-202
16. S.V.Chekanov, W.Kittel and W.J.Metzger,
Local Multiplicity Fluctuations in Final-State Hadrons produced in Z decay,
Nijmegen preprint, HEN-401, 1997
17. S.V.Chekanov,
Local Multiplicity Fluctuations in the Statistical Treatment of Cascade Process,
(Submitted to Nucl. Phys. B)
18. S.V.Chekanov, W.Kittel and W.J.Metzger,
Local Multiplicity Fluctuations in Angular Intervals and Analytical QCD Prediction
Nijmegen preprint, HEN-402, 1997

